University of Bremen
Faculty 1 of Physics and Electronics
Institute for Biophysics

Measuring creep response of soft samples by magnetic force microscopy

Dissertation in Partial fulfilment of the

requirements for the Degree of

Dr. rer. nat.

Examiners:

1. Prof. Dr Manfred Radmacher

2. Prof. Dr Dorothea Brüggemann

Presented and sat by

Achu Yango

Submitted on 02.10.2020

Colloquium: Bremen, February 07, 2023

Abstract

In this work, the creep response of soft gel and cell samples after applying a step in loading force by means of magnetic fields has been directly measured by Atomic Force Microscope. By analysing the creep data with the standard linear solid model, we can quantify the viscous and elastic properties of soft samples independently. Cells, in comparison with similar soft gels, are much more viscous, as has been qualitatively observed in conventional AFM force curve data before. With the new method the spring constant and the viscous damping coefficient of friction from the creep response data have been quantified. Two different modes for applying a force step have been proposed: (1) by raising the sample height an indirect force step is being applied, or (2) by employing magnetic cantilevers a direct force step can be applied. Both lead to similar responses, whereas the latter seems to be better defined since it resembles closely a constant strain mode. The former is easier to implement in most instruments, thus may be preferable from a practical point of view.

Acknowledgement

Foremost, I would like to express my sincere and deepest gratitude to my advisor Prof. Dr Radmacher Manfred for the continuous support of my Ph.D work and the research work, for his patience, motivation, enthusiasm, and immense knowledge on the diverse exciting projects. My three years of research in the biophysics Institute in the university of Bremen contributed to my professional life and especially my personal growth. Your guidance helped me in all the time of the work. I could not have imagined having a better mentor for my Ph.D work.

Besides my advisor, I would like to thank Prof. Dr. Dorothea Brüggemann and the dissertation committee, Prof. Dr Stefan Bornholdt, and Prof. Dr Martin Eickhoff who generously took without hesitating the academic responsibility for this work

My sincere thanks also go to Prof. Dr. Monica Fritz, her working group for their continuous encouragement, inter-disciplinary collaborations, insightful comments, refreshment activities constructive feedback and many interesting questions.

I thank in general my fellow laboratory mates and my colleagues in Biophysics Group: Dr. Meike Gummich, Katherina Gärtner, Dr. Carmela Rianna, Dr Jens Schäpe, as well to Prem Kumar for the stimulating discussions, for the sleepless nights we were working together before deadlines, and for all the fun we have had in the time of my work. It was great sharing laboratory with all of you during last four years.

Also I thank my friends in the University and to Marie-Ann for enlightening me the first glance of the work and introducing me to the laboratory, most of all the insightful and friendly discussions. Last but not the least, I would like to thank my entire family, to my father, mother, to my sister Akere, my brothers, and finally to Cathy, Akere, Ngwe, and Fonkwa: for their support and encouragements throughout till date.

And finally, last but by no means least, also to everyone in the Biophysics Institute especially Janka Heitz who spent some difficult times while prove reading the initial version of the work.

Table of content

List of Figures

1.0 GENERAL INTRODUCTION AND STATE OF THE ART

The invention of the microscope and its improvement over a period of 400 years did not only extend or improve our sense of seeing but also revolutionized our perception of seeing the world as important advances in biology and medicine. Of the five senses humans perceive, sight is often argued as the most magnificent; the one we would last live without. Extending this perception further and further has been the driving force of major scientific development. Although it is a significant product of evolution, our eyes have significant limitations. Local probe technique extends our sense of touching in the micro and nanoworld in this way we probe locally, complimentary new reproducible information in this world with microscopic techniques. Numerous techniques and experimental approaches are now available for exploring the mechanical properties of soft samples. The sensitivity may be dependent on the characteristics of the sample as well as on the sample preparation. The ability to reliably measure the local mechanical properties of the soft samples like living cells, subjected to variety of contributions in medicine, however, to the best of my knowledge currently surpasses our ability to quantitatively interpret the data in many cases.

This dissertation is divided into 7 chapters. The **Chapter 1** and its sub chapters we will focus firstly, on a pertinent theoretical background, literature review and the current state of the art of measuring visco-elastic properties of soft samples by Atomic Force Microscopy is given and then followed by a subsection with a brief summary of the critical issues with the AFM and motivations. In this work, the magnetic AFM step response setup has been employed to measure reproducibly the creep response of the cell sample in an environment, which mimics its natural environment. Within each chapter are relevant cited literature and figures. However, an exhaustive coverage of these techniques and methods may not be given in my work but we will take a brief look at a few representative examples relevant to my work. Lastly, the research goals and objectives work will be elaborated. **Chapter 2** describes the materials and methods, which have been used in this work. The creep data in this work were collected with an AFM. The electronics has been upgraded for magnetic AFM and to allow careful signal control. The AFM measurements have been performed using V-shaped magnetic cantilevers on the adhering live cells in a stiff petri dish found in their aqueous environment respectively. The experiments performed in this work will be restricted to soft spring cantilevers with blunt having opening angles of about 35°. Two different setups for

measuring the creep response of live cells and gels to a small loading force and unloading force after the initial creep of the approach ramp of the force curves. In a similar fashion the soft samples have been loaded and unloaded by AFM z-step response and the magnetic step response experiments. Firstly, by changing the sample base height by a well defined step with an experimental situation that not identical with a relaxation at constant strain, nor at constant stress. A magnetic step response setup has been implemented in which magnetic cantilevers are employed to apply directly a force step at constant z height, which is closer to the constant strain situation **Chapter 3** is the analysis section. The section readdresses the objectives of this work in terms of analysing the deflection data by employing SLS model, the mechanical equivalent circuit presented in chapter 2. Analysing the portion of the creep data after the approach ramp of the force curve the spring constants of the soft samples were derived. **Chapter 4** is the results section. The spring constants and the friction coefficients due to the creep of the mechanical data on the soft sample can be derived using the proposed model. In order to get a better understanding two different setups for measuring the viscoelastic creep response of living cells by AFM have been evaluated. **Chapter 5** is the discussion chapter. In this work the step response data is presented in an array of force curves by z step and the magnetic step setups to prove that viscoelastic creep response can be measured reproducibly by magnetic step response AFM in its aqueous environment. **Chapter 6** concludes this work and states a brief outlook. **Chapter 7** is the appendix where we show the more results, which are related to this work. **Chapter 8** is the bibliography containing the list of publications in a numerical order.

1.1 What is an Atomic Force microscope?

The Atomic Force Microscope (AFM) developed by Binnig, Quate and Gerber [1], enabled investigation of biomaterial surfaces at very high resolution and measuring interaction forces with high sensitivity. As shown on the schematics in figure 1, the AFM is made of three major components: a force transducer (a cantilever beam), an optical detection system to sense the cantilever deflection and the piezo element to position the sample (or the tip). The force transducer is a cantilever, which acts as a soft spring.[2] The AFM is operated for example in aqueous buffer solutions in direct contact with a substrate (sample) surface and exerts a force on the surface which otherwise is impossible by electron microscopy methods. The atomic force AFM is operated under constant force mode, which incorporates optical beam deflection for sensing the cantilever motion.

1.2 Working principle of the AFM

During an AFM experiment, a probe attached to the soft spring cantilever is brought in contact with the soft sample. The soft spring cantilever at the very tip-end has to be positioned over the sample to invoke physical interaction that can be captured accurately for quantitative data analysis as the sample is scanned laterally. A laser beam is directed towards the back if the cantilever in the experimental environment and it is directed towards a photo detector.

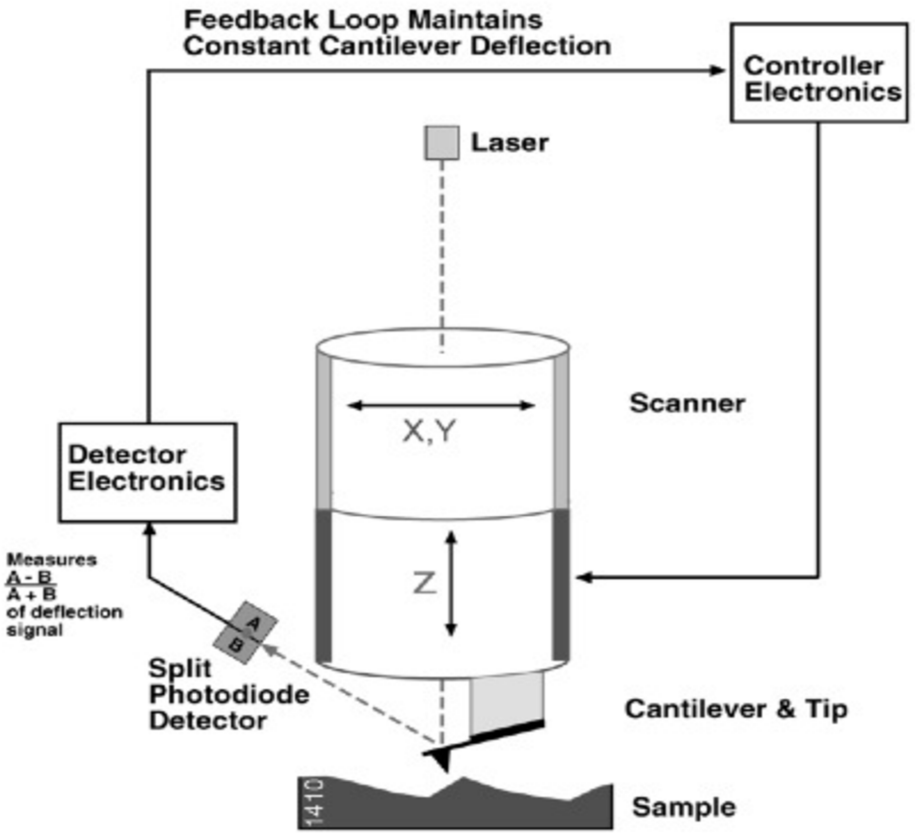

Figure 1: Schematic diagram illustrating the principle of the Atomic Force microscope. The motion of the cantilever is detected optically. The rest of the microscope (the inverted optical microscope typically beneath the sample) is not represented in the diagram. (Adapted from [2] and [3])

A feedback system for position control consisting of hardware and a software-based control unit is nowadays employed for the accurate control of the height (Δz) movements. Positional control was implemented in each of the three axes through an actuator and a sensor, both of which require specific data signals. This is important because the interaction between the tip and the substrate allows enables the AFM experimenters to acquire force curves (see force

curves section below).[2] The spring constant of the cantilever is required to be measured directly. The mechanical properties historically have been analysed from AFM force curves. This is because soft samples will deform in response to cantilever force. This provides a way to experimentally measure the mechanical properties. The quantity most characteristic for a cantilever is the spring constant k_c with units in [N·m^{-1}]. AFM applications extend into applications ranging from measuring colloidal forces to monitoring enzymatic activity in individual proteins to analysing DNA mechanics. The AFM indentation experiments on metastatic cancer cells discovered a significantly lower spring constant of the cancer cells compared to the healthy cells.[4] [5] Despite the morphological similarity of the cancer cells to the normal cells, it is suggested that the AFM might be more effective for cancer screening than visual examination of the cells. [6] [7]

The AFM cantilevers are usually made of several materials. Although a variety of methods have been proposed to calibrate the soft springs there are still some challenges, which may limit the sensitivity of the AFM output signals. Amongst these are (i) the AFM cantilever velocity in the aqueous medium (ii) the thermal noise (fluctuation) of the AFM cantilever. The thermal noise method has been based on the fact that the free end of the cantilever is continuously in motion. The random motion gives rise to thermal noise of the cantilever bending or a typical change in the orientation. Martin et al. in 1987 [8] performed the another practical demonstration of the cantilever setup in an AFM microscope with a vibrometer to measure the amplitude of the stiff spring cantilever vibration. [9] [8] At large penetration depths in the soft samples like live cells, the soft spring cantilevers can resolve better sensitivity measurements by applying smaller force steps of around 500 pN. This is a major step towards satisfying accurately the experimental conditions and the novel setups. To understand these challenges associated with these experiments using the AFM, it is important to review the AFM technique it self.

1.3 Implementation of the AFM technique

The AFM techniques are commonly employed in microbiology for their advantage over electron microscopy when measuring living cells. Although one of the most important applications of the AFM is the study of the mechanical properties of the soft samples like the cell sample [10], the extent to which the small loading force indents the sample will depend on the soft sample viscoelasticity. [11] Many applications now require that the spring constants be measured adequately. As we will see in this section we will give a brief background of the AFM technique. We will start with the description of the AFM cantilever.

1.3.1 Cantilevers

As shown on figure 2, the AFM cantilevers are typically supplied in wafers containing six ready to use probe chips for AFM experiments. The cantilever, the tip (the point where the force is applied on samples is usually a few microns away from the end of the cantilever, as the tip is not exactly at the end of the cantilever [12]) of the cantilever, and its carrier chip are typically fabricated from one piece of wafer. The AFM soft spring cantilever is important for the force and the mechanical property measurements of the soft sample like cells because it carries the load to the support where it is forced against by a moment or the shear stress. As previously stated the spring constants of the soft spring cantilever must be known in addition to the deflection in order to quantify the soft samples like the life cells and gels. To the best of my knowledge, until recently it has been considered the least frequently measured parameter in most AFM experiments. The Relevant to my work, an AFM cantilever may be a springboard-like or a triangular shaped beam that is fixed (clamped) at one end. It is typically positioned over a deposited sample like the cell, the petri dish or the gel. The most preferable amongst the researchers are the rectangular and the triangular cantilever. To localise and choose region of interest for the AFM measurements the cantilever may be supplied with varied shapes. The V-shaped cantilevers are typically employed in the contact mode of operation in which twisting of the cantilever is undesirable. To access different ranges of force on different samples, the experimenter is usually required to change the cantilever (as provided by the manufacturer and reviewed publications [13]). To the best of my knowledge, the range of geometries is wide and the rectangular cantilevers for the AFM applications are typically manufactured by the photolithography. The triangular (V-shaped) cantilevers are typically made by the wet etching techniques. These techniques offer the possibility to fabricate the AFM cantilevers with the desired force sensitivity. Until now it has been assumed by most researchers that the cantilever is massless and the whole mass is concentrated on the tip. Usually, as many experimenters have described it, the very tip end is the working end of the AFM. The AFM cantilevers tips shapes (i.e. the side not facing the tip of the cantilever) can further be modified, for soft sample measurements or by changing the geometry using modification techniques like the ion bombardment in order to improve the hydrodynamic drag imposed on the AFM cantilevers in aqueous environments. The AFM cantilevers are commonly coated with a thin metallic (e.g. gold) layer on the surface if

the reflectivity is of concern. Furthermore, it is of fundamental importance for the measurements performed in an aqueous environment because the reflectivity is greatly reduced by the aqueous medium.[14] In a special case as for the rectangular cantilever the spring constants k_c of the cantilever loaded at the very tip end will be a function of the geometric parameters (the length *l*, and the cross sectional width *w*, and the thickness *t*), and the Young's modulus is given by the analytical equation:

$$k_c = \frac{w * t^3}{4 * l^3} * E \tag{1.0}$$

Where *E* the elastic (Young's) modulus [Pa] of the cantilever tip geometry. One usually calculates the spring constant of the cantilever in the order of several N/m.. For example, a commercial AFM probe may consist of cantilevers of typical length 10-1000 microns and spring constant in the range of about 0.001N/m-1000 N/m. As such, due to the manufacturing processes, the dimensions of these cantilevers, especially in their thicknesses, are difficult to control along the length of the cantilever and may even vary for each individual cantilever on the same batch. The resonance frequency ω_0 is derived from the well-known expression for a harmonic oscillator, $((2\pi\omega_0)^2 = k_c/m^*)$, modified by an effective mass $m^* = 0{,}2427\rho Ltw$:

$$\omega_0 = 0{,}1615 \cdot \frac{t}{L^2} \cdot \sqrt{\frac{E}{\rho}} \tag{1.1}$$

With, $\rho = 2340\ kg/m^3$ being the density of silicon. The thickness of an AFM cantilever can be determined accurately by scanning electron microscopy and has not been done in this work. In some special cases, magnetic or spherical particles are attached to the cantilever to achieve specific surface properties and a controlled geometry. This also indicates the importance of calibrating the cantilever spring constants by a more appropriate method.[14] Although this calibration step is very time consuming, technically the calibration step is very relevant because the AFM may be tuned not only to provide a superior performance in terms of its resolution [11] or its force sensitivity but also to provide adequate information about the live cell, the mechanical properties or viscoelastic properties. If we assume that the largest uncertainty arises from the thickness of the cantilever beam, one can try to estimate

the spring constant of the AFM cantilever by eliminating the thickness and measuring the resonance frequency. Eliminating the thickness from the above equation leads to:

$$k_c = 59{,}31 \cdot w \cdot l^3 \cdot \omega_0^3 \cdot \sqrt{\frac{\rho^3}{E}} \tag{1.2}$$

Thus by comparing the nominal resonance frequencies and the measured resonance frequencies, one can estimate actual spring constants of the cantilever.

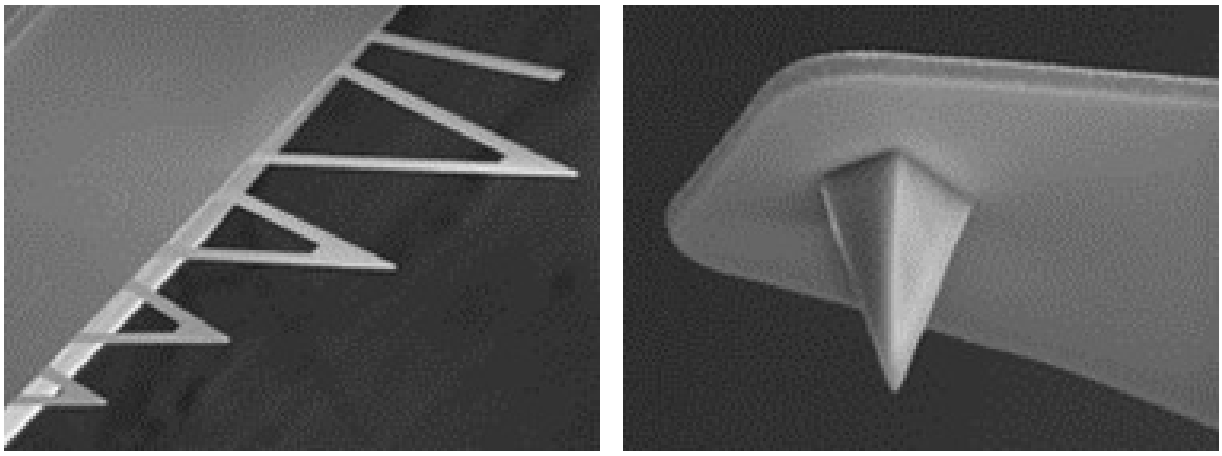

a) b)

Figure 2: Figure shows a diagram of four triangular and a rectangular shaped cantilever with the sharp tip. The example cantilever shown employs a pyramidal tip with asymmetrical tip geometry[13].

Transmission electron microscopy (TEM) have also been used to image uncoated tips by some researchers to determine the tip radius. [15] For example the cantilevers may be equipped with a bulk shaped pyramidal indenters, which may generally be blunted. They may have three or four sidewalls with a tip opening angle of ca. 35° and protruding length about 3-17 μm. The manufacturers typically adjust the production parameters to provide a range of commercially available dimensions on cantilevers with varying spring constants and cantilever properties.

The Coulomb force and the double layer force measurements have also been used to determine the tip size and shape. [16]. The small size and the structure of the cantilever together with the ability to operate in conditions such as in aqueous environment and in air makes cantilevers interesting as a force transducer. Many researchers have employed the colloidal probe technique in obtaining the force curves in order to overcome lack of information about the tip shape [17].

However, these techniques compromises the high temporal resolution offered by AFM and it hinders the mapping of physical properties using force curves due to the large tip radius. However the shape of the cantilever tip may be directly determined by the application and specific needs of the experiment. In this work the AFM cantilever geometry and shape has not been measured, rather it has been determined by the plan and its indentation compared to theory such that manufacturer specifications matches my data. When using 50 μm AFM cantilevers the assumption that the force acting is an end loading force is no longer valid.[16] In order to obtain the force curves and the mechanical property of soft samples like cells requires the individual calibration of the spring constants of the cantilever.

1.3.2 Contact mode AFM

Figure 3 shows a typical sequence of an AFM probe movement during the acquisition of a force curve. The contact mode is a mode of operating the AFM in which the feedback loop is used to monitor the cantilever response and then adjust the height accordingly to account for the changes in sample height. In this case the base of the cantilever is moved up and down over higher and lower parts of the sample in question. The sample is approached towards the tip end of the cantilever until it hits or indents the sample surface and the cantilever is deflected. In this mode the tip typically adheres to the sample surface and the deflection can be measured with a high spatial resolution. The finite adhesion forces deform the sample so that the contact covers over the finite area, which is increased by an additional spring force. The change in orientation causes a deflection of the very tip end of the cantilever and thus the angle between the sample surface and cantilever tip end. The change in orientation of the cantilever is measured optically. A larger deflection of the cantilever means a larger load force of the cantilever $F_c = k_c \cdot \Delta d$ with respect to the z-height of the piezo element. However, the z height information is not available for the user. In this work, in setting the deflection of the cantilever for measurements, we selected a preloading force controlled by the AFM trigger algorithm, provided the spring constant of the cantilever k_c is known. This is because we intend to avoid excessive cell indentation into the soft samples like cells. It was required the user performs the z-step response experiments at the dwell time. Two relevant feedbacks are employed. Typically the opened loop performed to the control the deflection during the approach ramp and the second closed loop feedback performed to

control the z-piezo height (for the LVDT) at the dwell time. However, the friction and properties of the soft spring cantilever and the sample may limit the reasonable precision.

a) *Force curve on stiff sample*

The mechanical properties of the sample can be extracted based on the cantilever response to a given indentation. All measurements in this work were performed with the commercial MFP-3D microscope. The AFM records the cantilever deflection (d) as a function of the distance Z between the sample and the cantilever rest position. Many conversions of the raw data have to be performed in order to obtain the real force curves. Igor Pro (Wavemetrics) software routines were used for conversion of the raw data, i.e. photodiode sensor output [V] vs. linear variable differential transformer (LVDT) output [nm] into deflection d [nm] vs. z-height [nm] in real time. A typical sequence of obtaining a force curve by AFM is shown on the figure 3

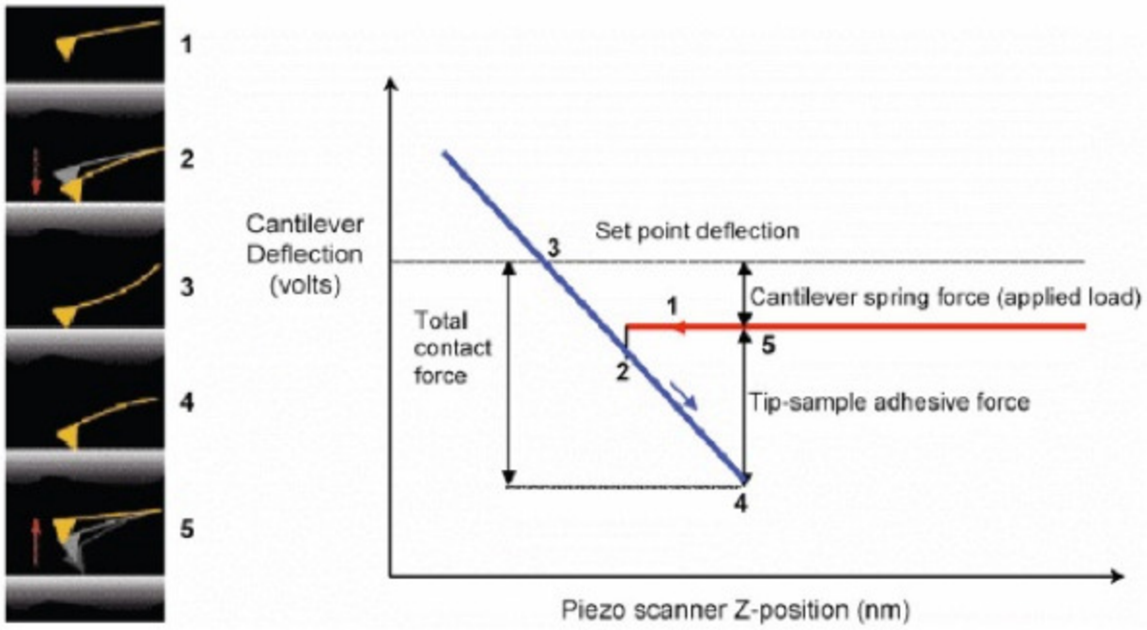

Figure 3: The typical sequences (1-5) of an AFM probe movement during the force curve data acquisition. The deflection (volts) is measured as a function of z-height (z-position) in (nm). The z piezo extends (1) and the tip descends (red). No contact with the sample yet. The cantilever is pulled down (2) by attraction to the surface. As the tip is pressed into the surface the cantilever bends upwards (3). The z piezo retracts (blue) and the cantilever ascends until the upward force cancels the surface attraction (4). The cantilever is momentarily returns to the original position (5). Right panel shows corresponding output: force curve plot.(adapted from [18])

The force curve (see figure 4) typically exhibits two linear regions: (1) the deflection is constant as long the tip does not touch the sample and (2) the deflection is proportional to the

sample height while the tip is in contact. The z height (z) in our AFM with a typical extension range of 5 - 10 µm has positioned the cantilever with a high resolution. The feedback controls the measurable force range $F = k_c * z$. The indentation is acquired by subtracting the cantilever deflection signal from the z height.

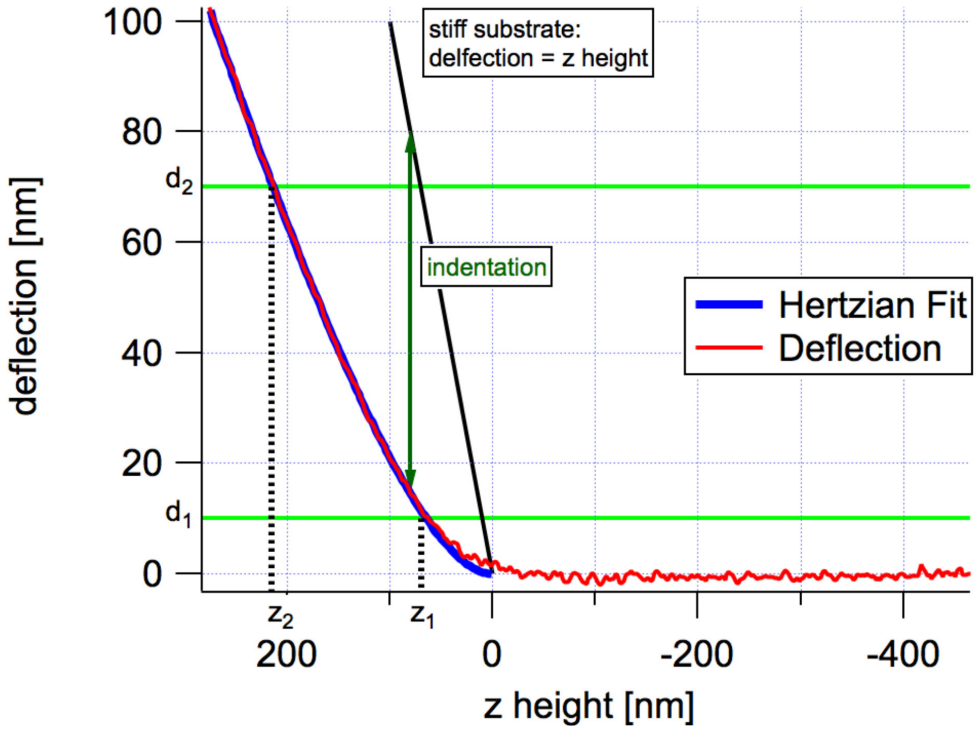

Figure 4: An illustration of the AFM indentation mode. In a force curve we will ramp the force to a certain value by ramping the z-position z_1. This corresponds to a deflection d_1 and an indentation δ_1, which has been calculated, from the measured cantilevers deflection and the sample height. The elastic modulus requires an appropriate model like the Hertz model. On stiff samples the force curve exhibits a sharp transition at the contact point, where the slope jumps from 0 (free cantilever) to 1 (in contact) with the sample (black line on force curve) after which the cantilever is retracted (not shown).

b) *Force curve on a soft sample*

In contrast to force curve on a stiff sample, the deflection is smaller than the movement in the sample height, due to indentation of the sample. For typical indenter shapes used in the AFM, this results in a non-linear force curve in the contact part. When this technique is applied over a grid of sample positions we call it the force volume technique.

1.2.3 Dynamic mode in AFM

In the dynamic mode thee AFM cantilever spring is excited to an oscillation at or near its resonant frequency. Experimentally, this is typically performed by the piezo electric element mounted on the AFM cantilever. Typical amplitudes of about tens of nanometres are

achieved. The excitation is kept constant during the whole the acquisition of the force curve. The observed quantities are the amplitude and the phase of the cantilever with respect to the excitation signal

1.2.4 Force volume

Many scientists have used the AFM to acquire data or map of interactions from various samples. In order to study the spatial variation of the soft sample interactions, force curves are acquired on several points over the scanned area. This therefore enables the experimenters to compare the cantilever-sample interactions or the derived quantities at different regions of the sample in study. While the cantilever is raster scanned over the sample from pixel to pixel, a force curve is recorded at each point. To compensate different sample heights, the range of force curve is moved up and down accordingly (trigger mode). The force curves are taken on definite intervals on the sample forming a grid of equally spaced force curves across the sample surface. This type of force plot acquisition is used to obtain a map of interaction forces for heterogeneous sample. The MFP 3D microscope has a built in force volume acquiring technique. The user can put in the number of points in both the x and y directions of the sample surface, where the force curves will be acquired in the force volume mode. In the force volume mode, all the force curves start at a fixed height. An approach (load the cantilever in a forward direction towards the sample) and the retract ramp (unload the cantilever from the sample surface in the reversed direction) are performed, then a lateral displacement away from the surface, again an approach withdrawal cycle and so forth till the end of the experiment. Usually in an AFM experiment, the first force curve will always be obtained from the left bottom of the force volume. An interesting observation on the force volume technique is that the sample is not damaged during the lateral displacements. The acquisition of force curves at every point on the scanned surface may be very time (several minutes) consuming. From the force curves the force versus indentation relation is calculated and a theoretical curve (Hertz model) fitted into the data. The Young's modulus of the sample is typically calculated from the fit procedure. A method of modifying the commercially available AFM is in principle to employ the magnetic cantilevers. The AFM can be modified with a fluid cell, which allows experimenters to measure under almost any kind of aqueous environment. For example, during experiments, a drop of fluid on top of a laboratory glass slide such that the sample is covered is by experience enough volume for the AFM experiments to be performed. The laser beam path can be focused to pass through the glass slide and the fluid in order to operate under fluids.

1.2.5 Vibration response

The Figure 5 shows the thermally driven motion of the triangular shaped AFM magnetic cantilever in an aqueous environment. The spring constants of the soft spring cantilever can typically be measured by inferring the results of the integral of the thermal noise and the temperature of the aqueous solution. The first step is typically to obtain the power spectrum of the freely vibrating cantilever with no excitation acting on it. In this method the cantilever is treated as a simple harmonic oscillator. Although the Sader method, which has been employed by many scientist can also be performed for a driven cantilever, the thermal tune methods relies only on the thermal excitation. The measurement for the thermal spectrum can be performed with the AFM itself. In many cases it is useful to employing an oscilloscope with higher sampling rate. The captured signal is Fourier transformed to the detector voltage power spectral density (PSD). The required natural frequency and the quality factor can be obtained from this voltage PSD by fitting a SHO model with the added background term the signal. The thermal noise calibration method, [19] has been preferred because it was quick and can be readily performed in the aqueous environment immediately after calibrating the deflection sensitivity.[20]

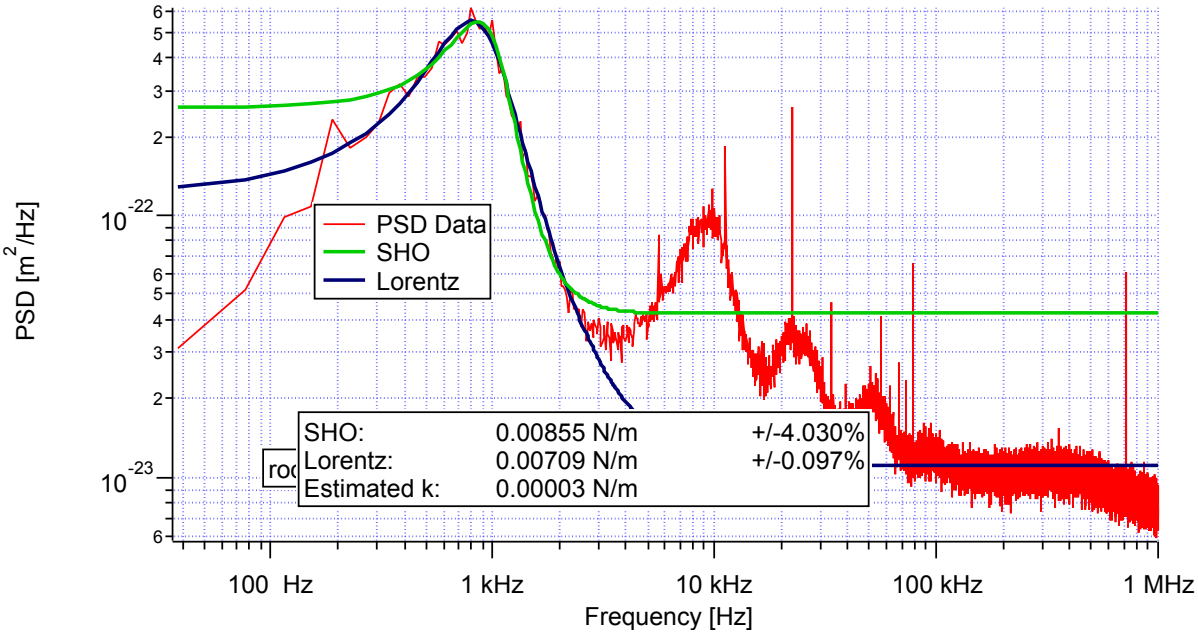

Figure 5: Thermally driven motion of a magnetic cantilever in an aqueous environment. The figure shows several higher modes due to thermal noise of the AFM cantilever. The spring constant of the cantilever obtained from the SHO and Lorentz fits to the first bending mode to the thermal noise data in the frequency domain. The AFM measures tilt and the sensitivity decreases for higher modes. The figure shows x-axis with the first and the second spectral peaks of the deflection data, which are obtained at approximately 850 Hz and 10 kHz for a wide range of frequencies respectively. The amplitudes (intensity in the thermal noise) of the deflection data on the y-axis span a wider range of $10^{21} \dots 10^{24}\ m^2 \cdot Hz^{-1}$ with the first frequency fit width smaller size than for the second bending modes.

The equipartition theorem, which says that if a system is in equilibrium, each mode of the cantilever on average contains an amount of energy $1/2\,(k_BT)$, is used to find the spring constant of the cantilever k_c by relating the thermal motion of the cantilever's fundamental mode to its thermal energy. Where k_B is the Boltzmann constant ($1.38\,10^{-23}J/K$, T is the temperature (K). The (time averaged) thermal noise in the deflection signal is given by:

$$\frac{1}{2}k_c\langle d^2\rangle = \frac{1}{2}k_BT \tag{1.3}$$

Where $\langle d^2\rangle$ in the left hand side is the mean square deflection caused by thermal vibrations. The force resolution (force fluctuations), if only thermal noise is considered, is be given by: [21]

$$\langle \mathrm{F}^2\rangle = k_B * \mathrm{T} * \mathrm{k_c} \tag{1.4}$$

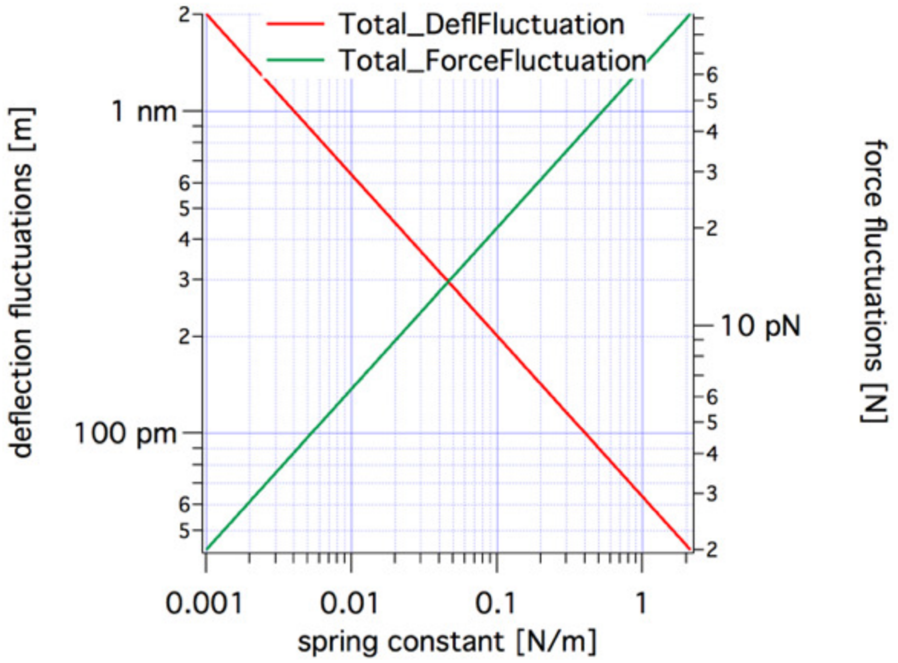

Figure 6: Thermal force and deflection fluctuations as a function of AFM cantilever spring constants. These numbers will give a lower limit for noise in the quantities force and deflection.

1.2.6 Sensitivity of the AFM technique

The cantilever deflection signal has been the output in volts of the PSD. The optical lever sensitivity of the soft spring cantilevers (as used in this work), enables the height quantification, is a required parameter in many AFM measurements especially in the contact mode of operation. The figure 7 shows the schematics of the AFM probe with integrated

cantilever tip and the beam bounce technique as may be employed by the AFM to obtain quantitative information about the local forces. As illustrated in the figure 7, the small portion closest to the sample dominates the sample interaction. The signals are generated by the segmented photosensitive diode (photodiode). As shown on figure 8, the AFM probes the surface of a soft sample typically by moving the sample beneath a tip attached into a weak cantilever spring while the tip is in contact with the soft sample, or near contact to the soft sample with the surface

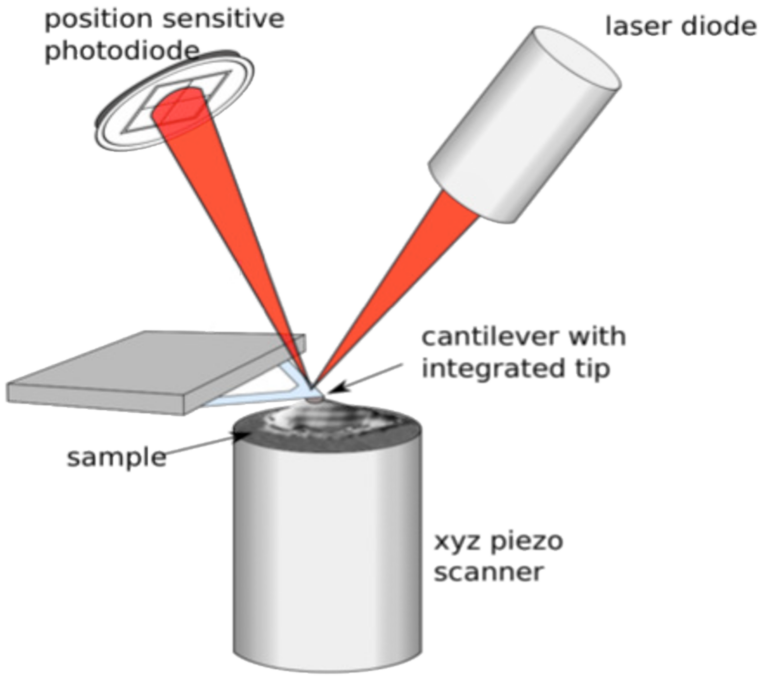

Figure 7: Illustration of the AFM optical lever beam bounce technique. The deflection of the cantilever is sensed with the optical detection. The very end of the soft spring cantilever bends upon contact with the surface, which is considered as the deflection. The reflected laser light from the very tip end of the AFM triangular cantilever creates a push pull error signal when the spot moves on the PSD.

As the AFM cantilever is moved closer to the sample, the cantilever will deflect because of long-range cantilever sample interactions. In the case where the AFM is operated in air or in vacuum with an electrically neutral sample, the only long ranged force will be the van der Waals (vdW) attraction. The mechanism leads to an attractive interaction potential. When the distance is reduced further, repulsion of the atoms sets in due to Pauli exclusion principle which can be tentatively described by a distance dependent $U_{vdW} = -C/R^6$. If the tip is far from the surface, its motion is only due to the thermal noise. With C being the interaction

parameter describing the molecular diameter. The sum of these contributions is named Lennard-Jones potential and describes the interaction between two atoms separated by the distance R.

$$U_{LJ} = -\frac{C}{R^6} + \frac{B}{R^{12}} = 4\varepsilon\left(\left(\frac{\sigma}{R}\right)^{12} - \left(\frac{\sigma}{R}\right)^{6}\right) \tag{1.5}$$

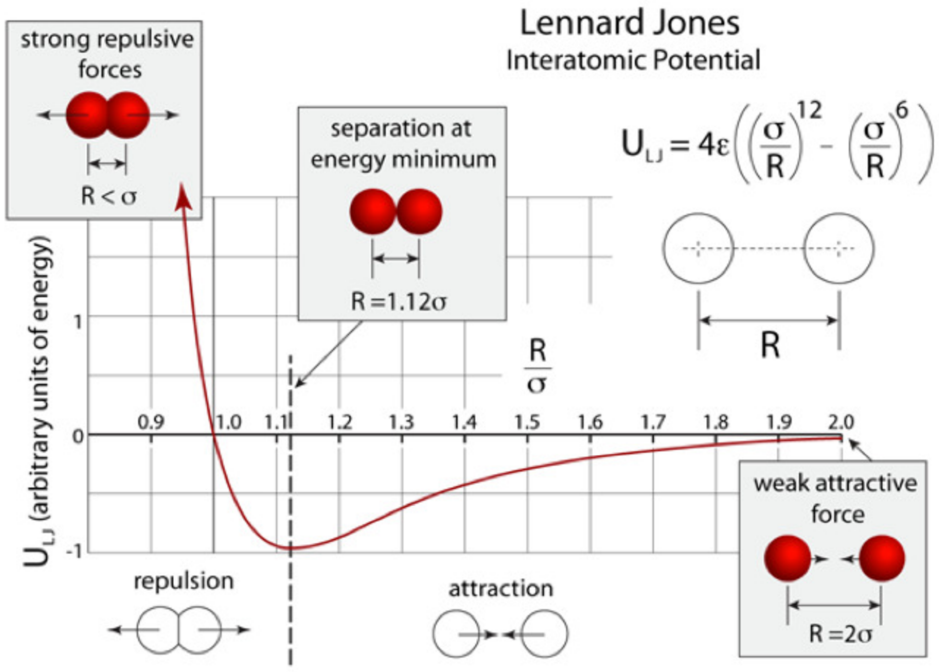

Figure 8: The graph plots the Lennard-Jones potential function, and indicates the region of attraction and repulsion. The AFM probes the surface of a soft sample typically by moving the sample beneath a tip attached into a weak cantilever spring while the tip is in contact with the soft sample, or near contact to the soft sample with the surface. The atoms try to minimize their potential energy and at the lowest temperatures are sitting at the bottom of the potential curve. When the separations are to the left of the minimum the atoms repel, otherwise they attract each other. [22]

Where ε and σ defines the depth in which the potential and the distance between the interatomic particles respectively. R is the distance at which the potential will reach its minimum. In addition to repulsive van der Waals force described in the figure, two other forces are generally present during contact-AFM operation. As shown on the figure 8, then the cantilever comes close to the surface, corresponding to the interatomic distances, it may happen that the chemical bonds are formed. Under ambient conditions all surfaces are rather covered by thin films and therefore the actual cantilever sample interaction may differ significantly from this model depending on the shape of the tip or the absence of absorbed

molecules on the surface. Additionally, a capillary force exerted by a thin water layer often present in ambient environments, and the force exerted by the cantilever itself. The capillary force arises when water wicks its way around the tip, applying a strong attractive force (about $10^{-8}N$) that holds the tip in contact with the surface. The magnitude of the capillary force depends on the cantilever to sample forces. The magnitude and sign of the cantilever force depends on the spring constant and the deflection of the cantilever.

Furthermore, the contact force is measured by detecting the deflection of the AFM cantilever. As previously described we typically measure the AFM cantilever deflection when it scans the soft and stiff sample surface. How much signal that is generated in the photodiode for a given amount of the cantilever deflection is called the optical lever sensitivity. The inverse optical lever sensitivity (invOLS) for the tilted soft spring magnetic cantilevers is typically obtained from a portion of the height data after obtaining a force curve on a clean cantilever glass slide. The cantilever deflection [nm] in the repulsive regimes of the force curve equals the inverse slope of the voltage output of the position sensitive sensor, $[\frac{\mathrm{V}}{\mathrm{nm}}]$, vs. the linear variable displacement transformer curves acquired on the samples. The voltage change is due to the same amount of deflection of the cantilever as the movement of the piezoelectric element $\Delta \mathrm{z}$. The cantilever deflection in the retraction part force curve is given by: $\Delta \mathrm{z} = \mathrm{V} \cdot InvOLS^{-1}$. Where V is the potential difference from a position sensitive detector. Here $InvOLS$ $[\frac{\mathrm{nm}}{\mathrm{V}}]$ is the inverse optical sensitivity. The inverse optical lever sensitivity depends on the dimensions and the shape of the laser spot on the photodiode and hence depends on the refractive index of the medium in which the measurements are performed. The z-height of the feedback loop keeps the cantilever at a constant deflection, such that the calibrated motion of the z piezoelectric transducer scales the height data. In order to show the linear regions of the force curves, the deflection of the cantilever was approximately 2 micrometres. The proportionality factor is checked and recalibrated each time before acquiring force curves or when the experimental conditions like change in medium is changed. In a force curve the retract regime is considered for the values in the range of the measured voltage change. The sensitivity in the tilt is taken into account during calibration and is not a problem, especially as one operates the AFM in closed loop feedback. For the data collected in this work, the magnetic sensitivity of the cantilever was calibrated individually. Many researchers have used the optical interferometer setups (vibrometer) as detection method to supplement the optical lever setups by the manufacturers in order to determine the small displacements of the cantilever with a good resolution. [2]

1.2.7 Indenting force

It is possible to correlate a change in the mechanical properties with the structural changes on the soft samples by AFM because the indentation that is created due to a loading force can be quantitatively and qualitatively analysed. The AFM contact force or normal force is the most important attribute of the mechanical data obtained by AFM, which is directly related to contact reliability. Accurate determination the samples mechanical and the viscoelastic response requires a specific force measuring design be capable of sensitive detection of the initial point of contact between the indenter and the soft sample. The indentation experiments by AFM employs an indenter with geometry, which is typically unknown to push into the cell and the cantilever response is then monitored. This is an essential tool for the characterization of the lateral variation of the sample mechanical properties and hence for the study of the soft samples. The spring constant of the cell sample has been determined on the basis of the force versus the indentation curves. As a soft sample spring being in series with the cantilever spring, the indenting force and its resulting indentation in the cells often follow the prediction of the Hertz contact model, which is linear. As theory suggest [23], Hertz model relates and describes the indenting force as a function indenting contact cantilever tip area[24], which is increased by the spring force for different contact tip geometries. Till date, most of the spring constant data collected in literature has been currently collected using the pyramidal, the conical or the spherical tip geometry. Based on the tip geometry (pyramidal, spherical or a conical tip) for contact measurements, the soft samples spring constant and the elastic properties can be described. Understanding the effects on the indenter geometry on soft samples opens more possibilities to directly compare data obtained with different indenter geometries [11]. Assuming the live cell is a homogeneous and isotropic material (for at least relatively small indentation) the live cell can be characterized by its Young's modulus and an assigned Poisson ratio. [25] For example in the case for a pyramidal tip geometry with a tip opening angle α, the elastic modulus E and the Poisson ratio v, we find widely cited and relationship between indentation δ and indenting force $F_{pyramid}$:

$$F_{pyramid} = \frac{1}{\sqrt{2}} * \frac{E}{1 - v^2} * \tan\alpha * \delta^2 \qquad (1.6)$$

The contact angle α is always defined with respect to the advancing sample substrate. From an experimental point of view, the contact angle occurs only visually. Experimental evidence reveals that for perfectly elastic samples the sample spring constant increase with increasing

contact angles and was proven by a separate experiment. However, for the perfectly elastic sample like the gel a single Young's modulus value seems only to define the response of the sample to deformation. Other models have been developed and have been employed by authors in the literature [26] and thin samples [27] by employing sharp tips. Spherical tips have been used to measure the response of the whole live cell. The indentation δ and the loading force F_{cone} for a conical tip shape is given by:

$$F_{cone} = \frac{2}{\pi} * \frac{E}{1 - \nu^2} * \tan\alpha * \delta^2 \tag{1.7}$$

1.4 Mechanical properties and analysis techniques

Mechanical properties of live cells, have gained a large interest and have seen rapid development in the last decade for two reasons. Firstly, the availability of the technics to measure cell mechanics with high spatial resolution and high sensitivity by AFM. For animal cells the mechanical response is mainly caused by the actin cytoskeleton [28] and internal stresses in this network [29]. Secondly, the field is very interesting because it has been discovered that mechanical measurements have some biomedical applications like monitoring and diagnosis of diseased cells. [30] For instance changes in mechanical spring constant of a cell can indicate disease or injury. These advances stemmed from observations of the dynamics of cell properties of deformability. The first application of the AFM on cancer cells was performed by Lekka et al., in 1999 [7]. In their work they suggested that cancer cells are softer than normal cells in AFM measurements, and this change in cellular spring constant are attributed to the changes in the organization of the cytoskeleton [7]. The argument that cancer cells seem to be softer than normal cells in AFM measurements has also been validated in subsequent studies [31], [32]. This rational has been additionally applied to numerous studies in the investigations of rheological properties if tissues like the lung epithelial cells [33], heart cells [34], the lamina of cell nuclei [35] and vascular endothelium [36]. A recent study shows that the property of the extracellular matrix like the spring constant modulates the viscoelastic properties of the live and the diseased cells thus normal cells appear softer than cancer cells on soft substrates. [37]. Nevertheless, their mechanical fingerprint or phenotype [4] is very different and clearly distinguishable from normal cells. So, the general idea using cell mechanics as a tool to detect the state of a cell, including its pathological state, or in the case of cancer cells its malignancy still holds and has been understood, and will have potentially many applications in the biomedical

industries. The feedback of local matrix spring constant on the cell state likely has important implications for development, differentiation, disease and regeneration. [38]

The deformation of soft samples like live cells or the diseased cells is as a result of an applied stress or strain evolving over time. [39] How cells respond to deformation has been investigated with many techniques in the laboratory and to the best of my knowledge the first reports on single cell mechanics were using the micropipette aspiration technique [40, 41]. The micropipette aspiration technique offers the advantage that it may be performed using equipment available in the laboratory to study the viscosity of the entire live cell. In this technique the micromanipulator is used to bring a micropipette into contact with the cell surface. The suction pressure is applied in the micropipette to deform the soft sample like the live cell surface. The live cells are not adherent to the stiffer substrate when employing this setup. However, the resultant deformation of the cell by the micropipette setup is suggestive of the global cellular mechanical properties, like viscosity since the entire cell sample is deformed.[41] In 1950, Crick et al., [42], pioneered a novel magnetic force experiment in which they employed controlled movements of micro magnetic particles of arbitrary shapes to measure the viscoelastic response of live cell. However, due to technical challenges and the lack of magnetic beads quantitative measurements were challenging. Following the rational performed by Crick et al., [42], Valberg et al., in 1987 [43] have extracted the viscoelastic properties of cells by studying the relaxation of the remnant magnetization or by tracking the translational motion of single particles. [44] [43]. Many other methods have been used to study soft samples including Scanning Acoustic Microscopy [45], magnetic twisting cytometry (MTC) by the application of the torque and no force [46, 47], the application of force by magnetic tweezers [44, 48], AFM [49], optical tweezers [50] and hydrodynamic stretcher [51]. The MTC however typically applies a magnetic field to generate the torque on the magnetic materials attached to the live cell surface. It is challenging to control the force and characterize the twisting with high resolution. The cellular spring constants have been derived from the applied torque and the twisting deformation relationship. [46] As compared to the loading techniques like magnetic tweezers or magnetic bead cytometry experiments where contact is made with the live cell sample by employing a magnetic bead, the contact between the sharp tip of an AFM can be reasonably well defined when the cell is indented in an almost vertical direction, normal to the petri dish or the support on which the cells are cultured. The conventional AFM method strongly relies on the knowledge of the area function of the indenter as a function of the tip geometry, which is known to a few degrees when the experiments are being performed. For the optical

tweezers, the forces applied on the soft samples depend on the spring constants of the optical trap and range roughly 1-100 pN. In a typical optical tweezers experiment a soft sample is specifically brought close to a bead in contact with the cell and trapped bead is controlled externally at the focal point of the laser. The force exerted on the soft sample may be determined from the offset of the trapped bead from the centre of the trap. Both the AFM and the optical tweezers are capable of generating relatively high forces, but generally have lower sensitivity in the low force regime partly because of the inherent challenges in measuring the slopes due to the noise. The AFM combines the capabilities of high force sensitivity with a quantitative mechanical probing at larger indentation depths. However, depending on the experimental setup (creep or modulation type) the analysis and the models employed vary strongly, and need to be refined accordingly. For a comprehensive review and discussion the reader may be inferred for instance to this review: [52]. Most importantly the difference between active and passive microrheology has also been emphasized, which gives the basis for detecting active processes in cells [53]. In a modulating experiment the timescale of the response can be set by the experimental parameters, since the frequency is swept over a given range. This allows seeing multiple relaxation processes, which may then result in power law behaviour of the viscoelastic properties [54]. In creep experiments only the most prominent relaxation process will be visible. However, this may very well be the most relevant time scale or process with which cells interact with their environment. This confirms the practical need to use creep experiments to complement other possibly more sophisticated methods.

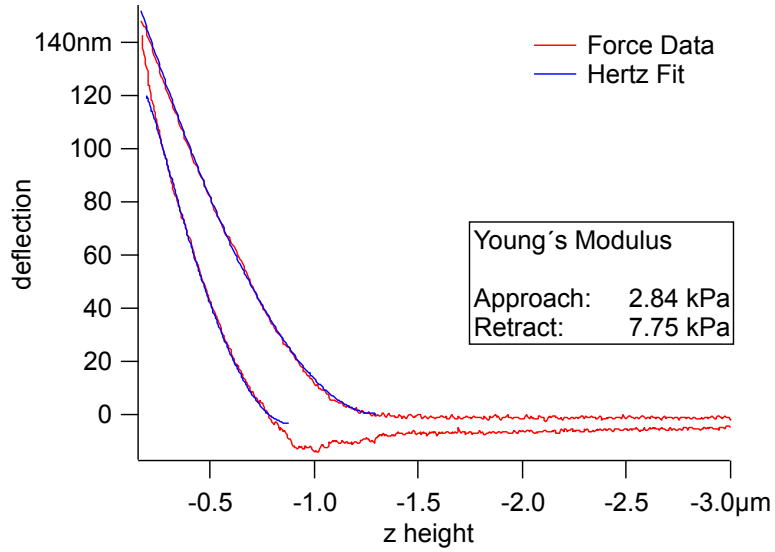

Figure 9: Hertz model fit on approach and retract deflection curves on a thyroidal S748 cell seeded on Petri dish. A large hysteresis between the two red curves can be seen; consequently, the Young´s moduli extracted from them are very different (E=2.84 kPa for approach and E=7.75 kPa for retract). [30]

In AFM, usually mechanical data, i.e. force curves, are analysed in terms of the Hertz model [55, 56], which only considers elastic properties of the sample as shown in figure 1. The use of the Hertz model is necessary, since due to the tip geometry (typically pyramidal or spherical tips are used), the contact area between the tip and the sample will increase while loading the cell, and hence the sample spring constant will be a function of loading force (and tip geometry and sample properties). The Hertz model is widely used when analysing mechanical data of cells by AFM [49]. However, analysing force - indentation data with the Hertz model neglects the contribution of viscous properties of soft samples, which is very important in the case of cells. In force curves, their contribution can be seen by a separation between the approach (loading) and retract (unloading) curve. The difference may also be due to plastic deformation, which does not seem to be an issue in cells, as can be seen by recording several force curves in the same area, which are identical to each other. Thus by applying the Hertz model, we will get different elastic moduli from the loading and unloading curve, which shall rather be called apparent moduli. Often only approach data are analysed to achieve comparable data between experiments and groups. In some reports - including one from our group [57] - it has been argued, without a strict and convincing derivation, that the average of the apparent moduli shall be close to the true elastic modulus, and their difference shall be a measure of the viscous properties. In some reports, the difference between approach and retract curves have been analysed to calculate viscoelastic properties [58] [57] [54]. However, during the approach ramp, the force and indentation are varying at a constantly changing rate, and the response of the cell is due to the retarded response during the entire approach or retract path, the analysis depends largely on the linearity and homogeneity of the sample. It is essential to compare these data with other data where the force or indentation are changed in a simpler way over a smaller range, where it can be expected that the sample reacts in an approximately linear fashion. An alternative (and scientifically more sound) approach is measuring the stress relaxation after the approach ramp in a force curve [59] or to apply an indirect or direct step in magnet or sample height after the initial creep of the ramp during a force curve has seized respectively.

Modulating the sample position sinusoidally has been used [33, 60] to measure viscoelastic properties of cells as a function of frequency as is done in polymer rheology. A modulating force can be applied by attaching a small magnetic particle to the very end of the cantilever. The force in magnet modulates the force on the tip end of the magnetic cantilever, which

will transmit a modulating indentation to live cells. [61, 62] [63]. In addition, the retract curves, adhesion may be present, which will make determination of the contact point difficult and may need to be considered as an offset of the acting curve. However the adhesion, which will be mediated by the extracellular molecules sticking to the tip, it is not clear at which point these molecular bonds are under tension and actually generate a force.

The viscosity of cells usually easily shows detectable relaxation phenomena following a perturbation. The viscosity mapping in biological systems is important for the understanding of the biophysical processes. In the past few years several scientific works have aimed to quantify this cell property by applying fluorescence imaging techniques, like the fluorescence recovery after photobleaching [64] [65], because by tuning the fluorescent properties of the employed probes, one achieves a high spatiotemporal resolution. However, the introduction of the fluorescent probes, in consequence, interferes with the intrinsic properties of proteins or the amino acids. On the contrary, there are very little direct experimental results on creep response. The magnetic force AFM is a powerful setup that can be used to measure the creep response of the soft samples like the cell. The AFM has the advantage in that the viscous response of the bulk sample can be quantified without the addition of fluorescent probes. Although the AFM which employs a sharp tip has very successfully been employed for qualitative analysis of cellular elasticity, the broad range of absolute elastic moduli reported for living cells under same conditions in the literature (100 Pa–100 kPa) is intriguing [66] [67]. The degree of quantitative information that can currently be extracted from the conventional force curve analysis of such ultra-soft samples like the cell is still limited and also very challenging. As shown in the recent work of Rianna et. al., in 2016 [37], the properties of the extracellular matrix like the stiffness modulates the viscoelastic properties of the live and the diseased cells. The AFM has been employed to obtain this type of information from ultra-soft samples as well as about the apparent elastic constants. However, it is interesting that the life and the diseased cells will exhibit a sharp change in the viscoelastic properties in response to the varying stiffness of the mechanical environment. Their rationale, which was based on applying an indirect force step by AFM on the diseased and the normal cell types and have reported a change in the storage modulus of the healthy cells from 1.2 to 2.7 kPa and the loss modulus of 300 to 735 Pa s while tuning the stiffness of the polymer gel substrate on which the cells are placed stiffness to higher values respectively. The diseased cells, on the other hand, showed a storage modulus of 1.4 kPa and a loss modulus of 400 Pas, which were virtually independent of the polymer gel

substrate stiffness. However, their findings showed the usefulness of the setup in measuring the viscoelastic properties of the normal and diseased cell samples. In contrast, intervening measurement methods such as the bead-tracking microrheology or the micropipette aspiration give values of 100–500 Pa for elasticity. [46] [44] The differences have been ascribed to cell substructure heterogeneity, the viscous properties and the far greater spatial accuracy of AFM measurements [66] [44]. On the other hand, adherent cells have been demonstrated to change their shape from round to fully spread without significantly altering their microfilament mass.

It is known that normal live cell types may tune their mechanical properties to the stiffness of the underlying substrates [68], however to my best knowledge similar works in which the creep responses are directly quantified by the magnetic step AFM have not been performed till date. It is important to carefully measure the viscous response and the elastic properties of live cells in response to the deformation achieved under different force steps and experimental conditions in order to compare the results. The main issue with such novel experimental setups, however, lies in the fact that it is challenging to directly measure the viscous contribution of the soft samples accurately on soft samples. The rheological properties are the key features of living cells [69] and have been also characterized in a few works by obtaining time-dependent measurements for small loading forces in their natural environment. [70] The relative contributions of the actin polymerisation-depolymerisation dynamics and tensile prestress to the live cells shape and stability are controversial. [70] It has been proven in several studies that cancer cells on such supports are at least one order of magnitude softer than normal cells, because of their different cytoskeleton structure and organization [71], however creep response measurements on the live cells response on the stiff Petri dishes with an alternative setup is still missing in literature. This indicates the practical relevance that viscoelastic properties of live cells and tissues need to be quantified directly by a more appropriate experimental setup even though in their natural environment the substrate stiffness may additionally tune the live cells samples mechanical properties. [70] Proper use of the AFM setup with novel methods allows mechanical probing of the soft samples without significant influence of the underlying substrate. There is the need for setups capable of addressing rheology of the living cells without disrupting the cytoskeletons underneath the cell. [72] [31] [73] [37]

In indirect loading setup such as the conventional AFM, the mechanical data are analysed in a quasi-static manner. The dynamic response from analysis of the force curves and contact mechanics is encircled with a number of challenges especially when characterizing the viscoelastic properties as has been discussed before. This is because a force balance in the conventional way of obtaining the mechanical data implies that a substantially slow measurement has to be performed. It thus seems to suffer from low-frequency noise, or the drift in the system, hence only one frequency can be employed at a time, and it is generally too slow to probe the cell mechanics. In this case of slow measurements, the viscous contributions of the live cell are typically minimized. If the measurement is performed too rapidly, the viscous contributions associated with the motion of the soft spring cantilever become significant. Viscoelasticity of the soft samples like the cell may also lead to the frequency-dependent response of the soft spring cantilever. This is because, besides their solid-like property, they show fluid-like properties and will have the ability to flow giving rise to entropic forces, capillary forces associated with the surface curvature, and the viscous forces that depend on the mechanical system.

1.5 Motivation and summary of critical issues

The AFM has been used for several years and it has been shown to be an accurate technique in accessing the mechanical properties especially on soft samples like life cells, even though the determination of spring constants has been a major challenge to nano- and biomechanics researchers. Prime examples of the successful application of the AFM cantilevers are present in many applications with the relevance to the high sensitivity, the quick response and the low power requirement applications range from the chemical to the biological sensors and the diagnosis of broad range of diseased cells [74] and even in glucose monitoring from unhealthy patients.[75] [76]

Thus, recently, much research has been carried out to calibrate the cantilever spring constant. To the best of my knowledge the calculation of the spring constant of cantilevers becomes very challenging when the cantilever thickness is less than $1\,\mu m$. Because of a large variability in the spring constants, the cantilevers will have to be calibrated on an individual basis. Contemporary research is urges users to study these key areas. To be practical, the best calibration methods must not damage the probe in the calibration process, and one must be able to perform them quickly and without the need for additional complex equipment if possible. In fact, because the deviations from the manufacturer's spring constants of the

cantilever from the nominal values often span over a factor of 3 in error in recent years, controversy has swirled around the need for independent, more precise and accurate methods for calibrating the spring constants of the cantilever. Example references and some fairly complete reviews can be read in the work of Burnham et al., [77].

A variety of these methods have been proposed on other works to calibrate the cantilever, with spring constants in the range 0.01 to 1 N/m and amongst them the thermal noise method is the most preferred by the researchers. More recently, researchers have been using the thermal calibration technique developed for laser Doppler vibrometry (LDV) to calibrate both the torsional and the flexural spring constants of the cantilever. By direct comparison of their obtained results with commercial referenced cantilevers using the LDV thermal and the electromagnetic force balance, an agreement of up to 2% or slightly better was demonstrated. [78] By using the reference cantilevers with spring constants determined from the instrumented and the calibrated nanoindenters Grutzik et al., [79] recently described a method to calibrate stiffer cantilevers (in the range 200 to 250 N/m), which has been based on International traceable chain, although the spring constants of the cantilevers are a lot stiffer than those used for the experiment in this work. Nevertheless, the majority of these methods to calibrate the spring constant of the cantilevers adapt the cantilever to a holder for force balance and the deflection due the cantilevers of a known spring constant by a technique originally proposed by Tortonese et. al., [80], or by the measurements of deflection due to the viscosity of the aqueous medium surrounding the cantilever. This results in a decrease in resonance frequency and to a widening of the resonance peak due to the viscosity of the medium that makes it harder to record good thermal spectra in water.[81, 82] In 1995, Sader et al., [20] introduced an alternative method to calculating the spring constants from an unloaded resonance frequency.[83] The mass of the cantilever was inferred from the geometrical dimensions. The thickness measurements requires typically the use of scanning electron microscopy (SEM) which is time consuming and cannot be routinely carried out for every AFM cantilever.[20] The method has additionally required the determination of the mass and the density, which could increase the amount of difficulty during the cantilever calibration process. This method is not used in this work because it requires the knowledge of geometrical parameters and may perform best for a cantilever that is very stiff. The same author has proposed a subsequent method whereby; the spring constants of the cantilever have been determined solely by its resonant frequency and the quality factor in air medium.[83]

The AFM force curves have been used for the studies of the material properties and for the characterization of material properties on the soft sample.[10] Therefore for different experimental purposes with different results, it might be useful to load and then to unload the cantilever directly or indirectly after an initial creep of the approach ramp on soft samples like cells by an external force in magnet or by employing the z-height by AFM.

When obtaining force curves in the contact mode, lateral forces seem to act on the cantilever due to the frictional forces in the system [84], although the lateral spring constants of the cantilever for triangular-shaped cantilevers has been questioned before.[85] Other recent works explore and measure synchronously in an SI traceable way the influence of AFM cantilevers undergoing torsional bending, which is associated to the torsional spring constants of the employed cantilever using the electromagnetic balance and the optical lever system.[84] This challenging scenario has led to efforts to standardize conditions and isolate critical variables or values with the hope that unambiguous results not only will demonstrate the existence of the minute changes in the spring constant of the sample but also will permit analysis of the underlying mechanisms in cell mechanics. However, the previous studies of the deflection sensitivity are mainly focused on measuring the vibrational or resonance characteristics and using these characteristics to determine the spring constants of the cantilever through mechanical or thermodynamic relations. [78] [14] In fact, the calibration uncertainties of currently used techniques are still relatively high, e.g., ranging from 10% to 30 % especially for cases where the spring constants of the reference cantilever employed are not guaranteed as compared to the manufacturers prescribed spring constant values [77] [86]. We expect that the magnetic force AFM based experiments –as described herein- to play an important role, like choosing favourable experimental conditions; with newer experimental setups to directly load and to unload after the approach ramp of a conventional force curve on the soft samples like the live cell.

In this work, the creep response of soft gel and cell samples after applying a step in loading force by means of magnetic fields has been directly measured by AFM. A second setup has been presented in which the loading force is applied indirectly after the approach ramp of the force curve by changing the z height of the AFM in a conventional fashion.

1.5.1 Theoretical fundamentals and an Experimental Approach

In order to access the effects, the environment will have on the motion of a cantilever, we have considered two general cases. When the cantilever is in (in contact) and not (off/no contact) in contact with the soft sample like the life cells and gels. The figure shows the cantilever oscillating off and in contact with the sample, with amplitudes of A_0 and A_1, respectively. It also shows a simplified spring dashpot model for the non-contact and contact measurement.

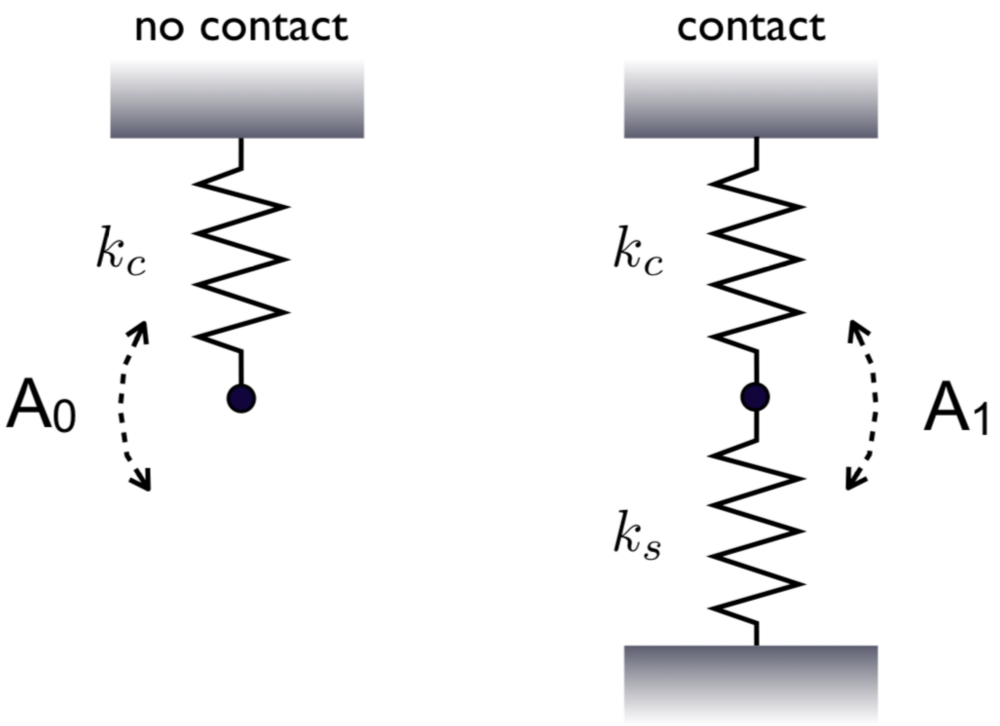

Figure 10 Association of the springs to determine the spring constants of the sample in terms of the spring constant of the cantilever and the oscillation amplitudes i) no contact A_0 and 2) in contact A_1

In the case where the vibrated cantilever is not in contact with the system has resonance frequency that is related to the spring constant cantilever as $m_0{\omega_0}^2 = k_c$. The AFM cantilever may be described as a damped harmonic oscillator with effective mass m_0. When in contact both the systems' effective mass and the resonant frequency changes, such that $m_1{\omega_1}^2 = k_c + k_s$. To be specific k_c is the spring constant of the cantilever while k_s is the spring constant of the soft sample. In both cases the motion of the cantilever and the reaction

of the cantilever to an external force field can be described within a good approximation by a damped and a driven harmonic oscillator. The equation of motion of the free cantilever is

$$F_{total}^{(free)} = F_{drive} + F_k + F_{viscous} \tag{1.9}$$

Is the oscillating magnetic force, F_k is the restoration force due to the deflected cantilever, which can be described by Hooke's law $F_k = k_c(z - \bar{z})$, (where z is the cantilever deflection and $\bar{z}$ is the equilibrium cantilever deflection), and $F_{viscous}$ represents the viscous force due the hydrodynamic interaction of the cantilever in liquid. The equation for the free cantilever is (assuming, $\bar{z} = 0$):

$$m_0 \frac{d^2 z(t)}{dt^2} = F_{drive} - k_c z_0(t) - \eta_0 \frac{dz_0(t)}{dt} \tag{1.10}$$

Where m_0 is the effective mass of the cantilever, k_c is the spring constant of the cantilever, $z_0(t)$ is the free cantilever deflection, z_0 is the free equilibrium deflection. The viscous force was written in the form:

$$F_{viscous} = \eta_0 \frac{dy_0(t)}{dt} \tag{1.11}$$

The resultant force on the magnetic cantilever magnetic cantilever in contact with a viscoelastic sample and exposed to an oscillating magnetic field will be given by:

$$F_{total}^{(contact)} = F_{drive} + F_{contact} + F_k + F_{viscous}^{\dagger} \tag{1.12}$$

Therefore, the effective equation of motion of the cantilever in contact $z_1(t)$ is given by:

$$m_1 \frac{d^2 z_1(t)}{dt^2} + \eta_1 \frac{dz_1(t)}{dt} + k_c z_1(t) = F_{drive} + F_{contact} \tag{1.13}$$

The surrounding medium and the sample typically exerts a force $F_{viscous}^{\dagger}$ when the cantilever is contact with the soft sample, which is proportional to the velocity.

$$\frac{dz_1(t)}{dt} \tag{1.14}$$

The differential equation to be solved for the non-contact scenario will be described by:

$$\frac{d^2z(t)}{dt^2} + b_0 m_0 \frac{dz_0(t)}{dt} + {\omega_0}^2 m\, z_0(t) = F_{drive} \tag{1.15}$$

While the cantilever is in contact, the scenario can be described in two ways: 1) In the first case we explicitly add the contact force to the resultant force acting in the cantilever, which be subsequently be labelled CM1.

$$m_0 \frac{d^2z_0(t)}{dt^2} + b_1 m_0 \frac{dz_0(t)}{dt} + {\omega_0}^2 m_0 z_0(t) = F_{drive} + F_{contact} \tag{1.16}$$

Where the proportionality coefficient typically written in the non-contact case as b_0 and b_1 for the contact case is the damping coefficient. Again, the viscous force of the contact case is written as:

$$F^{\dagger}_{viscous} = \eta_1 \frac{dz_1(t)}{dt} \tag{1.18}$$

Here η_1 is the effective hydrodynamic viscous coefficient of the liquid + viscoelastic sample when in contact with the soft sample.

2) Alternatively, we can write the effective model equation such that contact is described by a change in the effective cantilever mass m_1 or resonant frequency $\omega_1$of the system. This will be subsequently labelled as CM2.

$$m_1 \frac{d^2z_1(t)}{dt^2} + b_1 m_1 \frac{dz_1(t)}{dt} + {\omega_1}^2 m_1 z_1(t) = F_{drive} \tag{1.19}$$

In this equation $z_0(t)$ denotes the cantilever motion being off or $z_1(t)$ in contact with the sample. $F_{drive} = F_B e^{-i\omega t}$ is the driving magnetic force acting on the cantilever (magnetic) and $F_{contact}$ represents the force between the cantilever and the sample (CM1). F_B is a parameter that depends on the magnetic dipole moment of the coil and the magnetic cantilever, and the distance between the magnetic cantilever and the coil. As it has been

previously described, $b = \eta/m$ or better-written $b_n = \eta_n/m_n$ is the damping coefficients of the viscous force due to either liquid (off contact regime) or the liquid + sample (in contact regime). In steady state, these equations have solution of the type

$$z_n(t) = A_n \exp i(\omega t + \phi_n) + \tilde{z}_n \tag{1.20}$$

where ω is the angular frequency of the AC (alternating current). ϕ_n is the phase shift due to the viscous forces. $\tilde{z}_n$ is the equilibrium cantilever deflection. The phase shift $\phi = \phi - \phi_0$ is due to the sample viscoelasticity. By solving the solution $z_0(t)$ we obtain the following expression for the amplitude of vibration A_0 as function of frequency. The evolution is characterized by a resonance curve of the form

$$A_0 = \frac{F_B}{k_c} \frac{1}{(1 - (\omega/\omega_0)^2) + i(b_0\omega/{\omega_0}^2)} \tag{1.21}$$

When the tip approaches the surface, the sample forces may modify the vibration. The contact (surface) forces (F[Z+z(t)]) has to be added where, Z is the distance between the surface and the mean position of the cantilever tip and z(t) is vibration around this mean position. $F'_{Contact}$ is the derivative of the contact force between the cantilever and the sample. $F_{contact}$ has two components: 1) the contribution due to z-step displacement that brings the cantilever into contact $F_{contact}\,(\delta_0)$ and causes an indentation δ_0. This quantity is typically estimated as $F_{contact}\,(\delta_0) = k_c\, d_{trigger}/2$, where $d_{trigger}$ is the maximum cantilever deflection of the force curve taken before a dynamic measurement. 2) The other force component is due to the oscillation contribution due to the magnetic field F_{drive}. For the typical modulation experiments the contact force will oscillate around $F_{contact}\,(\delta_0)$. We can expand in a Taylor series to determine the effective modulation of the contact force due to the magnetic field. The solution for the contact and the non-contact cases in the contact mechanics 1 (CM1) and the contact mechanics 2 (CM2) approaches are, respectively

$$A_1^{(CM1)} = \frac{F_B}{k_c} \frac{1}{[1 + (F'_{contact}\,\delta_0/k_c) - (\omega/\omega_1)^2] + i(b_1\omega/{\omega_0}^2)} \tag{1.22}$$

$$A_1^{(CM2)} = \frac{F_B}{k_c + k_s} \frac{1}{[1 - (\omega/\omega_1)^2] + i(b_1\omega/\omega_1^2)} \tag{1.23}$$

Where $b_1 = \eta_1/m$ and $\omega_1^2 = [\omega_0^2 + F'_{contact}(\delta)/m_0] = \omega_0^2[1 + F'_{contact}(\delta)/k_c]$. This equation states the contact of the cantilever with the viscoelastic surface induces a small change of resonance frequency. At a given distance from the surface, there is a resonance at a frequency lower than far away from the surface. The shift of the resonance frequency is directly related to the force gradient. At constant applied frequency, the shift of the resonance curve results in a decrease of the amplitude of the vibration whose measurement of the spring constants of the sample it self directly.

1.5.2 Magnetic properties, force and the choice of magnetic particles

It is known that magnetic particles when placed in medium and exposed to large enough external magnetic fields are subjected to the induced forces in magnet exerted on them by the magnetic field [87]. The ability to concentrate the magnetic field on the magnetic cantilevers of interest with high sensitivity has been particularly crucial for the success of the novel AFM magnetic step response applications in the laboratory and for the subsequent measurements. The sensitivity of the magnetic cantilever should be large to create a measurable cantilever displacement. In 2016, Tasci et. al. [87] showed that the behaviour of the movement and aggregation of magnetic particles in the magnetic fields could both appear as if they are in the inhomogeneous or in the uniform magnetic fields. Majority of the magnetic particles available for non-invasive work are the weakly ferromagnetic (composite of 20-90% by weight of Fe_2O_4 % or Fe_2O_3 nanoparticles embedded in polymer matrix) and this includes the available paramagnetic beads. The paramagnetic particles are defined by the size of the nanoparticles they contain. Even though it holds for all materials including ferromagnets, the relationship between the magnetic field (B) and magnetic field strength (H), may depend on the previous magnetisation of the ferromagnetic material or its magnetic history. The magnetic field is no longer linear with the induced field H. On the other hand, if the magnetic content is known, and the smaller magnetic particle is known, the magnetic susceptibility could be read directly from relationship of magnetisation curves provided to experimenters by the vendors (in the so called B–H curves). [88] The magnetic response to a magnetizing field may differ greatly in the strength and the mass. The magnetic materials employed on the magnetic cantilevers during this work were interesting for us to employ because they were readily available and could be routinely prepared.

Nevertheless, the magnetic particle selection requires not only a good understanding of the desired performance in an applied field, but also the data sheet information available on the magnetic particle provided by the vendors. The bacterial organelles called magnetosomes are promising in enhancing the sensitivity of the force transducers. This is because they are ferromagnetic and possess (fixed magnets) magnetic crystals of sizes between 35 and 120 nm. This is interesting because the ferromagnetic particles are preferred in applications where the external field is weak and the particle size is limited, due to their high saturation magnetisation. The force in magnet induced on the magnetotactic bacteria causes them to align in the presence of an external magnetising field. A vast number of reviews and books have been published on application of magnetic particles. [89] [90] [88].

1.6 Research goals and the objectives

In this work we employ the standard linear solid model, a mechanical equivalent circuit, to analyse our data, which is the simplest combination of spring and dashpots, which reproduces the experimental results obtained on cells. When changing the sample base height by a step, this position change will be transmitted through the cell and deflect the cantilever, which will creep to a new equilibrium position. During creep the loading force (which is proportional to the deflection) and the indentation (which is z sample height minus deflection) will both change. Thus the experimental situation is not identical with a relaxation at constant strain, nor at constant stress, which is preferred to use in polymer rheology. Thus, in addition to this conventional z step scenario, we also implemented here a method to apply directly a magnetic force step at constant z height, which is closer to a constant strain situation.

Our objectives are (i) to induce steps in forces either by changing the sample height or applying a magnetic force to the very end of the cantilever in physiological conditions and (ii) to adequately analyse the creep response data of soft samples like the live cell samples by after the magnetic step in force and the z step after the approach ramp of the conventional force curve respectively. The novel magnetic step response setup has enabled the slow time dependent monitoring of the creep response after the approach ramp of the force curve as well data for comparison. The localized, concentrated and spatially reconfigurable magnetic field has been necessary in order to achieve a precise, biocompatible and the well-defined loading and unloading force steps in magnet during the dwell time. To my knowledge no similar commercial setup was available commercially to perform the experiments.

Experimentally, the local response to the deformation on soft samples will be performed firstly indirectly and then directly to load and then to unload the live cell sample and the gel sample after the creep due to the visco-elastic of the sample in question has relaxed considerably respectively. A descriptive statistics of the experimental results, which represent the median values of the interquartile range of the measured force curves by AFM have been presented. The spring constants values of the live cell and the gel sample have been quantified from the creep response experiments by the magnetic step response AFM. The spring constant values have been compared to prove the reliability and reproducibility of the results derived by both setups respectively. The key advantage of this magnetic step AFM response setup lies in its capability to perform slow local measurements directly after the approach ramp of the force curve in the aqueous buffer solution. We will demonstrate that the design of this experiment and the data analysis does handle viscous properties sufficiently.

2.0 MATERIALS AND METHODS

The chapter is the material and method section. It entails firstly the description of the cell sample, then the polymer gel sample and lastly the magnetic cantilever preparation as employed in the course of this work respectively. For each AFM experiment performed the samples were either polymer gels or cultured cells placed on different glass slides and Petri dishes respectively. First, a brief explanation of the AFM employed and then the cantilever will be given. Then follows a description of the setup as employed for this work. All the experiments have been performed in the AFM contact mode of operation. The optical lever design will be described, followed by the explanation of the designs for force measurements. The creep response curves have been recorded by monitoring the deflection of the cantilever after loading and unloading the soft sample in force by the magnet or by increasing the z height. For stress relaxation, the two loading schemes in z step and the magnetic step have been performed and will be described in this section. The pyramid indenter with a 35° opening angle and the indentation of the tip has defined the mechanical contact between the tip and the ultra-soft samples. The measurements of the soft samples material properties will be described.

2.1 The AFM apparatus and description

In general, the Atomic Force Microscope has been operated under constant force mode, which incorporates optical beam deflection for sensing the cantilever motion. The most common detection scheme is the optical beam deflection, which is also used in our setup. A schematic of the AFM showing the most important components is shown in Figure 4 A laser beam emitted by the laser diode is directed onto the cantilever and reflected onto an array of four photodiodes. The corresponding signals are acquired and processed by a feedback electronic. By subtracting opposite diode signals, the vertical as well as the torsion of the cantilever can be detected. The optical lever method of detecting cantilever deflection signal is shown in the Figure. Due to the difference in bending shapes of different cantilever modes proportionality constant is required for each mode.[21] [2] [91] [12] [16, 92]

2.2 Sample preparation

The live NIH-3T3 fibroblasts cells (cells) and the ultra-soft polymer gel (gel) have been subjected for the characterization of the visco-elastic creep response by AFM z response and magnetic response. The material properties of the gel samples could be tuned for

biocompatibility and mechanical stability. The local viscoelastic creep response of the cell sample with the magnetic cantilevers will be described for the two designs. Depending on the sample in its environment newly prepared magnetic cantilevers have been employed to characterize the soft samples viscoelastic properties.

2.2.1 Cell culture

Cells were cultured in low glucose DMEM (Dulbecco's Modified Eagle Medium), supplemented with 10 % FBS (Fetal Bovine Serum) and incubated at 37°C in a humidified atmosphere of 95% air and 5% CO_2. Cells were cultured typically for two days after splitting on plastic Petri dishes prior to AFM measurements. The plastic petri dish was then mounted in a home built aluminium holder and fixed with vacuum grease. Experiments were performed at room temperature in 5% CO_2 atmosphere.

2.2.2 Gel preparation

Acrylamide and Bis-acrylamide solutions were purchased from Bio-Rad. N,N,N′,N′-Tetramethylethylenediamine (TEMED), TC-119 medium, N-[3-(Trimethoxysilyl)propyl]ethylenediamine silane and dichlorodimethylsilane solution were purchased from Sigma. Sodium hydroxide (NaOH) and ammonium persulphate (APS) were purchased from Merck and circular cover glasses (22 mm diameter) from VWR Scientific. Glutaraldehyde, ethanol and other solvents were purchased from Panreac AppliChem. Polymerization of the gel solution [93] was carried out between two glass slides, silanized with amino- or chloro- silanes, respectively. In details, for the amino-silanization, round cover slips were first washed in absolute ethanol, then covered with 0.1M NaOH for 3 minutes and finally activated with the amino-silane N-[3-(Trimethoxysilyl)propyl]ethylenediamine for 3 minutes and fixed with 0.5% glutaraldehyde for 30 minutes. For the chloro-silanized glass preparation, a dichlorodimethylsilane solution was poured on the cover slides for 5 minutes; glasses were later extensively washed with ultrapure water (MilliQ systems, Molsheim, FR) and dried. Polyacrylamide gel solution was prepared by mixing 40% Acrylamide with 2% Bisacrylamide in ultrapure water. Polymerization was initiated by APS and TEMED. The solution was dropped on the amino-silanized glass and covered with the chloro-silanized one slide to avoid the presence of oxygen that would inhibit the polymerization. After 30 minutes the upper slide was removed, leaving the gel on the amino-salinized support. The polymer gels (gel as a simple acronym

used through out this work) on amino-salinized support were then stored in humid conditions for future use.

2.2.3 Magnetic cantilever preparation

The magnetic AFM cantilevers have been prepared by gluing a 20 μm permanent magnetic fragments to the back side of the cantilever opposite to the AFM tip and stored at room temperature for use. The usage is illustrated on figure 3 where the magnetic fragments have been positioned at the rare end to the back of the cantilever. I have employed V-shaped cantilevers (MLCT, Bruker, Germany) [13] with a nominal *spring constant* ≈ 10 mN/m (resonant frequency in air ≈ 7 kHz) for cell experiments and micro lever (DNP-S, Bruker, Germany) with a nominal *spring constant* ≈ 60 mN/m (resonant frequency ≈ 23 kHz) for the experiments on gels. Small magnetic fragments of about 20 µm in diameter were prepared by sanding a strong samarium cobalt magnet (IBS, Berlin, Germany) with an electrical tool (Dremel, Breda, NL) [94]. We placed a new cantilever chip into a cantilever chip holder, with the probe of the chosen V-shaped AFM cantilever facing upwards. A tiny drop of 2-component epoxy glue (18g+15g /2 x 15ml, Uhu Plus endfest 300, Uhu GmbH, Bühl, Germany) [95] was mixed and put on a glass slide next to a small amount of magnetic fragments. The glass slide with glue and magnetic fragments was placed on the optical microscope stage (Zeiss, Axiovert 300, Oberkochen, Germany) [96]. The AFM cantilever tip has been carefully dipped into the droplet of glue and then quickly to the region containing magnetic fragments by optical microscopy. Excess glue (if any) was removed by slightly touching the cantilever tip on a bare portion of the glass slide. An easy way of handling was by micromanipulation. In this way it possible to translate the cantilever tip in three-dimensions on a suitable magnetic fragment and off the glue on the laboratory glass slide in a precise manner. Once the AFM cantilever and the magnetic fragment come in contact, the AFM cantilever was withdrawn by lifting the AFM cantilever chip holder off the surface of the glass slide.

2.3 Descriptions of setup with magnetic cantilevers

The AFM enabled the installation of the magnetic cantilevers in air and in aqueous environment like the cell culture medium. A schematic of the force microscope (MFP-3D Asylum Research, Santa Barbara, CA, USA) has been employed for this work. Our AFM has been operated in contact mode whereby the soft spring cantilever exerts a force on the sample surface. The MFP-3D AFM operates both in liquid and air medium and measures the force between the sample and soft spring cantilever. The cantilever can be moved in the Z directions and it is positioned with nm accuracy relative to the sample surface by a piezo electric transducer. The feedback system for position control consists of a hard ware and software based control units. By monitoring the z height, the force curves such that additional creep and non-linearity are ruled out.

The magnetic force microscope resides on a commercial optical microscope (Axiovert 200, Zeiss, Oberkochen, Germany). Cell populated PA supports were placed in Petri dishes, fixed to an aluminium holder with vacuum grease and mounted on the AFM stage with two magnets. All the set-up was enclosed in a homebuilt polymethylmethacrylate (PMMA) box in order to inject and maintain 5% CO_2.

As shown on figure 3a, to apply a magnetic force to the magnetic cantilevers a coil of 100 turns around a soft iron core was attached to a polyvinyl chloride (PVC) tube, which fitted to the microscope objective placed under the AFM. The soft iron had a sharp pin in order to create a large gradient of the magnetic field. Typically, currents of 1.5 A were used in our measurements. The step like voltage signal was generated by the AFM controller and amplified with a home-built high current OP-AMP. Readout, control of cantilever motion and analysis of the signal were done using home written routines in IGOR (Wavemetrics, Lake Oswego, OR, USA).

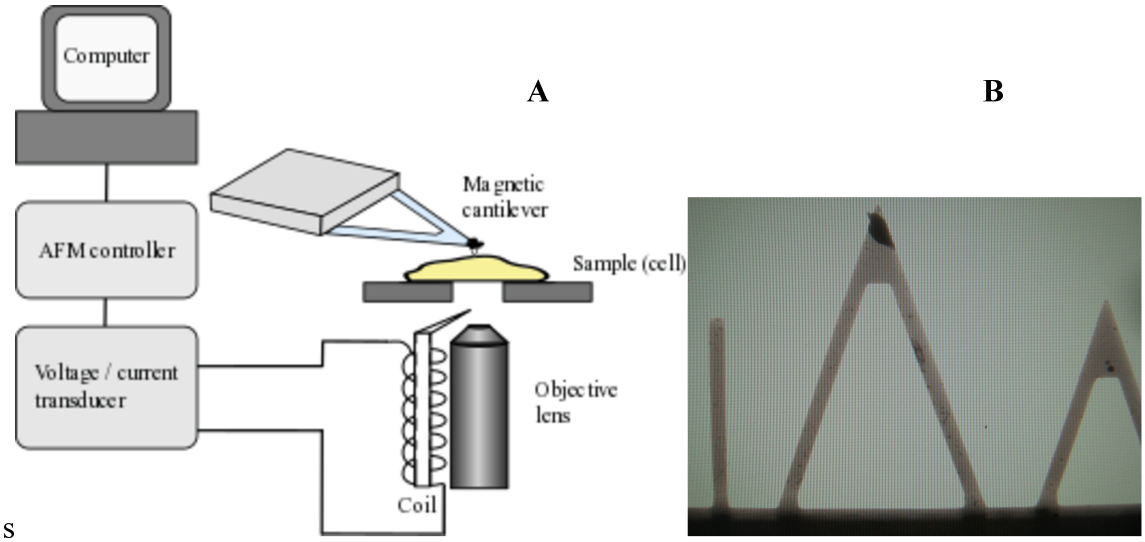

s

Figure 11: Schematic setup of magnetic AFM cantilever including the electrical assembly. The coil has been connected to a voltage/current transducer. The AFM controller links the transducer to the personal computer. The sample is mounted on the x-y piezo of the AFM. A coil is attached firmly to the microscope objective lens, which is placed under the AFM tip in the combined optical/force microscope (panel A) and a 3 mm gap spacing below the AFM sample holder (diagram modified from [63]. The core material of the coil has a sharp pin in order to concentrate the gradient of the magnetic field. In panel B three AFM cantilever with varied lengths. The longest (middle) 320 μm triangular AFM cantilever shows an glued magnetic particle to the tip.

The detection laser of the AFM had to be aligned to an area of the cantilever, not being covered by glue. The deflection sensitivity of the magnetic cantilever was calibrated by obtaining a force curve on a stiff substrate, usually petri dish.[19] The cantilever was then withdrawn a few micrometres from the surface and the thermal motion of the free cantilever was recorded to obtain the spring constant following the method by Butt et al., [21]The soft cantilevers for cells and slightly stiffer ones for the gels have been used. By applying a voltage step to the free cantilever and measuring its deflection the magnetic sensitivity was obtained. The linearity of the response was checked to take care that the coil is not operated in saturation. Typical maximum forces were around 0.8 nN. The magnetic force could be increased by using a larger magnetic particle or by bringing the coil closer to the AFM cantilever[48]. Since, for our applications the force was sufficient we did not try to increase further. [16]

Essentially, we glued a small magnet in the back of a regular AFM cantilever (referred to as a magnetic cantilever, or MC), and placed a coil below the sample stage such that the magnetic cantilever (MC) is positioned at a distance x of the coil such that the tip lies in coil axis.

Flowing through the coil there is an alternative current of the form:

$$i_{AC}(t) = i_0 \exp i\omega t \tag{2.1}$$

Where ω is the oscillation frequency and i_0 is the current amplitude. The magnetic field in the proximity of the magnetic cantilever (MC) can be approximated by the magnetic field of N loops of a radius a at a distance x along the axis, such that:

$$\vec{B}_{AC}(t) = \frac{\mu_0 N i_{AC}(t) a^2}{2(x^2 + a^2)^{3/2}} \hat{x} \tag{2.2}$$

We can also write $\vec{B}_{AC}(t)$ in terms of the magnetic dipole moment of the coil $\mu_{coil}(t) = (\pi a^2) N i_{AC}(t)$ as

$$\vec{B}_{AC}(t) = \frac{\mu_0 \mu_{coil}(t)}{2\pi(x^2 + a^2)^{3/2}} \hat{x} \tag{2.3}$$

Where μ_0 is the vacuum permeability. This AC magnetic field is not uniform since the magnetic field lines out side of the coil are divergent. However what really matters here is whether the magnet is glued to the cantilever will interact with the $\vec{B}_{AC}(t)$. Since the MC has a permanent magnetic dipole moment μ_{MC}, the potential energy of μ_{MC} in the presence of $\vec{B}_{AC}(t)$ is given by:

$$U = -\vec{\mu}_{MC} \cdot \vec{B}_{AC}(t) \tag{2.4}$$

In principle, we do not know which is the direction of $\vec{\mu}_{MC}$ but it is applicable (it works) as long as we have the vertical component to couple with $\vec{B}_{AC}(t)$. Assuming that $\vec{\mu}_{MC} = \mu_{MC}\hat{x}$ an approximate form of the force acting on the magnetic cantilever (MC) due to $\vec{B}_{AC}(t)$ is given by:

$$\vec{F}_{AC}(t) = \nabla\left(\vec{\mu}_{MC} \cdot \vec{B}_{AC}(t)\right) \tag{2.5}$$

Finally, the approximate vertical force acting on the magnetic cantilever (MC) located at a distance x above the coil is:

$$\vec{F}_{AC}(t) = -\frac{3}{2\pi} \frac{\mu_0 \mu_{MC} \mu_{coil}(t) x}{(a^2 + x^2)^{5/2}} \hat{x} \tag{2.6}$$

By expanding the above expression around an average distance x_0 between the MC and the coil, we obtain:

$$F_{AC}(x) - F_{AC}(x_0) = -\frac{3\mu_0 \ \vec{\mu}MC \ \mu_{coil}(t)}{2\pi}\left[\frac{1}{(a^2 + x_0^2)^{5/2}} - \frac{5x_0^2}{(a^2 + x_0^2)^{7/2}}\right](x - x_0) \quad (2.7)$$

Replacing $\mu_{coil}(t) = \pi a^2 i_0 e^{i(\omega t)}$, we obtain the effective driving force on the MC has in the form:

$$F_{drive} = G(a, N, i_0, x_0, \mu_{MC})\ (x - x_0)\ exp(i\omega t) = F_B exp(i\omega t), \quad (2.8)$$

Where the amplitude of the driving force F_B depends on a few parameters of the experimental setup namely 1) The geometrical characteristics, 2) the current amplitude of the coil, and 3) the magnetic dipole moment of the cantilever.

2.3.1 AFM force curves

The AFM force curves have been a plot of the deflection of the cantilever versus the extension of the z piezo height. The conventional and the stress relaxation curves were recorded on a cell and gel and sample in order to study the viscoelastic property. The conventional and the stress relaxation curves started at a point where cantilever and the sample are far apart and the cantilever were not deflected. Force curves were taken typically at a sample rate of 1 Hz, maximum deflection was set to 100 nm, and a typical travel range of 2µm. The time for a complete cycle was chosen in such a way that the retracting and the approaching part of the force curves in the non-contact part of the force were not separated by the viscosity effects. The forces curves obtained here are ramped up and down with constant speed, except at the turning points. For the stress relaxation force curves, z motion was stopped for a dwell time of 2 s after the trigger threshold was achieved (cantilever deflection of 150 nm).

From the slope s of the force curve and the spring constant of the cantilever k_c, we calculated the spring constant of the sample k_s, by:

$$k_s = k_c * \frac{s}{1 - s} \quad (2.9)$$

I have recorded force volumes (6x6, or 10x10 force curves) at a typical spacing of 100nm to test homogeneity of samples and reproducibility of force curve data.

2.3.2 AFM z step response:

For step response, we kept the z voltage constant for a prolonged time (2s) after approaching the sample as in a regular force curve described above. After 1s of dwell time, the z height was increased by a small amount (typically 100nm) towards the soft sample and then withdrawn again after 0.5 s, (see figure 12) while the deflection signal was monitored showing the creep response of the sample. The creep response can be modelled by a spring and dashpot combination, usually called the general linear solid model. We could calculate the viscoelastic properties of the sample as described below.

2.3.3 AFM magnetic step response

Alternatively, to change the z height of the sample, we could apply a magnetic force step using magnetic cantilevers during the dwell time as described above. Typically, a force step of 0.4 nN was applied, while the z-height was kept constant and the deflection signal is recorded showing the creep response of our sample (see figure 13). The soft spring magnetic cantilever comprising of glued magnetic particle of volume V had magnetic susceptibility χ was exposed to the external magnetic field (B). The magnetic AFM cantilever experienced a gradient field of the form [97]

$$F_m = \chi * V * \frac{(\nabla \cdot B)}{\mu_0} * \vec{B}_{AC}(t) \tag{2.10}$$

F_m is the force a paramagnetic particle of magnetic susceptibility χ feels in a magnetic field. The response of the magnetic cantilever to the drive current a magnetizing field B_{AC} has been applied to the magnetic AFM cantilever.

In both experimental approaches used in this work, neither the force nor the indentation can be kept constant. Even in magnetic step response, where a constant external force is applied, the indentation is changing and hence the deflection of the cantilever, and hence the force exerted by the cantilever is changing. In z step response, it is even clearer that force (being proportional to cantilever deflection) and indentation (being z height change - deflection change) are changing after applying the step during the observed creep response. Technically speaking the stress (i.e. force) and the strain (i.e. indentation) are changing in our experiment.

Since normally stress relaxation is used in a condition where the strain is constant, and vice versa, we do not use the terms stress or strain relaxation here for our experimental conditions. Even though, stress and the strain are relaxing (both) in our experiments.

3.0 DATA ANALYSIS AND MODELLING

The chapter describes the data analysis of the deflection data obtained from the conventional force curve, z step response and the magnetic response design respectively. The objective of this section is to show that the creep response of cells samples by z step response and the magnetic step AFM design could be adequately quantified by employing the standard solid linear model. The standard linear solid model (SLS) has been employed to analyse the data from the magnetic step and the z step AFM design, which is the simplest combination of springs and a dashpot, which reproduces the experimental results obtained on cells. The viscous properties of the live cell samples will be derived in terms of the viscous damping coefficient of friction (friction coefficient) and the relaxation times.

Force curve data (conventional approach and retract, as well as creep response data after z-step or magnetic force step) were analysed offline using home-written routines in IGOR (Wavemetrics, Lake Oswego, OR, USA). Since in cell data creep even over the dwell time of 2s was still substantial, one subtracted an exponential fit over the entire dwell time (excluding those data when the step has been applied) to subtract the global creep. The loading and unloading step was fitted by a single exponential function to the corrected data. By employing the standard linear solid model (see figure 13), the spring constants of the sample k_1 and k_2, the friction coefficient f and the relaxation time constant τ can be obtained. One gets two sets of values, one for the loading step, and another one for unloading step.

Nomenclature

Since there are several quantities discussed in this manuscript, which all have units of a spring constant, we use the following nomenclature: We use *spring constant* when addressing the spring constant k_c of the cantilever; we use *spring constant* when addressing the spring constant k_s of the sample determined by a force curve, and we use k_1 and k_2 when addressing the spring constants of the sample derived from z-step response and magnetic step response data analysed within the framework of the standard linear solid model.

3.1 Spring constant of the sample derived from the force curves

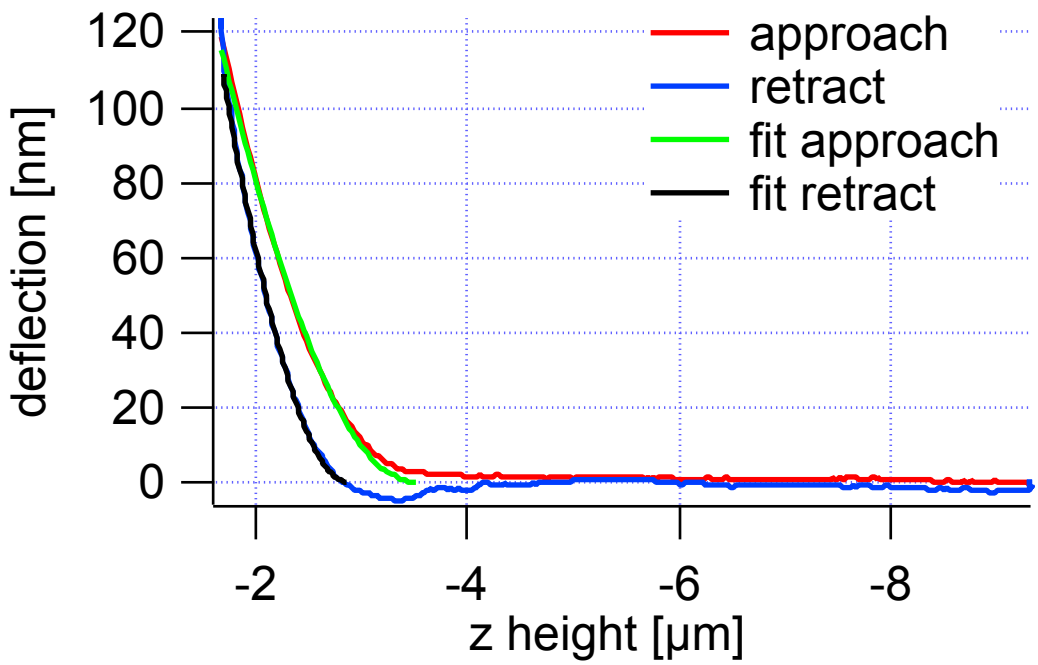

Figure 12: Typical force curve recorded after ramping cantilever on top of a cell. The figure shows plot of the approach (red trace) and the retract (blue trace) curves for contact mode cantilever in an aqueous environment. The deflection of the cantilever is recorded versus elongation of the piezo-electric scanner in the vertical direction. The simulated fit (green and black) is drawn on the approach and the retract regime of the force curves respectively.

When loading the soft sample as it has been described before with the AFM cantilever, at each given loading force F_1, which can be measured by its deflection d_1, one will create a sample indentation. In the force curve one measures the deflection as a function of z height of the sample. From the mechanical data one can derive the spring constants of the sample from the slope of the plot deflection versus z-height. The slope s is defined as:

$$s = \frac{\Delta d}{\Delta z} \qquad \text{(A3.01)}$$

Where Δd is the change in the deflection and Δz is the change in the z height. From the slope s of the force curve and the spring constant of the cantilever k_c, one calculated the spring constant of the sample k_s, by:

$$k_s = k_c * \frac{s}{1 - s} \qquad \text{(A3.02a)}$$

Since the slope, s, may be different on approach or retract, I distinguish both. In cells, due to a high viscous contribution $k_{approach}$ and $k_{retract}$ will always be substantially different. This is better illustrated on the deflection time data.

3.2 Analysis of Creep Response Data from z response experiment

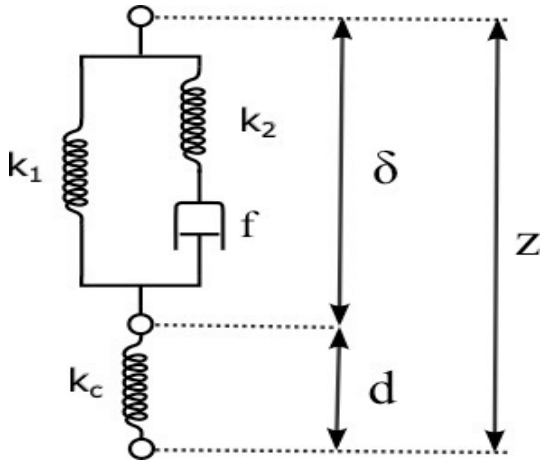

Figure 13: The Standard Linear Solid Model. The sample is modelled by a Zener element, where a spring k_1 is in parallel to a Maxwell element, consisting of a spring k_2 and a viscous damping element f. The cantilever is characterized by its spring constant k_c. Viscous (hydrodynamic) damping of the cantilever is neglected here, due to the slow creep response of the sample, which is the predominant viscous contribution. Motion of the sample height z is resulting in a deflection d of the cantilever or indentation d of the sample.

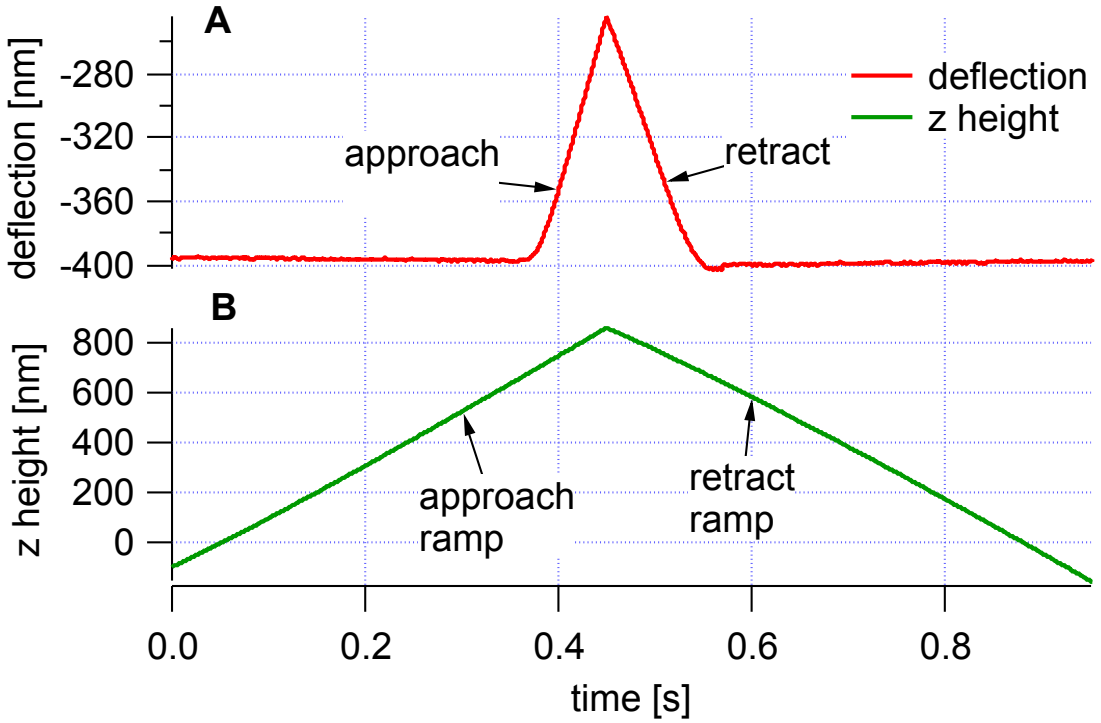

Figure 14: Typical conventional force curve obtained on a cell sample. The deflection data (A) and the loading step in z height (B) for 1 second. For quantitative analysis the indentation is calculated as the z height (B) minus the cantilever deflection (A).

We apply a step force when in contact with the sample at a z-position z_1, the deflection will be d_1, and the indentation is δ_1. Before the step the force equilibrium will be:

$$k_c * d_1 = k_s * \delta_1 = k_s * (z_1 - d_1) \quad \text{(A3.02b)}$$

We have used here the general relation between z-height, deflection and indentation, which will be always obeyed:

$$z = d + \delta \quad \text{(A3.02c)}$$

Since the forces are in equilibrium at this point, we can simplify our calculations by redefining the origin such, that

$$d_1 = z_1 = \delta_1 = 0 \quad \text{(A3.02d)}$$

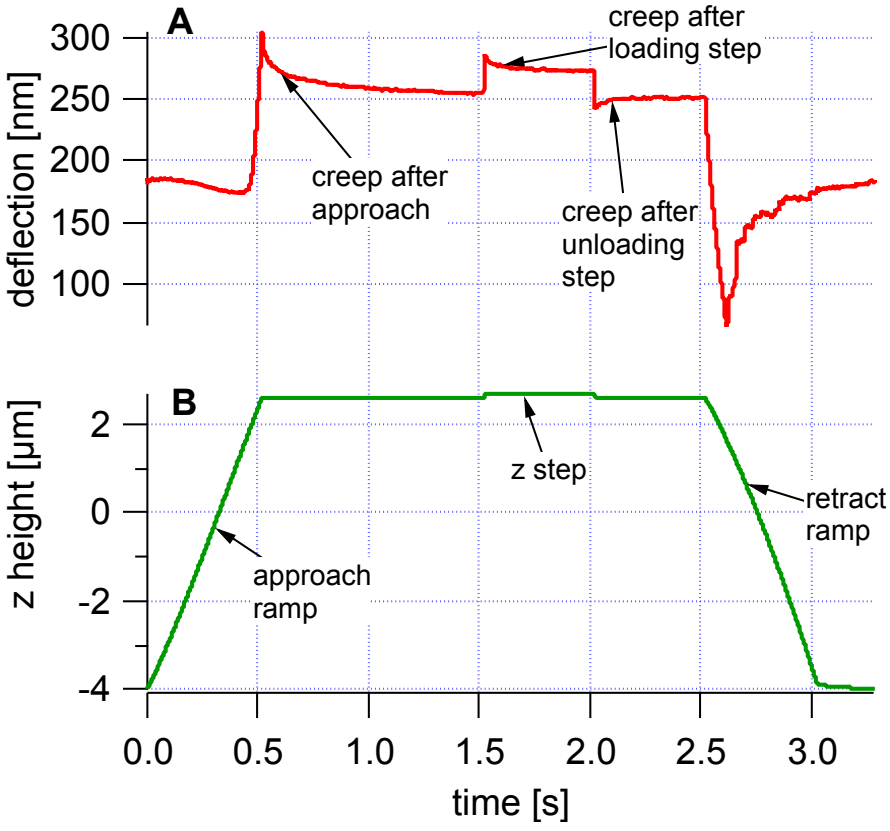

g

Figure 15: Typical creep response of a cell after applying a z step. Panel A shows the deflection data, while the z height (B) is first ramped as in a conventional force curve (approach ramp), then kept constant for 2 seconds, except a small step in z-height, which is applied after the creep of the cell, caused by the approach ramp, has relaxed appreciably. Then, finally the sample is retracted again (retract ramp). After the step (applied from time 1.5 to 2.0 seconds) the creep response to the loading and unloading step is analysed in detail. The indentation is the difference between the z height and the cantilever deflection.

3.3 Conventional step by increasing z-height: z-step

When externally applying force steps in indentation on the sample with the AFM cantilever at contact during a dwell time, by a jump in z height one will increase the z-height to:

$$z_2 = z_1 + \Delta z = \Delta z \tag{A3.03}$$

After relaxation, the deflection will have a new value d_2:

$$d_2 = d_1 + \Delta d = \Delta d \tag{A3.03b}$$

One models the sample by a combination of two springs and a dashpot, termed the general linear solid model, which is the minimum model to reproduce the measured creep behaviour above. After relaxation, the spring k_2 will be relaxed due to the creep of the viscous damping element f, so the force balance looks like:

$$k_c * d_2 = k_1 * \delta_2 = k_1 * (z_2 - d_2) \tag{A3.04}$$
$$k_c * \Delta d = k_1(\Delta z - \Delta d)$$

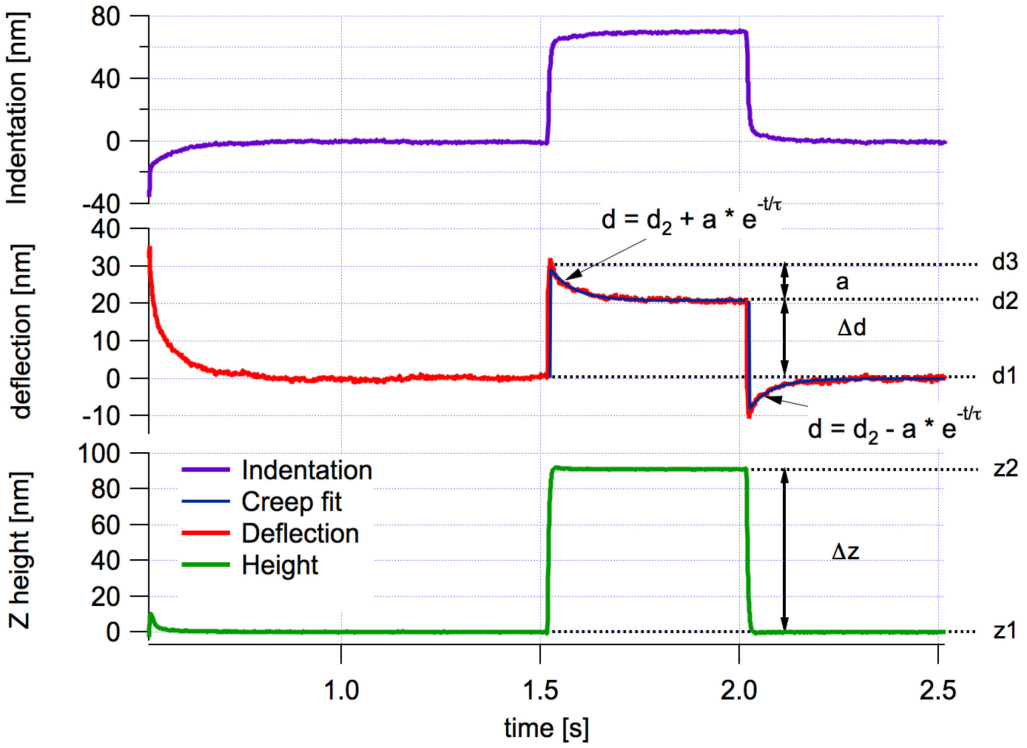

Figure 16: Creep response at dwell after applying a loading step in z height at t = 1.5s and an unloading step at t = 2.0s. The indentation is calculated as the difference between z height and deflection. The deflection data are fitted with an exponential function, which will give k_1, k_2 and f as results. The creep response at the dwell time is zoomed for better visibility.

The spring constant k_1 can be derived from the measurable quantities Δd and Δz:

$$k_1 = k_c \frac{\Delta d}{\Delta z - \Delta d} \tag{A3.05}$$

Right after (the infinitely step) z-step, the viscous element can be considered as a stiff rod. Thus, the force balance looks like:

$$\begin{aligned} k_c * d_3 &= (k_1 + k_2) * \delta_3 \\ k_c(\Delta d + a) &= (k_1 + k_2) * (z_2 - d_3) \\ k_c(\Delta d + a) &= (k_1 + k_2) * (\Delta z - \Delta d - a) \end{aligned} \tag{A3.06}$$

So, I can derive the spring constant k_2 from the measurable quantities Δd, Δz and from the initial value a of the deflection

$$k_2 = k_c \frac{\Delta d + a}{\Delta z - \Delta d - a} - k_1 \tag{A3.07}$$

After relaxation, the spring k_2 will be relaxed due to the creep of the viscous damping element f. For describing the creep responses, one employs the following ansatz for the relaxation process:

$$d = d_2 - d_1 + a * e^{-t/\tau} = \Delta d + a * e^{-t/\tau} \tag{A3.08}$$

The amplitude a, and the relaxation time τ can be obtained by an exponential fit of the data. The force equilibrium for any point in time is given by:

$$F_c = F_1 + F_2 \tag{A3.09}$$
$$F_2 = k_c * d - k_1 * \delta$$

The equation implicitly relates the dynamic values, which are a function of coefficient of viscous friction. Further the force in the Maxwell element will follow the following dynamic equation:

$$\dot{\delta} = \frac{\dot{F}_2}{k_2} - \frac{F_2}{f} \tag{A3.10}$$

In the experimental scheme an ideal step loading cannot be achieved. The loading has been accompanied by a very small rise time of the cantilever. The creep in terms of the true sample spring constant could be described by:

$$\delta = z - d \tag{3.11}$$
$$\delta = \Delta z - \Delta d - a e^{-t/\tau}$$

$$\dot{\delta} = a * \frac{1}{\tau} * e^{-t/\tau} \tag{A3.12}$$

The force F_2 in the Maxwell element can be rewritten using our ansatz eq. (A3.09):

$$F_2 = k_c \left(\Delta d + a e^{-t/\tau}\right) - k_1 * \left(\Delta z - \Delta d - a e^{-t/\tau}\right) \tag{A3.13}$$

$$F_2 = k_c * \Delta d \; - k_1 * (\Delta z - \Delta d) \; + \; k_c \, a \, e^{-t/\tau} \; + k_1 \, a \, e^{-t/\tau}$$

Using the above equilibrium of forces (A3.09) this will reduce to:

$$F_2 = k_c \, a \, e^{-t/\tau} + k_1 \, a \, e^{-t/\tau} \tag{A3.14}$$

$$\dot{F}_2 = -k_c \, \frac{a}{\tau} \, e^{-t/\tau} - k_1 \, \frac{a}{\tau} \, e^{-t/\tau} \tag{A3.15}$$

Entering the expressions from eq. A3.14, eq. A3.15, and eq. A3.12 in eq. A3.10 we get:

$$\frac{a}{\tau} \, e^{-t/\tau} = -\frac{k_c \, \frac{a}{\tau} \, e^{-t/\tau} + k_1 \, \frac{a}{\tau} \, e^{-t/\tau}}{k_2} - \frac{-k_c \, a \, e^{-t/\tau} - k_1 \, a \, e^{-t/\tau}}{f} \tag{A3.16}$$

$$1 = -\frac{k_c + k_1}{k_2} + \frac{k_c + k_1}{f} * \tau$$

$$f = k_2 * \tau \; * \frac{k_c + k_1}{k_2 + k_c + k_1} \tag{A3.17}$$

The relaxation time constant τ is the apparent time in the experimental setup, which not only depends on the materials properties k_1, k_2, and f, but also on the cantilever spring constant k_c, i.e. experimental parameters. The intrinsic relaxation time constant is defined by the ratio of coefficient of friction f and k_2:

$$\tau^* = \frac{f}{k_2} \; = \tau \; * \frac{k_c + k_1}{k_2 + k_c + k_1} \tag{A3.18}$$

3.3 Analysis of Creep Response Data from magnetic force steps

For the magnetic force step eq. (A3.02a) for the situation before the step still holds:

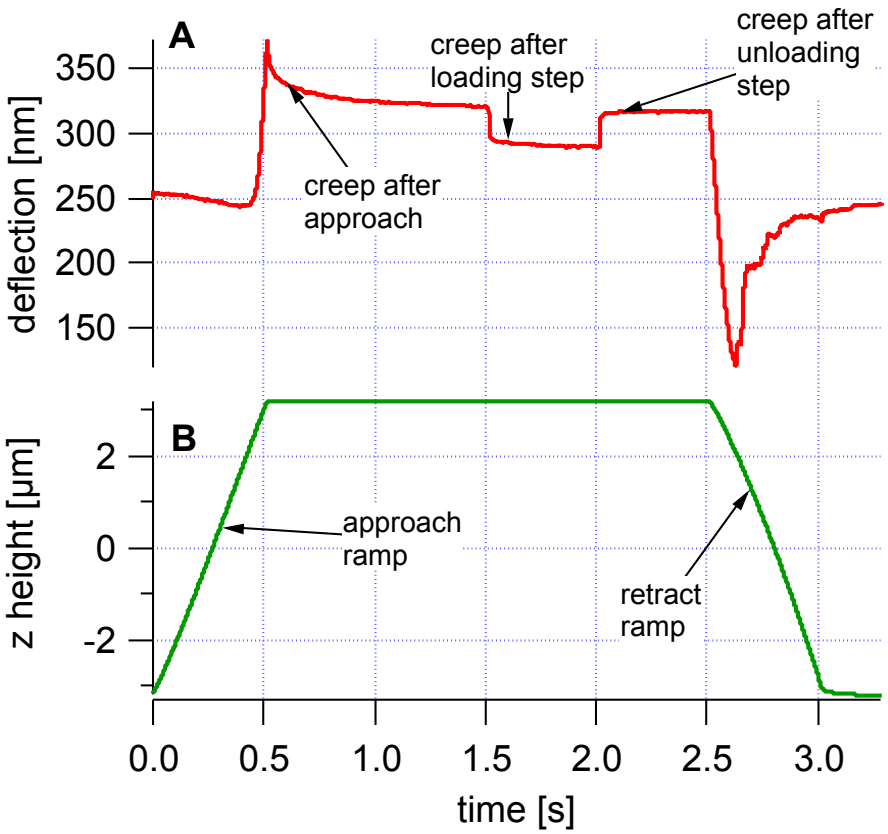

Figure 17: Typical creep response of a cell after applying a magnetic step. Panel A shows the deflection data, while the z height (B) is first ramped as in a conventional force curve (approach ramp), then kept constant for 2 seconds, except a small step in z-height, which is applied after the creep of the cell, caused by the approach ramp, has relaxed appreciably. Then, finally the sample is retracted again (retract ramp). After the step (applied from time 1.5 to 2.0 seconds) the creep response to the loading and unloading step is analysed in detail. The indentation is the difference between the z height and the cantilever deflection.

After the approach ramp of the force, it is required that the z-height remains constant for some time as seen in the figure 17B. Because the step is not changed we derive:

$$z_1 = z_2 = 0 \qquad \text{(A3.19)}$$
$$\Delta z = 0$$

When applying the external magnetic force F_m, one will first observes a sudden jump in deflection d_3 and then a relaxation to a deflection d_2.

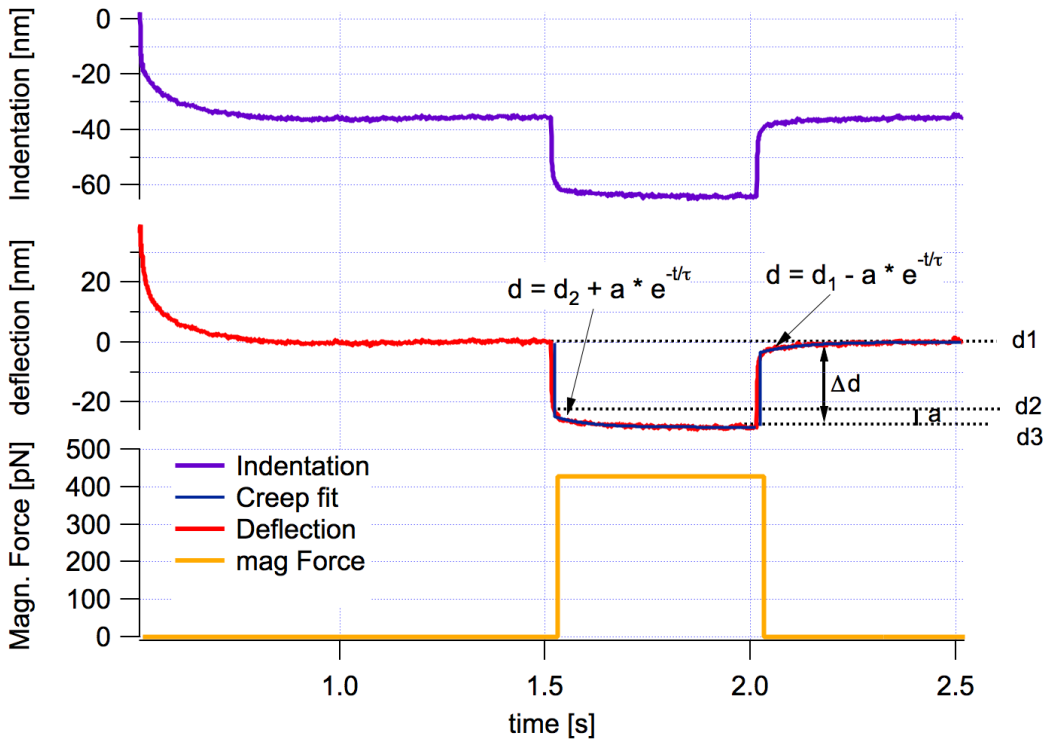

Figure 18: Creep response on the cell sample during 400 pN magnetic step force step starting at t = 1.5s. The deflection changes slowly resulting to the sample indentation, which is then followed by an unloading step at t = 2.0 s. For the loading step the change of deflection Δd is negative, since the indentation (30 nm) change is positive. The change in z height is zero during the direct step in force experiment. By applying an exponential fit we gain the spring constants k_1, k_2 of the cell sample and the viscous properties of the cell sample.

Since z is zero during the entire process, the indentations and the deflection are directly linked:

$$\delta_1 = -d_1 = 0 \qquad \text{(A3.20)}$$

$$\delta_2 = -d_2 \qquad d_2 = \Delta d + a$$

$$\delta_3 = -d_3 \qquad d_3 = \Delta d$$

For the loading step the change of deflection Δd is negative, since the indentation change is positive.

The creep amplitude a is positive, since d_2 is larger than d_3. After relaxation to deflection d_2 the force balance is:

$$k_c * d_3 = k_1 * \delta_3 + F_m \qquad \text{(A3.21)}$$

$$k_c * \Delta d = -k_1 * \Delta d + F_m$$

$$k_1 = \frac{F_m}{\Delta d} - k_c \tag{A3.22}$$

The initial response after the force step obeys the following force balance:

$$k_c * d_3 = (k_1 + k_2) * d_3 + F_m \tag{A3.23}$$
$$k_c * (\Delta d + a) = (k_1 + k_2)(\Delta d + a) + F_m$$

$$(k_1 + k_2) = \frac{F_m}{\Delta d + a} - k_c \tag{A3.24}$$

$$k_2 = \frac{F_m}{\Delta d + a} - k_c - k_1 \tag{A3.25}$$

For the relaxation one employs the same ansatz as above in eq. A3.08

$$d = d_2 + \ a\, e^{-t/\tau} \tag{A3.26}$$
$$d = \Delta d + \ a\, e^{-t/\tau}$$

The force balance needs to be expanded because of the magnetic force F_m:

$$F_c = F_1 + F_2 + F_m \tag{A3.27}$$
$$F_2 = k_c * d - k_1 * \delta - F_m$$

$$F_2 = (k_c + k_1) * d - F_m \tag{A3.28}$$

The force dynamics for the Maxwell element is also necessary here.

$$\dot{\delta} = \frac{\dot{F}_2}{k_2} - \frac{F_2}{f} \tag{A3.29}$$

Using the ansatz from equation A3.08 one can calculate F_2, its time derivative and the time derivative of the indentation

$$F_2 = (k_c + k_1) * \left[\Delta d + \ a\, e^{-t/\tau}\right] - F_m \tag{A3.30}$$
$$\dot{F}_2 = (k_c + k_1) * \left(-\frac{a}{\tau}\right)\ e^{-t/\tau}$$

The indentation and its time derivative are given by:

$$\delta = -d \tag{A3.31}$$

$$\delta = -\Delta d - a e^{-t/\tau}$$

$$\dot{\delta} = -\dot{d} = \frac{a}{\tau}\, e^{-t/\tau} \tag{A3.32}$$

This will be entered in the dynamic equation of the Maxwell element A3.10:

$$\frac{a}{\tau}\, e^{-t/\tau} = \frac{k_c + k_1}{k_2} * \left(-\frac{a}{\tau}\right) e^{-t/\tau} + \frac{(k_c + k_1) * \Delta d}{f} + \frac{(k_c + k_1) *\ a\, e^{-t/\tau}}{f} - \frac{F_m}{f} \tag{A3.33}$$

This relation can be split in its time dependent part and those terms, which do not depend on time:

$$\frac{a}{\tau}\, e^{-t/\tau} = \frac{k_c + k_1}{k_2} * \left(-\frac{a}{\tau}\right) e^{-t/\tau} + \frac{(k_c + k_1) *\ a\, e^{-t/\tau}}{f} \tag{A3.34}$$

$$0 = \frac{(k_c + k_1) * \Delta d}{f} - \frac{F_m}{f} \tag{A3.35}$$

The equation can be simplified and will give us a relation for the friction coefficient:

$$1 = -\frac{k_c + k_1}{k_2} + \frac{(k_c + k_1)\ *\ \tau}{f} \tag{A3.36}$$

$$f = k_2 * \tau\ * \frac{k_c + k_1}{k_2 + k_c + k_1} \tag{A3.37}$$

This relation is identical to the case of the z step. The intrinsic relaxation time constant is defined by the ratio of coefficient of friction f and k_2:

$$\tau^* = \frac{f}{k_2}\ = \tau\ * \frac{k_c + k_1}{k_2 + k_c + k_1} \tag{A3.38}$$

3.4 Analysing spring constants from a magnetic force modulation experiment.

In the previous section (section 1.5.1) we have described the motion of the free cantilever and the cantilever in contact with the visco-elastic sample in terms of the driven harmonic oscillator. The free motion is described by a mass connected to a single spring. As shown in figure 19 the in contact motion is described by a mass connected to a single spring.

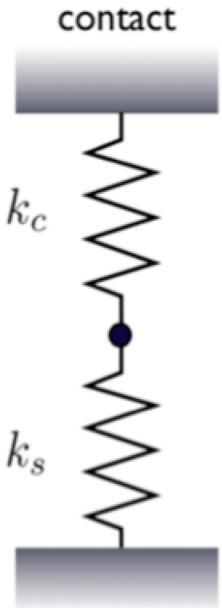

Figure 19: An equivalent mechanical circuit of the sample spring in series with the cantilever spring in the in contact motion. The motion (oscillations) of the cantilever spring in contact with the viscoelastic sample having amplitude A_1. The elastic properties could be described until the preset loading force of the conventional force curve.

The in-contact motion can be described by a mass connected to two springs (representing the cantilever and the sample.) Assuming that we pull down the mass with the given force, F_m, in both systems (e.g., the magnetic force). In the free cantilever model, forces act on the cantilever immersed in aqueous oscillating with the displacement amplitude is A_0 as well as when the cantilever is in contact with the soft sample.

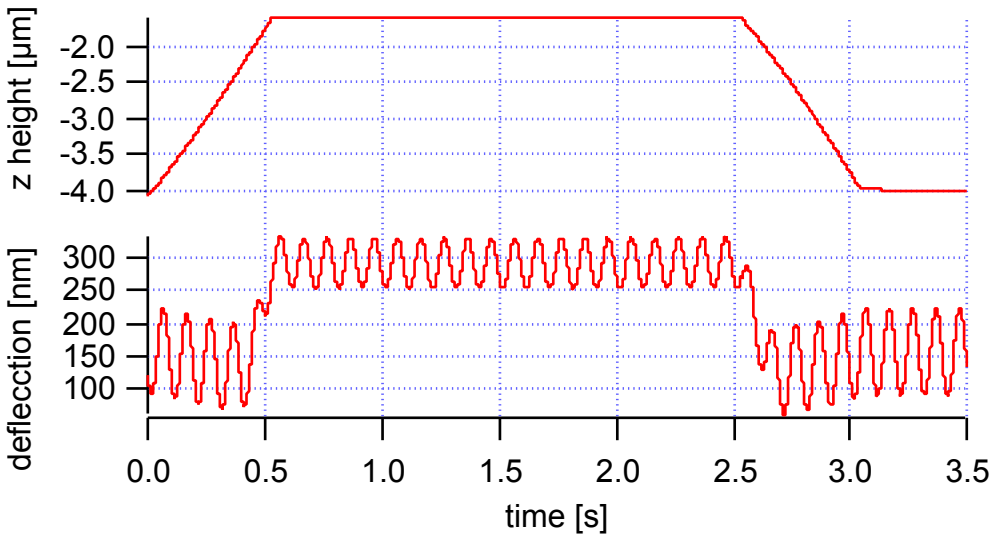

Figure 20: Figure shows stress relaxation data on a gel sample after a modulation force. The upper panel shows the z height profiles versus the time. The z-motion was stopped (t = 0.5 seconds) for 2 seconds. During this time the stress relaxation after the approach ramp of the cell has relaxed (with displacement A_1) and then retracted at t = 2.5 seconds. The bottom panel shows the deflection data in nm versus the time off and the in contact with the gel sample after the application of the modulation force in magnet for 3.5 seconds. Before contact the displacement of the free cantilever is A_0. For the in-contact system since the same force has to deform two springs, we obtain a smaller displacement A_1 (A_1<A_0).

We describe the motion of the cantilever free magnetic and in contact with a viscoelastic sample in terms of the solution of the driven harmonic oscillator. When the cantilever is in contact with a viscoelastic sample and also subjected to a magnetic field, the equation of motion will be given by eqn. 1.12.

As it has been described, when in contact, we will have the modulating force that makes the cantilever oscillates with the given frequency, the restoration force acting on the deflected the cantilever. as well as the viscous forces due to the liquid and the soft sample. The differences between the motions are:

1) The oscillations are different, being A_0 for the free cantilever and A_1 for the cantilever in contact with a viscoelastic sample.
2) The resonant frequencies and phase angles for both motions are also different ($\omega_0 \neq \omega_1$ and $\phi_0 \neq \phi_1$)

To estimate the spring constants, we simplify both free and in-contact motion by a simple arrangement of springs.

For the in-contact system since the same force has to deform two springs, we obtain a smaller displacement A_1 (A_1<A_0). By equating the forces as had been described before, we then obtain $k_c A_0 = (k_c + k_s) A_1$, which leads to the spring constants k_s of the soft sample that can be determined in terms of A_0 and A_1

$$k_s = k_c \left(\frac{A_0}{A_1} - 1\right) \qquad \text{A3.39}$$

On a very stiff sample, no indentation will occur, thus the amplitude in contact A_1 will be zero, leading to $k_s \longrightarrow \infty$. For every soft sample the amplitude in contact $A_1 \rightarrow A_0$, which leads to $k_s \rightarrow 0$. In the limit of $\omega \rightarrow 0$ we only have the elastic response because the viscous components vanishes as $dz_n/dt \rightarrow 0$. For $\omega > 0$, the viscous effects are present and k_s represents and effective spring constant.

3.5 The phase lag between free and in contact motions of the cantilever.

The phase lags of the cantilever motion are directly related to the internal viscosity if the sample, is calculated by

$$\emptyset = \emptyset_1 - \emptyset_0 \qquad \text{(A3.40)}$$

The phase angles of each type of the cantilever motion is

$$\tan \emptyset_n = I_m [A_n]/R_e[A_n] \qquad \text{(A3.41)}$$

For small angles one has within the CM2 approach

$$\tan \emptyset_n \approx \emptyset_n = \frac{b_n \omega}{\omega^2 - \omega} \qquad \text{(A3.42)}$$

We can make further approximations assuming $\omega_1 \approx \omega_0$ to determine the phase difference as

$$\emptyset \approx \frac{(b_1 - b_0)\omega}{\omega^2 - \omega_0^2} \qquad \text{(A3.43)}$$

Since b_1 describes the viscous damping due to the aqueous environment + sample, and by b_0 is only due to the aqueous environment, the phase difference $\emptyset$ carries only the information about the viscosity of the sample.

4.0 RESULTS

This is the results section. The viscoelastic creep response of living cells and gel was measured by AFM stress relaxation experiments. In addition to this conventional z step scenario, we also implemented here a method to apply directly a magnetic force step at constant z height, which is closer to a constant strain situation. In this section the results are shown and have been described. The spring constants from the cell and the gel sample have been quantified in adequate manner and then summarized in a tabular form. To avoid confusion the viscous property of the soft sample, friction coefficient, which has been derived, will be given the acronym, f, in the rest of the manuscript

Figure 21 shows the entire data sequence (z height (fig 21A) and deflection (21B)) as a function of time, as well as a zoom-in in the region of interest during the dwell time ((z height (fig 21C) and the deflection (21D)). As can be seen from the raw data, the relaxation time is on the order of 0.1 seconds, thus we choose to wait for 1s, before the step is applied. Even this prolonged waiting time is not sufficient so some residual creep from the approach is still visible. Thus, we needed to subtract an exponential function, to remove the global creep (green curve in Fig 21B). Here an exponential fit is applied to the entire dataset, excluding those data points next to the loading and unloading step. This detrended data set is actually shown in Fig 21D, which shows the corrected deflection data to be analysed. As can be seen here, after detrending, the loading and unloading step give similar (except sign) results, and the cell achieves - after creep - the same deflection position as before the step is applied. We have fitted then locally an exponential function to describe the creep response after the loading and unloading step (blue curves in Fig 21D). If we model our sample response by the linear solid model, which is the simplest combination of springs and dashpots reproducing the observed creep response data, we find that the deflection shall follow a single exponential behaviour (see analysis section for the derivations). The fit parameters (time constant τ, deflection plateau after creep has relaxed, and amplitude of the exponential decay) can be converted in the elements of the linear solid model circuit k_1, k_2 and f. Where k_1 will be the spring constant of the sample after relaxation, $k_1 + k_2$ will be value for the initial elastic constant of the cell sample right after the step has been applied, and f will be the friction damping coefficient. The apparent relaxation time constant τ will be determined by the sample's viscoelastic properties plus the cantilever spring constant. The intrinsic relaxation time constant τ^*, defined as f / k_2 will be independent of experimental conditions. Table 1 summarizes the results from analysing the force curve and the step

response data presented in figure 21. The values presented in table 1 will depend on the contact area, which is a function of loading force or indentation. By applying a suitable model (like the Hertz model often used in AFM), these values can be converted to materials properties like storage or loss modulus. However, since the validity f these models, especially on the microscopic scale used here, may be questionable we did not refrain to this option within this work.

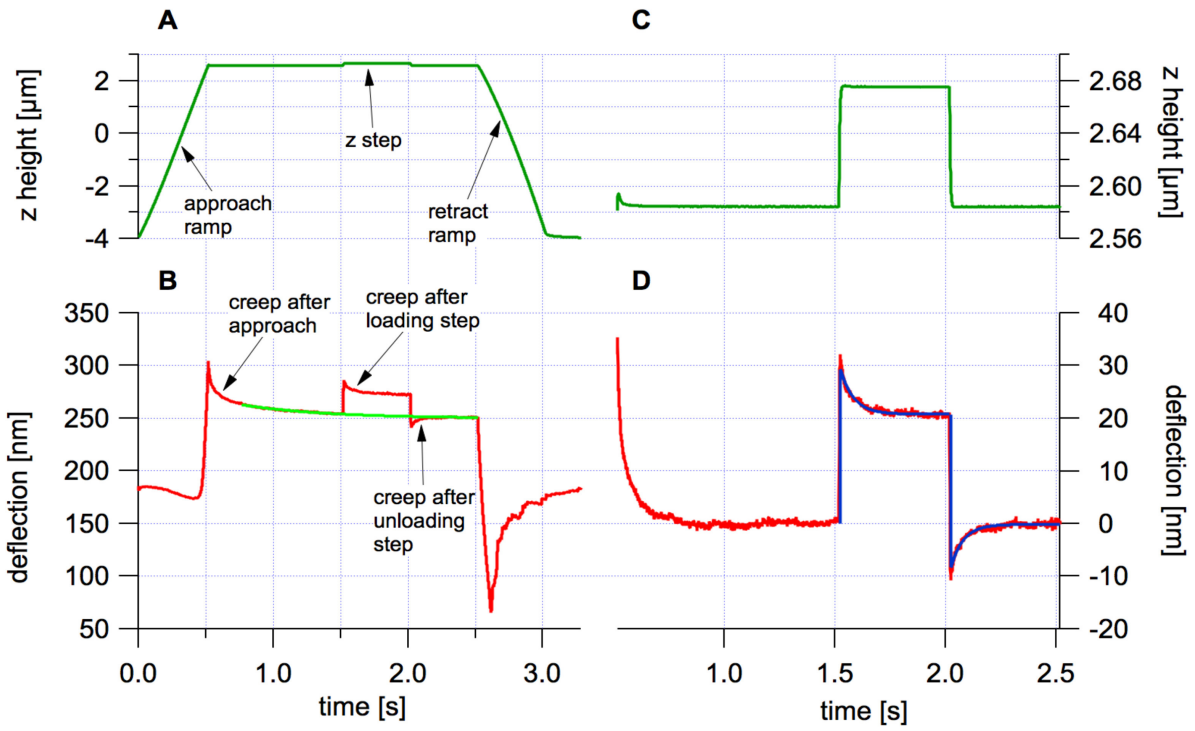

Figure 21: Typical creep response of a cell after applying a z step. Panel A shows the deflection data, while the z height is first ramped as in a conventional force curve (approach ramp), then kept constant for 2 seconds, except a small step in z-height, which is applied after the creep of the cell, caused by the approach ramp, has relaxed appreciably. Then, finally the sample is retracted again (retract ramp). After the step (applied from time 1.5 to 2.0 seconds) the creep response to the loading and unloading step is analysed in detail (see panel B & D for a zoom in). The deflection data is fitted with an exponential function, which is analysed in terms of the standard linear solid model.

Experiment type		**k, k1 [mN/m]**	**k2 [mN/m]**	**τ [ms]**	***f*** **[µNs/m]**
Force Curve	Approach	3.78			
	Retract	7.99			
z step	Loading	3.42	2.10	52.4	110
	Unloading	3.52	2.01	49.4	99.3

Table 1: Summary of spring constants of the cantilever and the spring constants of the cell sample and the viscous properties derived by analysing the force curve and the z step response data presented in Figure 3

As can be seen in table 1, the spring constant derived from the slope of the approach and retract branch of the force curve at a force corresponding to those applied during the step, deviate largely from each other, since this type of analysis does not consider any viscous contribution of the sample, but rather assumes that the response is purely elastic. Since this is definitely not the case, the numbers will be wrong by some degree and shall rather be called apparent spring constant values. On the contrary, the spring constants of the cell sample derived from the loading and unloading step are very close to each other, demonstrating that the design of this experiment (and the analysis of the data) does handle viscous properties adequately and will result in reliable numbers for the viscous properties of the cell sample. K_1 is the spring constant of the cell after creep has seized, so this should correspond to the spring constant of a force curve taking at an infinitely small loading rate, which is not possible. Not surprisingly, the spring constants of the cell sample determined from the force curve are larger than k_1. K_2 is the additional spring constant of the cell sample in the visco-elastic branch, so somehow the ratio of k_1 and k_2 measures whether the cell sample is purely elastic (k_2 should be zero then), or has both contributions. In our case in cells, k_1 and k_2 are of the same order, so cells are elastic and viscous at the same time at roughly the same proportion. The friction coefficient will be due to the internal viscosity of the cytosol, the organelles, and the cytoskeleton being pulled through the cytosol. From an experimental point of view, the relaxation time τ may be more interesting, since this sets the time scale at which viscous contributions will be apparent ($t <= \tau$) or not ($t >> \tau$). The observed relaxation time will be the most prominent, in terms of response amplitude and in terms of time scale, i.e. the longest time scale as selected by the experimental scheme and the analysis procedure. It is conceivable that in a cell, there will be many more relaxation processes at a multitude of time scales, depending to different modes of creep response, which have not been analysed or detected within the framework of this work.

In z step response a sudden change in z height is applied to the sample base, which will be transmitted through the cell and deflect the cantilever. The cantilever deflection is then slowly relaxing in a new equilibrium position, which implies that the loading force (which is proportional to the cantilever deflection) is changing. The sample deformation, which is the z-height minus the cantilever deflection, will also be changing (and relaxing slowly). See the results shown in figure 16, where the indentation during a step response has been calculated and plotted. So, this type of experiment will neither be a constant stress (i.e. constant force), nor a constant strain (i.e. constant sample deformation or constant indentation) type

experiment, as is usually used in creep experiments in soft matter physics. Thus we designed a variant of this experiment, where the sample z-height is kept constant, while a magnetic force step is applied directly to the cantilever during the dwell time (see figure 22).

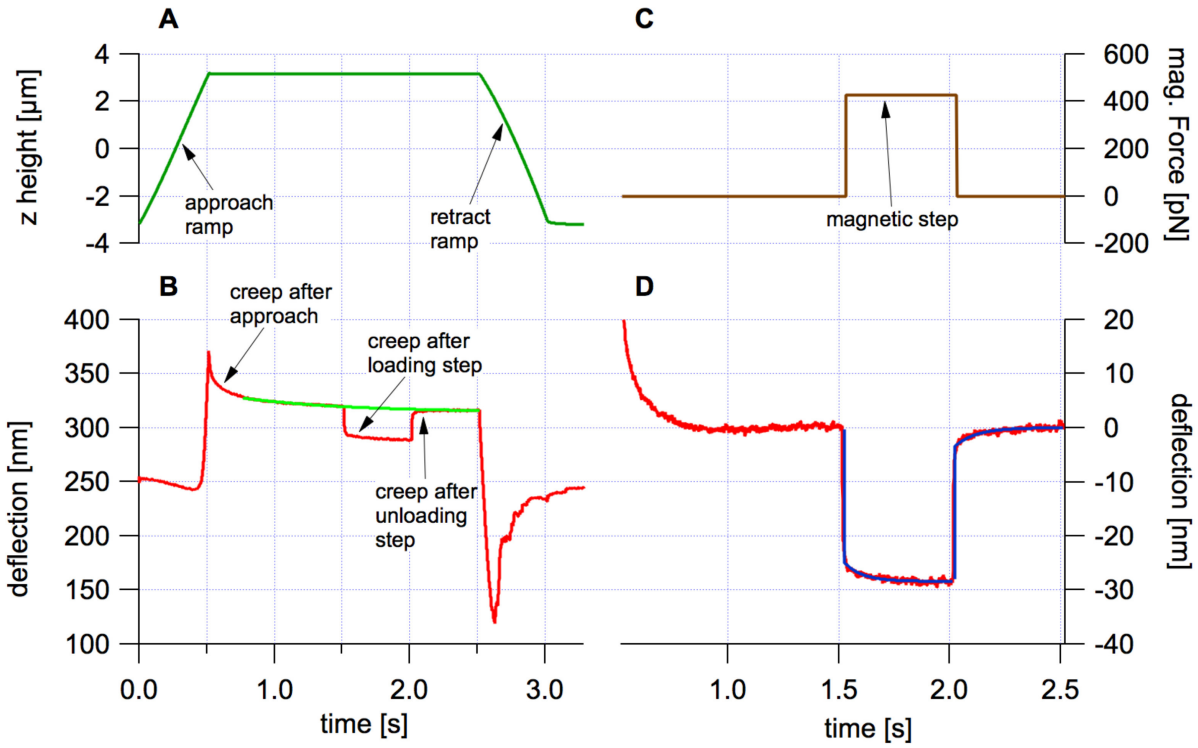

Figure 22: Creep response of a cell after a magnetic force step. Here the z height is kept constant for 2 seconds, after the approach ramp (22A and B). At time 1.5 s (after 1 second of dwell) a magnetic force is applied to the cantilever (fig. 22C), which leads to a change in indentation of the sample (Fig 22D), which in this case can be read directly from the deflection signal. As in the z-step, we can see an instantaneous jump in deflection followed with a slow creep. Here, due to the different experimental scheme, both effects go in the same direction, and thus appear to the eye very different than the equivalent creep response process in fig 21D. (same cell as in figure 21)

Figure 22 shows the response of a cell after applying a magnetic force step in contact with the cell. The experimental sequence is very similar to the z step response in figure 21. After approaching the cell the z height is kept constant now for the entire dwell time (0.5 .. 2.5 seconds) and the cantilever tip is retracted after dwell. After 1 s dwell (at t = 1.5s) a magnetic force of 400 pN is applied directly to the cantilever, which is turned off after 0.5 s (at t = 2s) (see figure 22A and 22B for the z-height and the deflection as a function of time during the entire sequence). The creep response can be observed from the deflection signal. As in the case of z step response the global creep (caused by the approach ramp of the force

curve) has to be subtracted (green line in figure 22B) to get the detrended deflection signal to be analysed further (figure 22D). We also fit a single exponential function to the deflection data after the loading (at t= 1.5s) and the unloading step (t=2.0s) of the magnetic force (Fig 22D), which is then also analysed in the frame work of the linear solid model, to get the same spring constants ($k_1 + k_2$) of the cell and the viscous quantities (f and τ) as in the case of z step. Table 2 summarizes the results of the analysis for the data presented in figure 22. As in the case of z step, we observe a large discrepancy for the spring constant values of the cell sample derived from the approach and retract force curve, but very good agreement of the viscoelastic properties derived from the loading and unloading step. As in the case of z step response, the sample indentation will be the difference between z height (which is constant in this experimental scheme) and deflection. The data presented in figure 22 have been recorded at the same cell in roughly the same area as the z step data of figure 21, except for some small drift or movement of the cell, which is inevitable during the time needed for acquiring data and switching from one mode to another (some 20 minutes in this case). Thus the numbers in table 2 are not identical but very similar to those in table 1.

Experiment type		**k, k1 [mN/m]**	**k2 [mN/m]**	***τ*** **[ms]**	***f*** **[µNs/m]**
Force Curve	approach	3.78			
	Retract	7.45			
Magnetic Step	Loading	2.86	2.08	70.2	146
	unloading	2.91	2.04	83.8	171

Table 2: Summary of spring constants of the cell (k1 and k2) and the viscous properties derived by analysing the force curve and magnetic step response data presented in Figure 22

In this work one has recorded step response data in an array of force curves (6 X 6 curves at a spacing of 100nm) to show that viscoelastic properties can be measured reproducibly by these methods. Figure 23 shows k_1 values as well as spring constant of the cell sample calculated from the approach and retract ramp of the force curve. As in the case of single force data above (figure 21, summarized in table 1) we can see that except for the spring constant values, k, calculated from the retract curves, which shows a large variation, the other quantities, and most importantly the k_1 from loading and unloading step are very accurately determined. To further stress this point, one has averaged the spring constants and the relaxation time τ determined by z step and magnetic step data for comparison in figure

24. There is some slight deviation between magnetic and z step data, although they were recorded on the same cell, however there may have been some drift or movement between the two measurements. Other possible error sources will be discussed below. Recording the entire force map took 4 minutes plus some time for switching from one mode to another. This may explain the slight deviation easily.

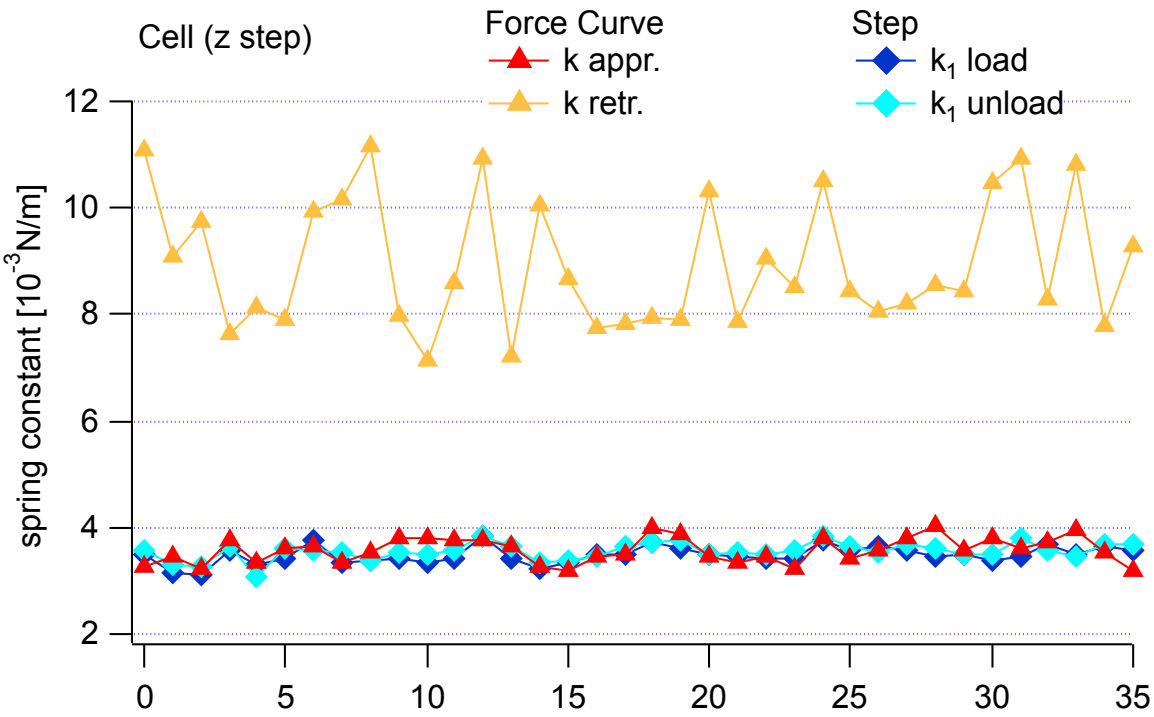

Figure 23 Comparison of spring constants of the cell sample calculated from force curve data (k approach and k retract are the values from the corresponding branch of the force curve) and from step response data (k_1 loading step and unloading step). The graph is a compilation of all 36 force curves from a 6 by 6 force volume over an area of 600nm.

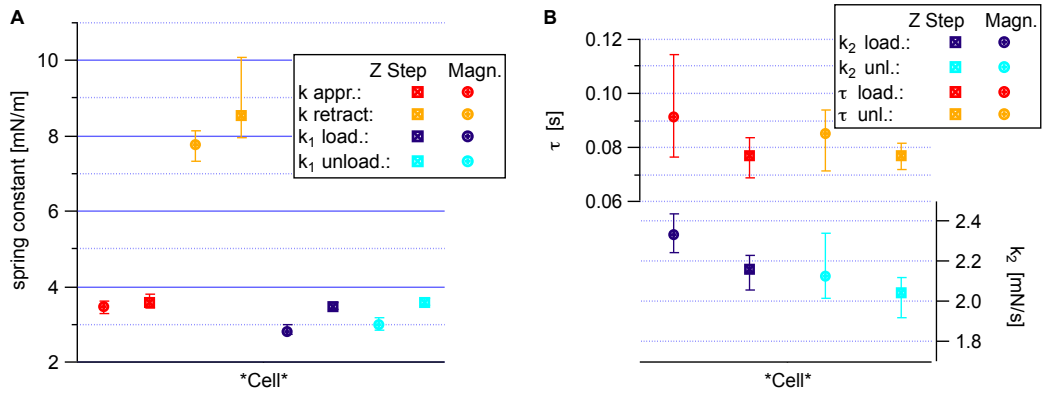

Figure 24: Spring constant (A) and viscous (B) properties of cells. The values correspond to the medians of the respective quantity from the 36 values measured in a force volume over a square area of 600nm. The spring constants derived from the step (k_1 loading and k_1 unloading) are very similar for both methods (z step and magnetic step), whereas the spring constant (k's) derived from approach and retract force curves deviate largely due to the neglect of viscous response in this type of analysis. The viscous properties (the relative strength compared to the elastic properties is measured by k_2, whereas τ is the relaxation time) are also determined reproducibly in both step methods (z step and magnetic) for loading and unloading steps.

Figure 25 shows the creep response of a cell, when applying a step in the z-height. The cell sample is loaded in a conventional fashion until the preset loading force (approach ramp) and then kept constant for two seconds except for the small well defined loading step in the z-height that was applied after the creep caused by the approach ramp had relaxed considerably. A 100nm in deflection typically corresponded to about 1 nN of the loading force. A modulating force was applied by attaching a small magnetic particle to the very end of the cantilever. The force in magnet modulates the force on the tip end of the magnetic cantilever, which will transmit a modulating indentation to live cells (see the results in figure 26). Due to the visco-elastic properties of the cell sample, we observed a large creep after the approach ramp-of the loading curve. This first (and large) creep response is very challenging to treat analytically. The figure 26 illustrates the derived spring constants and the amplitude rations after a force modulation experiment obtained by AFM magnetic force modulation. In different regions of the soft sample the amplitude indicates both the type of contact and the position of the cantilever. The shows the usefulness of the complimenting the technique for the measurement of the viscoelastic properties of the cell and gel sample.

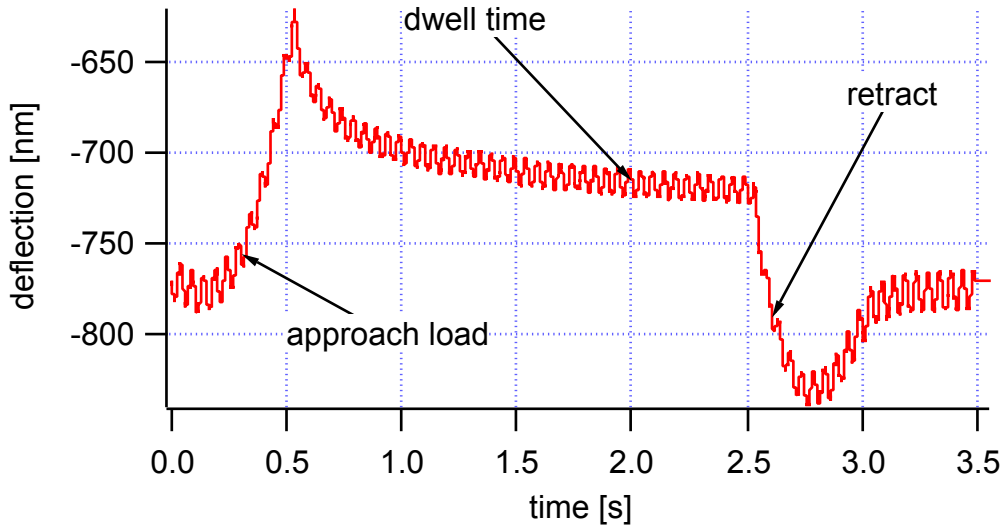

Figure 25: Representative stress relaxation data on a cell sample from force modulation experiment. The upper panel shows the z height profiles versus the time. The z-motion was stopped (t = 0.5 seconds) and the direction reversed after 2 seconds. During this time the stress relaxation after the approach ramp of the cell has relaxed considerably.

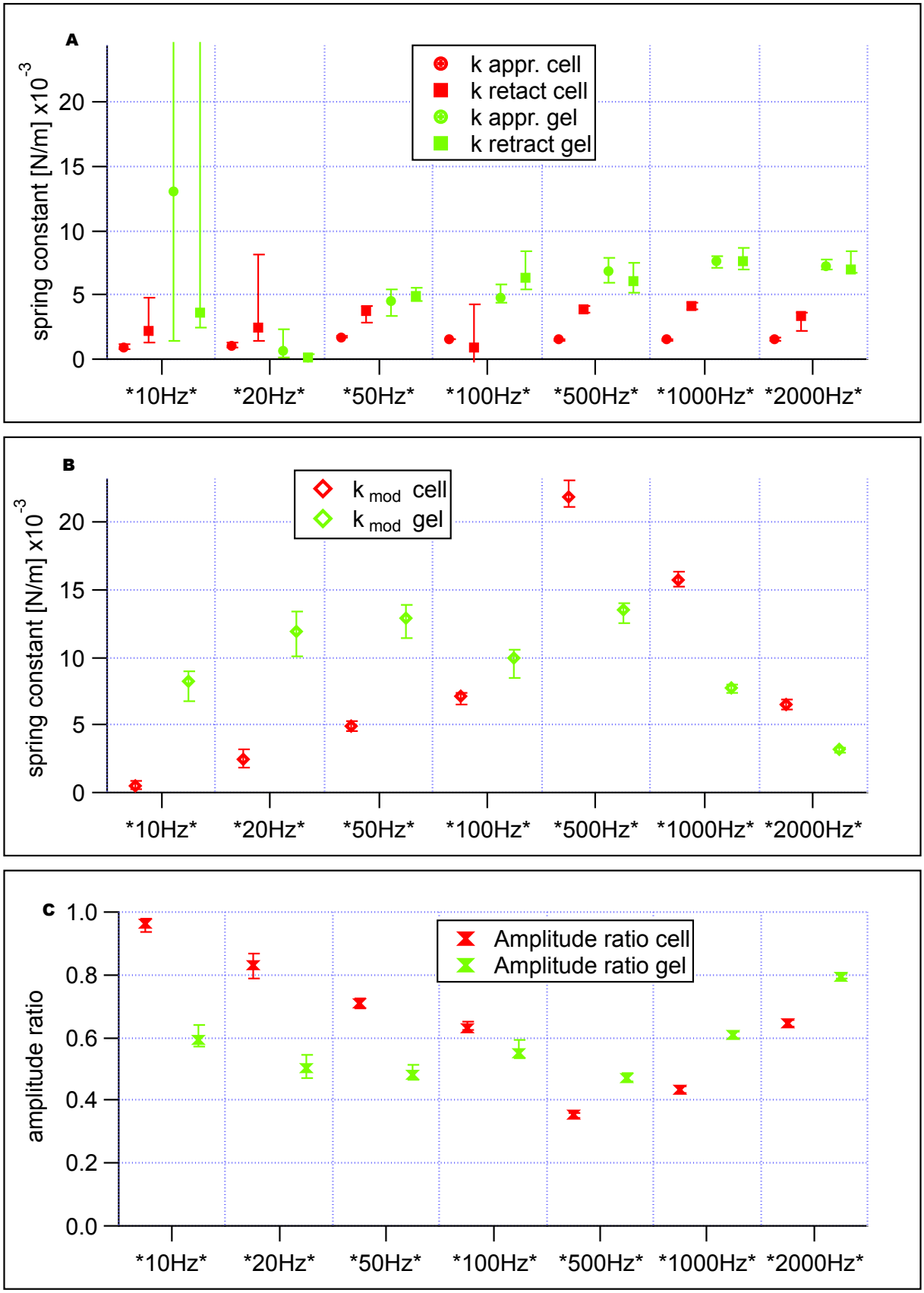

Figure 26: The deduced effective spring constants (figure A and B) and the response amplitudes ratio (C) for different frequencies during a force a modulation. The spring constants were measured in the part of the FC after the creep had relaxed. Figure represents the median values amplitude as the magnetic cantilever was oscillated over physiological relevant frequency range acquired on the cell sample and gel sample.

5.0 DISCUSSION

This is the discussion section. In this work, the creep response of soft gel and cell samples after applying a step in loading force by means of magnetic fields has been directly measured by AFM. Besides analysing the creep data with the standard linear solid model, we can quantify the viscous and elastic properties of soft samples we prove that the AFM can be employed to measure the visco-elastic property of living cells.

Hydrodynamic drag of cantilever

The viscoelastic properties of cells by recording the creep response have been analysed after applying a z-step or a magnetic force step. Both types of creep data were analysed in the framework of the linear solid model (figure 9), which is a combination of two springs and one dashpot. This is the simplest model, which reproduces the observed creep response data. The AFM cantilever has been modelled just by its spring constant, neglecting hydrodynamic damping of the moving cantilever. Thus is justified to consider hydrodynamic effects of the cantilever to be small compared to the sample viscous contribution. This assumption was tested by looking at the creep response of polyacrylamide gels under the same experimental conditions. On the gel one only sees very little creep after applying a step. Some creep is visible after the approach ramp, which applies a much larger force than the subsequent steps applied here. On gels, one is not able to separate the hydrodynamic contribution of the cantilever and the viscous contribution of the sample. However, one can consider the combined viscous effect in the gel experiment as an upper limit for hydrodynamics in the cell experiments. And since this combined viscous effect is much smaller than in cells, we can safely say that the predominant viscous effect in cells comes from the sample and hydrodynamics can be neglected in cell data.

Error sources in step response data

Besides systematic errors (like tip shape, changes in cells induced by temperature or pH changes, and so forth), the major experimental error will come from the accuracy of deflection calibration. By measuring force curves on the bare substrate, we have observed that variations in slope of the force curve can be around 5..10% despite the fact that force curves on a stiff support shall have a value of 1. This problem is very serious when

investigating cells, since in cell samples even bare areas of the substrate are coated to some degree with extra-cellular matrix material excreted by cells. But even on ultra-clean samples (like carefully cleaned glass slides) a similar, maybe slightly smaller variation, of slope values is observed. In these samples the effect may be due to tip contamination, stick-slip motion of the tip along the substrate, or other sources. Let's assume that the deflection calibration is off by p per cent or some factor e = 1 + p (which will typically be on the order of 0.95 to 1.05 corresponding to a 5% error). The spring constants have been calibrated by recording thermal fluctuations of the free cantilever, where the calibration of the power spectral density will then be proportional to e^2. The spring constant will be inverse proportional to the PSD, so it will be off by a factor of $1/ e^2$. Any mechanical measurements, regardless whether it is based on the slope of the force curve, or step response, will eventually boil down to a relation where the sample spring constant k_s is proportional to the ratio of loading force and indentation. In AFM the indentation is given by the difference between z height and deflection. The exact relation may look different (see the analysis section), but for the sake of error propagation, one can write a kind of archetypical equation:

$$k_s = \frac{\Delta F}{\Delta \delta} = \frac{k * \Delta d}{\Delta z - \Delta d}$$

Since the change in deflection is much smaller than the change in z (in case of a z step on cells since the slope is on the order of 1/10), one can neglect the error in the denominator, so the total deviation of the elastic properties in z step will be proportional to 1/e, or also p per cent.

In magnetic step, Δz is zero, so the errors in Δd will cancel, and we will end up with an error of $1/e^2$, which will be proportional to 2*p, if p is small.

So, magnetic step response will be more prone to errors in deflection calibration. However, if calibrated cantilevers can be used, e.g. those where the spring constant had been measured with the help of a vibrometer, then the only error would be in the deflection signal, which would actually cancel.

Change in Contact Area during Step

The rationale behind the experiments reported here assumes that the sample reacts linearly while applying a step. This requires that the force applied, and the indentation change resulting from that force, is small such that the mechanical properties do not change

considerably. This may not always be given, especially with highly structured samples like cells. The consequence is to increase the force sensitivity as much as possible to be able to apply very small force steps. Since the main limitation in current state of the art AFMs is not instrumental noise, but rather thermal noise in the cantilevers, it is essential to use very soft cantilevers. For the cantilevers used here, thermal noise levels will be around 7 pN. One has used here the softest cantilevers available for cell work, however it would be favourable if softer cantilevers will become available.

When applying a force step, the indentation and hence the contact area between a pyramidal tip and the sample is changing. This will lead to a change in contact spring constant. In our case a typical indentation change was 70 nm for z-step, and 30 nm for a magnetic step, whereas the indentation before the step was applied was about 700 nm in both cases. So, the change in contact area will be 10% for z-step and less than 5% in the case of magnetic step. This will lead to a systematic error in spring constant values of the sample. This situation can be improved by applying smaller steps, if force sensitivity is sufficient. Even better, is the use of blunt (e.g. cylindrical) tips, which will result in a constant contact area regardless of applied force. This has been suggested by Rico et al [98] however these tips are not commercially available despite their merits for mechanical measurements.

Comparison of step response data and force curve data

When recording a force curve one constantly changed the z height, while the sample is indented. Therefore, one basically apply a continuous series of little steps, each will cause a relaxation over a time scale of the observed relaxation time. The observed viscous effect will be the superposition of the individual creep response, where retardation has to be taken into account. Since force-loading rate is changing constantly during the approach rate, there is no simple way to disentangle spring constants of the cell and viscous contributions in force curves. Thus, usually force curves are only analysed in terms of elastic properties, which inevitably leads to different values for approach and retract ramps, as can be seen in tables 1 & 2. Analysing step response data with the help of the linear solid model will not only result in identical spring constants of the soft sample for loading and unloading, but it also will quantify the viscous response of the sample in terms of the friction coefficient and the relaxation time τ. This is a major improvement compared to the previous conventional way of taking force curve data and analysing them only in terms of apparent elastic properties.

The mechanical data in Table 1 and 2 agree reasonably well, as can be expected from subsequent measurements on cells. Even if technically they have been taken on the same position, there is always motion and shape changes of cells going on, so that you cannot expect exactly identical numbers here. On gels, which are stable and very homogenous, we were able to achieve results, which were reasonably close together (5-10%).

Comparison of z step and magnetic step data

In soft matter physics creep experiments are usually done after applying a well-defined step in force and keeping the applied spring constant (constant stress) and monitoring the creep in strain (corresponding to indentation in our experiment), or operating at a constant strain (after applying a jump there) and following the creep response. Our experimental condition is neither constant strain nor constant stress, since both quantities (force being proportional to deflection and indentation) change. However, as long as the material acts linearly, which needs to be assumed anyhow in the framework of our analysis, we can deal with strain and stress being not constant. The analysis presented in the material methods is based on the actual experimental conditions.
Nevertheless, the magnetic force step approach was designed, to come closer to a constant stress situation. In this approach one does not change the z-height but apply an additional force directly to the tip of the cantilever by a magnetic field. However, since this additional force will indent further the sample, we also see a creep in the deflection. So, again one is not at a constant stress situation, but somewhat closer. AFM would allow keeping deflection constant by adjusting the z height of the sample. Since the response of the system is rather slow, it would interfere with the relaxation times we observe in cells. Thus, a rather simple approach has been used in this work.

Multiple Relaxation times

You would expect that complicated soft matter like the cytoskeleton of the cell will exhibit multiple relaxation times, which will be linked to different molecular or physical processes, like friction of the cytosol, like internal friction in the bending of actin filaments, or the time scale of the activity of myosin cross-linkers, just to mention a few. This will ask for a more complicated model as the general linear solid model, which will have multiple Maxwell elements, one for each relaxation time. Here, one wanted to follow Ockam's razor and try to

use the simplest model, thus implementing only one relaxation time. Since this model fits the data very well, one does not see a need to extend our model, since this will only introduce additional parameters, which cannot be linked easily to molecular or physical processes. In the future, or in different experimental conditions, it may be essential to extend the model used for analysis.

When looking carefully on our creep response data (e.g. in figure 21 and 22) we can clearly see evidence of slower (beyond 0.5s) and faster timescales (below 10 ms). For the very slow processes, it is probably more appropriate to term them active motion or shape changes of the cell, than mechanical creep. They are not caused by the step applied to cell, but occur always in a more random or not predictable fashion as would be expected from active cellular processes. So, one did not follow and record the processes over longer times than 0.5 seconds, since they are due to other processes. The faster processes, which are visible where the exponential fit does not match nicely the data for times close than 5ms to the step, may very well be analysed within the framework of mechanical response of the cells. However, since our soft cantilevers have response times on the order of 1 ms, one do not have the appropriate time resolution to analyse these processes. This, in essence, lead one to focus only on a single exponential fit.

Comparison with other data

The focus of this work was to evaluate two different schemes for measuring the creep response of living cells by AFM. Therefore, we have presented our results as model free as possible, i.e. using the simplest mechanical circuit, which needs to be employed to describe our data. Calculating spring constants of the cell or gel (and dynamic viscosities) will reflect to some part sample properties, but will also depend on tip geometry, or more precisely to contact area. In conventional force curves, usually the Hertz model (or its variants) is used to get the material's properties (like Young's modulus) from the raw data. This can also be done from step response data, and will be reported in another publication [37]. However, since the Hertz model requires several assumptions (homogeneity, isotropy, linearity of the material, large thickness of sample), which are all questionable to some degree, one would rather omit these issues here in the context of this work. Along the same line, in cell rheology often more complicated models as the standard linear solid model are used, e.g. power law behaviour. Again, this applies to assumptions; specifically, here a power law behaviour can be expected by the superposition of an (infinite) number of relaxation processes, each of which will be characterized by its own spring constant and relaxation time. There will be a

general relation between the relaxation time and the length scale of these modes, both increasing in a correlated fashion. One believes, that in the data, since we are measuring the slowest modes of cellular mechanics, one is at the extreme end of a (otherwise) continuous spectrum, and thus the application of a power law behaviour may questionable again.
In future work, one will look into differences in visco-elastic properties of cells and to elucidate the role of certain molecular components of the cytoskeleton (actin, myosin, cross linkers, adhesion sites) and their role in viscoelasticity.

6.0 CONCLUSIONS AND OUTLOOK

In this work the viscoelastic properties of live cells with a new experimental approach inspired by polymer rheology has been measured: steps in forces either induced by changing the sample height or applying a magnetic force to the end of the cantilever. Although both approaches are not equivalent with constant strain or constant creep response experiments used in soft matter physics, they can be analysed in the framework of linear elastic theory to yield elastic and viscous properties of the sample. This is a major improvement in comparison to standard force curves, which clearly show the influence of viscous properties, by the difference of approach and retract curves, however usually they are not (cannot easily be) analysed to include this viscous response. If analysed in the standard way, the spring constants derived from force curves will deviate for loading and unloading, and shall rather be called apparent spring constants. The spring constants of the cell and the viscous properties derived from the loading and unloading step are identical, even with experimental errors, and thus reveal in quantitative and reliable manner the true viscoelastic properties of cells.

Although it has been shown in this work that soft magnetic cantilevers could be employed to measure the viscoelastic creep response of the soft samples like cells accurately the work will be improved if different a forms of magnetic materials will be employed in the future. For the controlled movements of the loading and unloading step forces in magnet the soft spring cantilevers have been made more sensitive by equipping them with permanent magnetic fragments to measure the creep response of the live cells and polymer gels. However, the magnetic step response AFM experiments performed in this work have not been achieved with the available smallest ferromagnetic materials. The geometries of the

magnetic fragment glued to the back of the soft spring cantilevers typically unknown, which leads to complications in the orientation of the step forces in magnet especially the mechanical properties. These magnetic responses for the various cantilevers differ greatly in strength. However, the results in this work demonstrate the usefulness revealing the creep response while employing the soft spring magnetic cantilevers to loading and to unload the of cell samples. The current work has not been performed with the smallest available ferromagnetic materials. There is lack of information about the spring constant and the mass of the employed cantilever. One will like to employ for the future preferably a smaller ferromagnetic particle in the order of a micron. As a good alternative magnetosomes could be employed because they are small and they are closer to a perfect ferromagnetic material. For this reason, the soft spring cantilevers could be prepared in the future with the magnetic materials like the magnetosomes. More interestingly, the Hertz model might prove to be more useful in a future work, if it is included to the mechanical equivalent circuit presented in this work to fit and hence derived the material properties of the soft samples like cells.

APPENDIX

A1 Spring constant of the sample derived from force curves

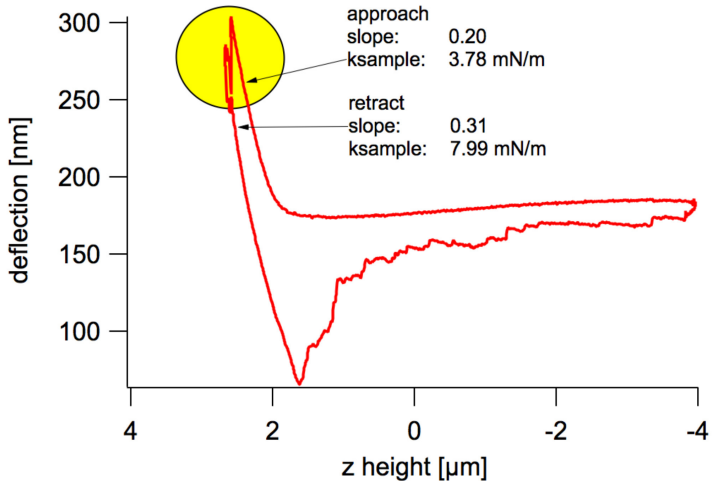

Figure 27: Force curve on a cell while at maximum force a z step is performed (see yellow circle). The figure shows the same data as in figure 3, here in the conventional scheme of deflection versus z height as is usually done in force curves. The slopes and the corresponding spring constants of the sample, which can be calculated from the approach and retract part of the data are also indicated in the annotation.

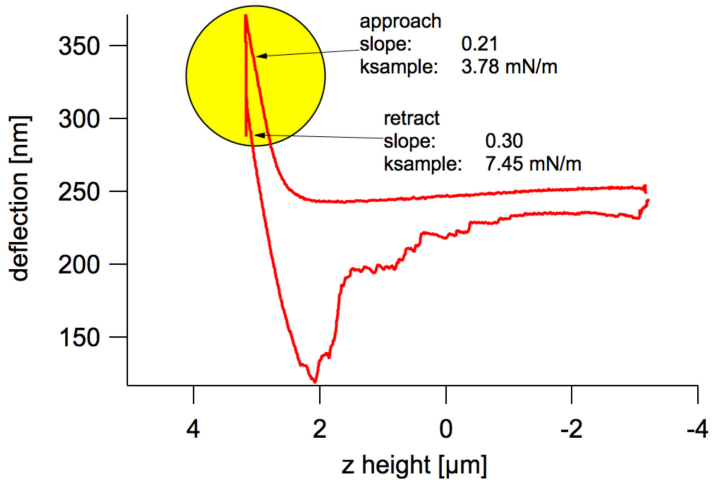

Figure 28: Force curve on a cell while at maximum force a magnetic step is performed. The figure shows the same data as in figure 4, here in the conventional scheme of deflection versus z height as is usually done in force curves. Since in a magnetic step, only the deflection changes due to the magnetic force (z is kept constant) the effect of the step is harder to see than in fig S1. The slopes and the corresponding spring constant of the sample, which can be calculated from the approach and retract part of the data are also indicated in the annotation.

A2 Analysis of Creep Response Data from z steps and magnetic step on gel sample

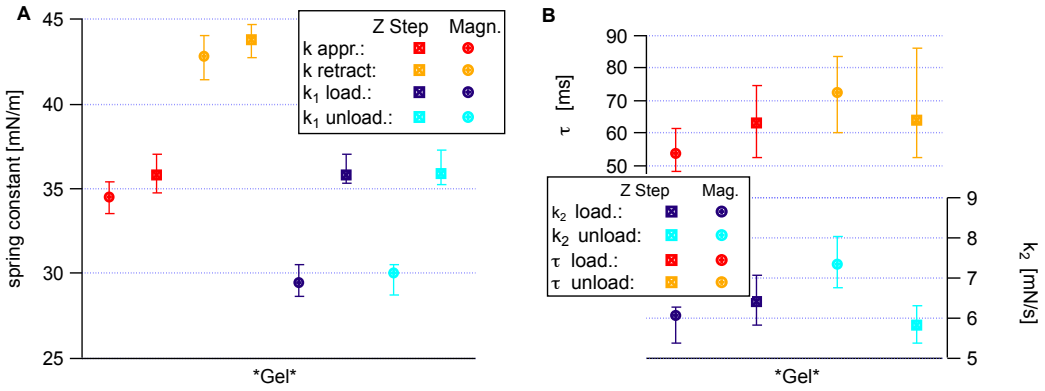

Figure 29: Analysis of step response data on polyacrylamide gels. Panel A shows a comparison of spring constant value calculated from approach and retract curve with the spring constant k_1 values from step response. Panel B shows the creep response time and the spring constant of the sample k_2 values. All values are very close for unloading and unloading, except the approach and retract data calculated from the force curves, as expected.

A3 The magnetic coil

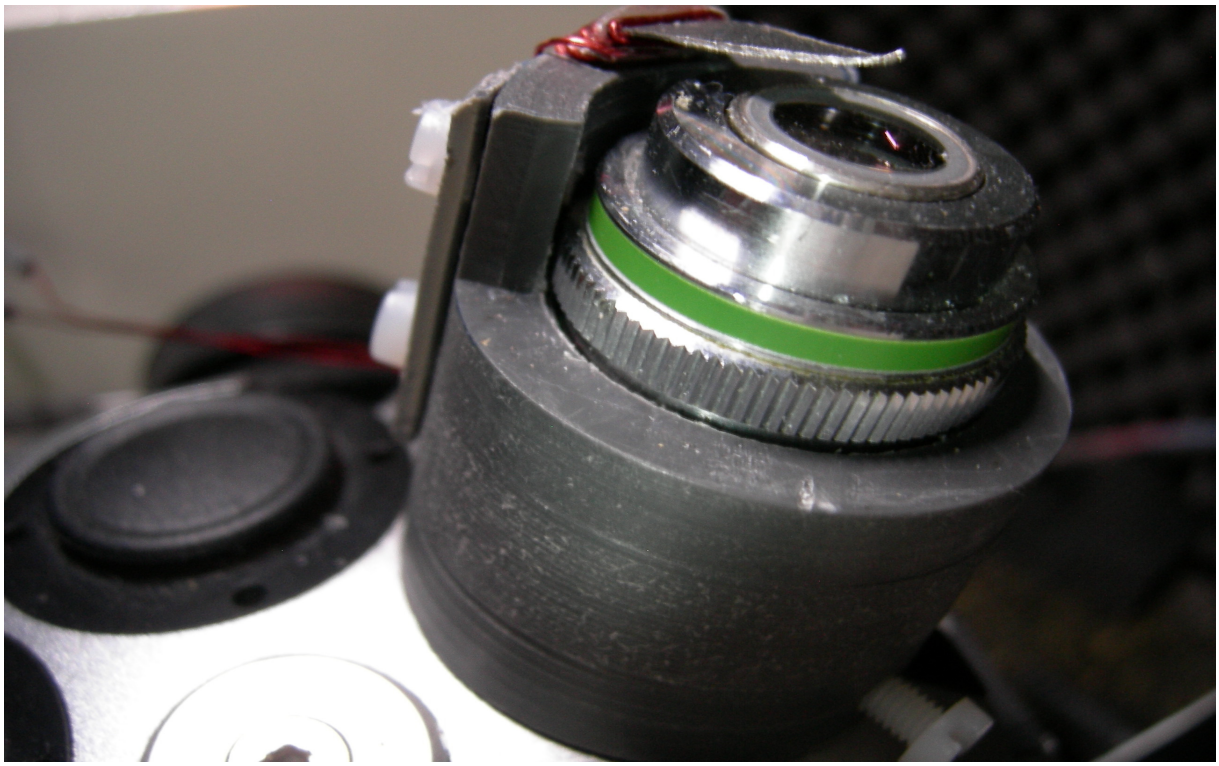

Figure 30: Setup of the magnetic coil used for loading magnetic particles via the external magnetic fields. Image shows a side view of magnetic adapted on the 20 X objective lens of the AFM. The image shows the strip of the sharp transformer metal core with copper wire windings. The core material aided to create the large gradient of the magnetic field.

A4 Elastic and viscous properties of the cell and the gel sample derived from the magnetic step and the z step response experiments

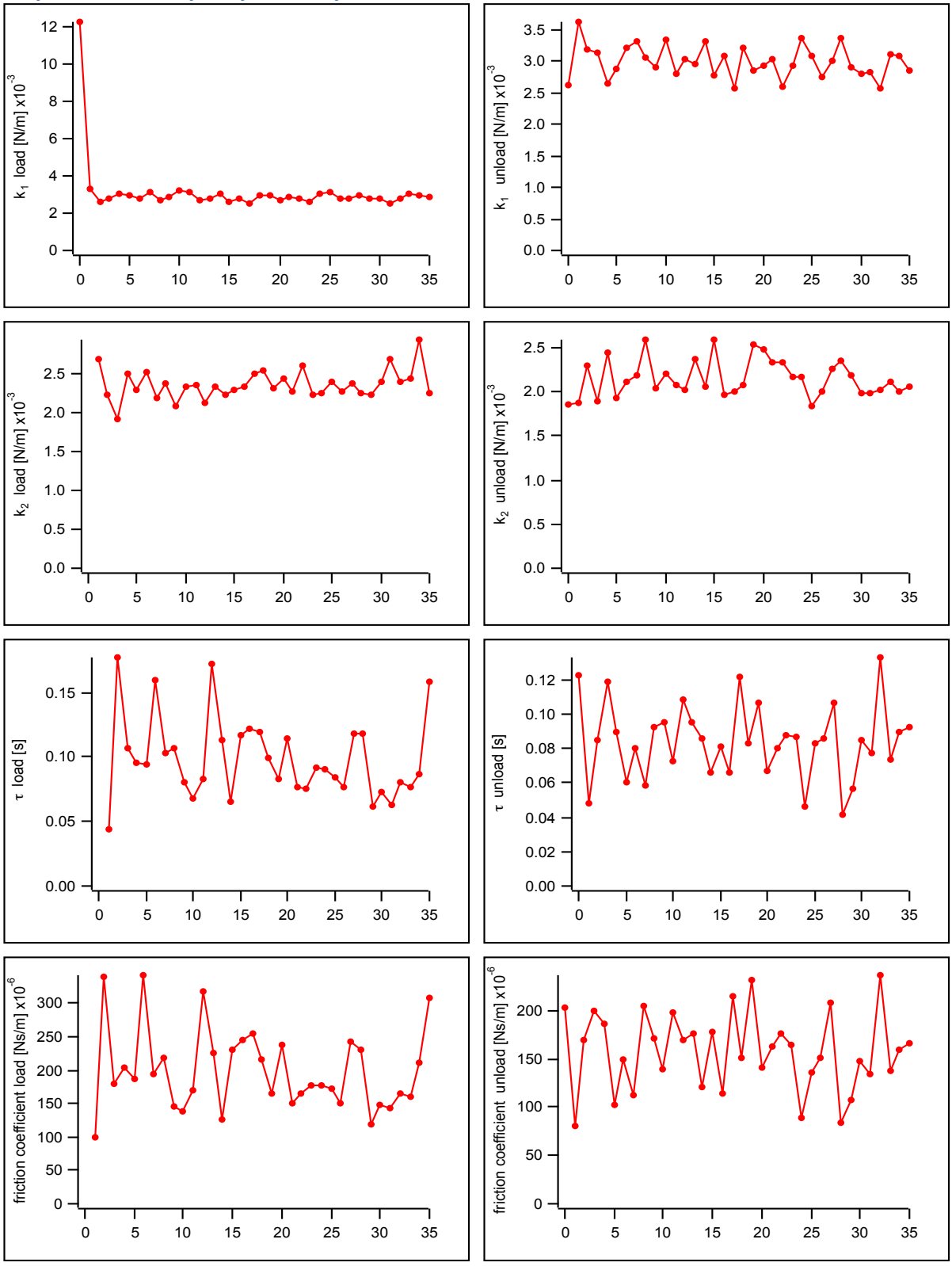

Figure 31: Spring constants and viscous values obtained after a magnetic step response on the cell sample. The loading (left panel) and unloading (right panel) values were obtained by analysing the creep data after the approach ramp of the force curve. The graph is a compilation of all 36-force curves (6 by 6 force volume) over an area of 600 nm.

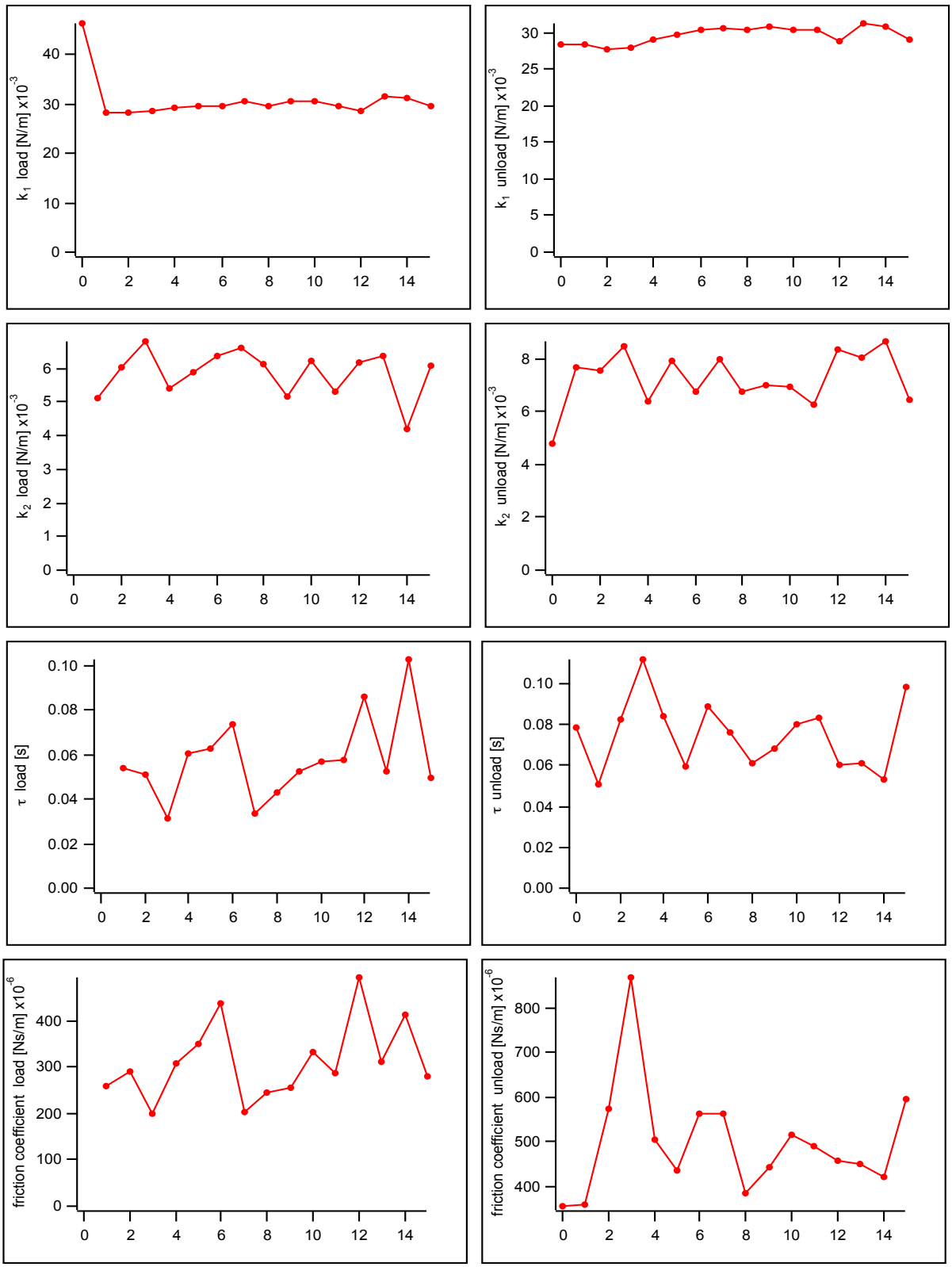

Figure 32: The spring constants and viscous values obtained from the z step response data on polymer gel sample. The stiffer cantilever was employed. The loading (left panel) and unloading (right panel) values were obtained by analysing the creep data after the approach ramp of the force curve. The graph is a compilation of all 16-force curves (4 by 4 force volume) over an area of 600 nm.

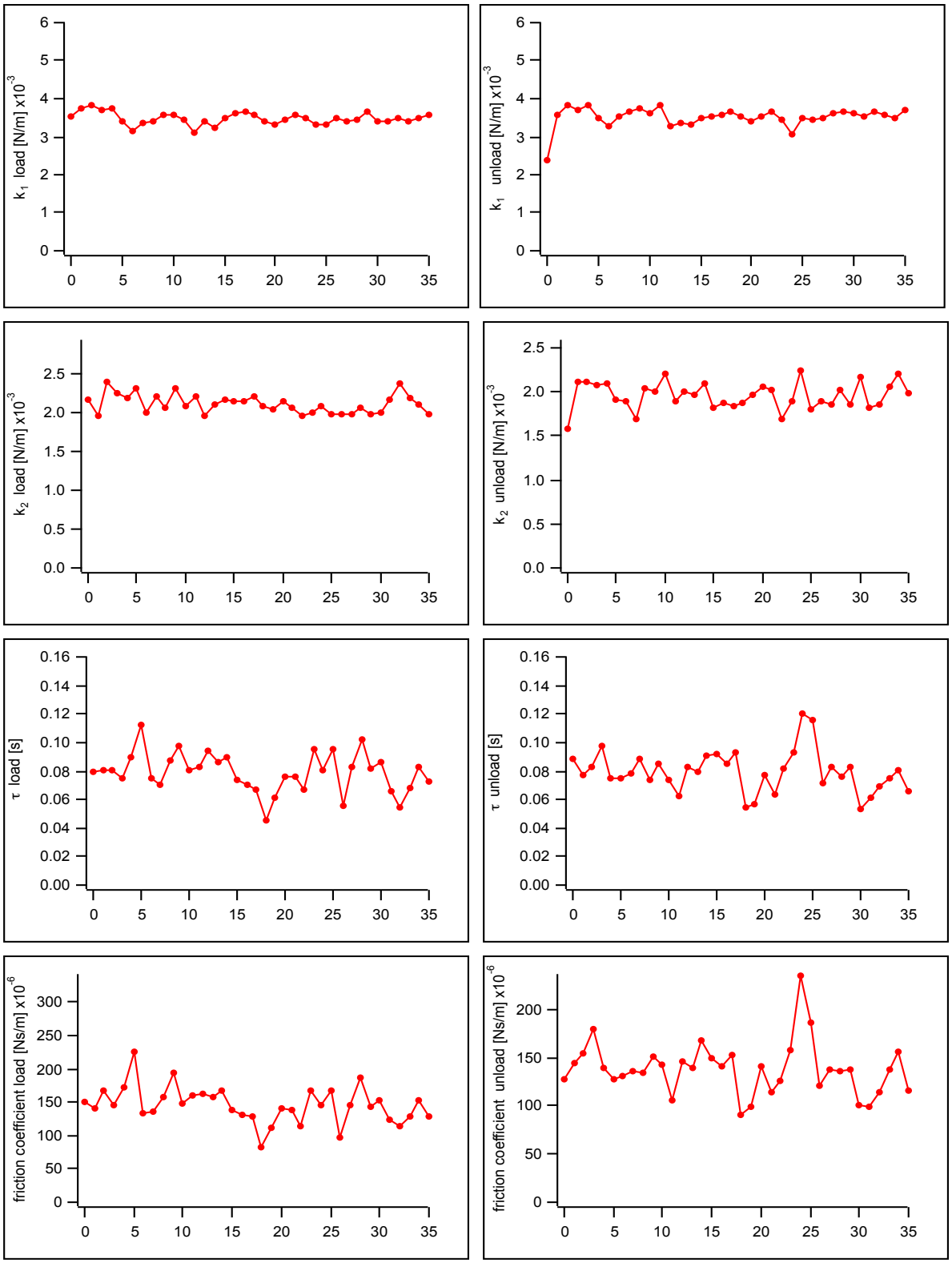

Figure 33: The spring constants and viscous values of the cell sample obtained from a z step response. The loading (left panel) and unloading (right panel) values were obtained by analysing the creep data after the approach ramp of the force curve. The graph is a compilation of all 36-force curves (6 by 6 force volume) over an area of 600 nm.

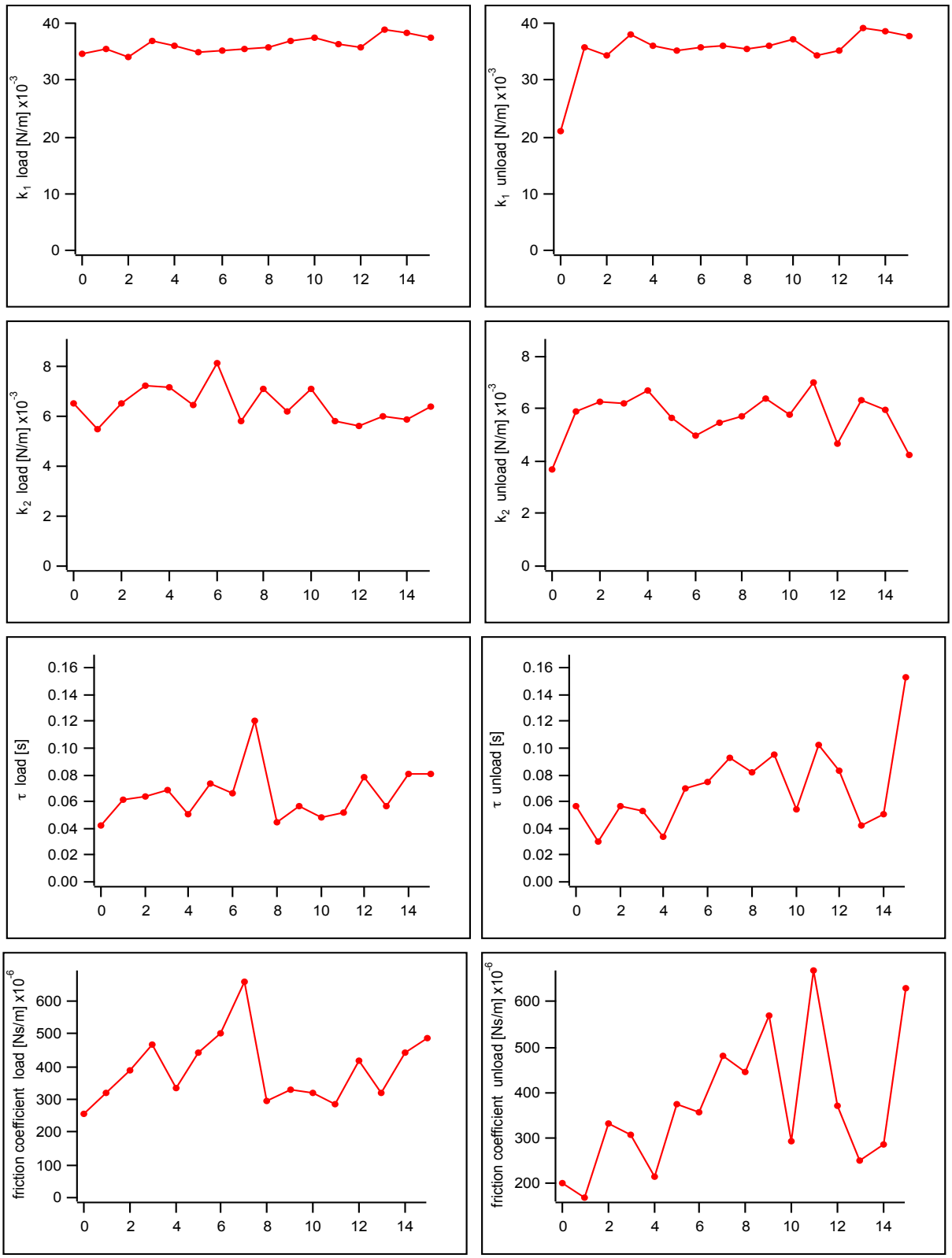

Figure 34: Spring constants and viscous values obtained from a magnetic step response data on gel sample derived after the approach ramp of the force curve. The loading (left panel) and unloading (right panel) values were obtained by analysing the creep data after the approach ramp of the force curve. The graph is a compilation of all 16-force curves (a 4 by 4) force volume. The panels have been zoomed in for better visibility

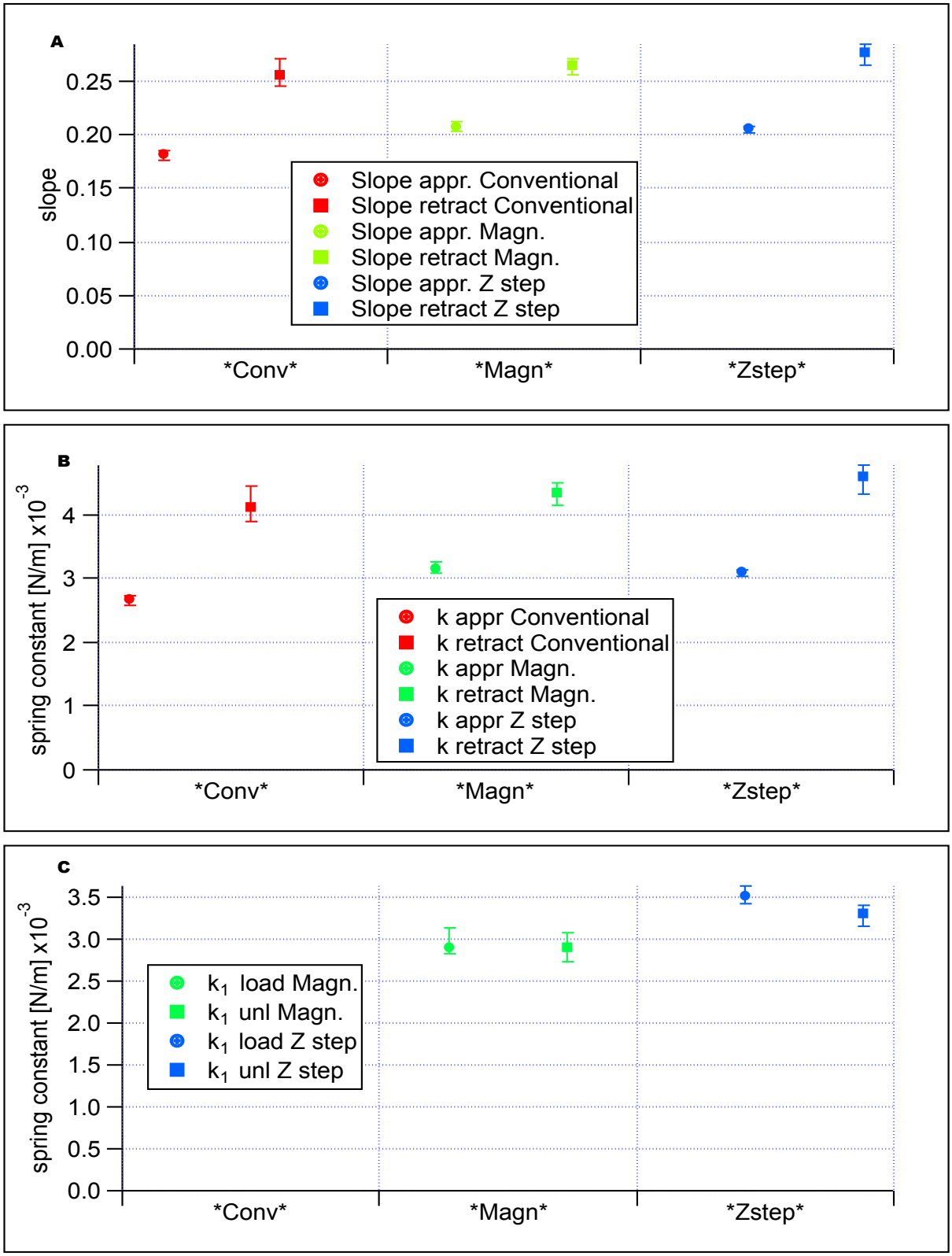

Figure 35: The cell samples spring constant and the slopes after applying a step in loading force by means of modulated ramping while in contact, the magnetic force and z step. It illustrates the usefulness of the complimenting the AFM technique. Comparison of the spring constants of the sample after a AFM force modulation in magnet compared on a cell sample. The spring constant of the cell sample is obtained by analysing the creep data after the approach ramp of the force curve (Conv.). The graph is a compilation of all 36 force curves each from a 6 by 6 force volume over an area of 600.

BIBLIOGRAPHY

1. Binnig, G., C.F. Quate, and C. Gerber, *Atomic force microscope.* Physical review letters, 1986. **56**(9): p. 930.
2. Bhushan, B. and H. Fuchs, *Applied scanning probe methods VII*. 2007: Springer.
3. AZONANO. *Atomic Force Microscopy and Using It for Investigating Gene Delivery Vehicles*. 2006, 05, 12 [cited 2015; Available from: https://www.azom.com/article.aspx?ArticleID=3278.
4. Lekka, M., et al., *Cancer cell recognition–mechanical phenotype.* Micron, 2012. **43**(12): p. 1259-1266.
5. Lekka, M. and P. Laidler, *Applicability of AFM in cancer detection.* Nature nanotechnology, 2009. **4**(2): p. 72-72.
6. Lekka, M., et al., *Cancer cell detection in tissue sections using AFM.* Archives of biochemistry and biophysics, 2012. **518**(2): p. 151-156.
7. Lekka, M., et al., *Elasticity of normal and cancerous human bladder cells studied by scanning force microscopy.* European Biophysics Journal, 1999. **28**(4): p. 312-316.
8. Martin, Y., C.C. Williams, and H.K. Wickramasinghe, *Atomic force microscope–force mapping and profiling on a sub 100 ‐Å scale.* Journal of Applied Physics, 1987. **61**(10): p. 4723-4729.
9. Martin, Y. and H.K. Wickramasinghe, *Magnetic imaging by "force microscopy"with 1000 Å resolution.* Applied Physics Letters, 1987. **50**(20): p. 1455-1457.
10. Cappella, B., *Physical Principles of Force–Distance Curves by Atomic Force Microscopy*, in *Mechanical Properties of Polymers Measured through AFM Force-Distance Curves*. 2016, Springer. p. 95-230.
11. Radmacher, M., M. Fritz, and P.K. Hansma, *Imaging soft samples with the atomic force microscope: gelatin in water and propanol.* Biophysical journal, 1995. **69**(1): p. 264.
12. Braga, P.C. and D. Ricci, *Atomic force microscopy: biomedical methods and applications*. Vol. 242. 2004: Springer Science & Business Media.
13. Bruker. *MLCT - Bruker AFM Probes*. 2016; Available from: http://www.brukerafmprobes.com/p-3444-mlct.aspx.
14. Ohler, B., *Practical advice on the determination of cantilever spring constants.* Application Note AN94, Veeco Instruments Inc, 2007.
15. Butt, H.-J., M. Jaschke, and W. Ducker, *Measuring surface forces in aqueous electrolyte solution with the atomic force microscope.* Bioelectrochemistry and Bioenergetics, 1995. **38**(1): p. 191-201.
16. Butt, H.-J., B. Cappella, and M. Kappl, *Force measurements with the atomic force microscope: Technique, interpretation and applications.* Surface science reports, 2005. **59**(1): p. 1-152.
17. Hillier, A.C., S. Kim, and A.J. Bard, *Measurement of double-layer forces at the electrode/electrolyte interface using the atomic force microscope: potential and anion dependent interactions.* The Journal of Physical Chemistry, 1996. **100**(48): p. 18808-18817.

18. AZONANO. *Fundamentals of Contact Mode and TappingMode Atomic Force Microscopy*. 2012, 18, 05; Available from: https://www.azonano.com/article.aspx?ArticleID=3010.
19. Hutter, J.L. and J. Bechhoefer, *Calibration of atomic‐force microscope tips.* Review of Scientific Instruments, 1993. **64**(7): p. 1868-1873.
20. Sader, J.E., et al., *Method for the calibration of atomic force microscope cantilevers.* Review of Scientific Instruments, 1995. **66**(7): p. 3789-3798.
21. Butt, H.-J. and M. Jaschke, *Calculation of thermal noise in atomic force microscopy.* Nanotechnology, 1995. **6**(1): p. 1.
22. Feynmann, R. *Lennard Jones* 2015, February 4; Available from: LennardJones.png&imgrefurl=http://www.atomsinmotion.com/book/chapter5/md&h=422&w=600&tbnid=6DR1r7LpWBx2bM:&zoom=1&tbnh=90&tbnw=128&usg=__Q4ZLANgGBeVoVKRoc719d1rGdbM=&docid=bt2Ent88N_ADjM&sa=X&ei=NsDRVOqQKczraqf5gtAJ&ved=0CDsQ9QEwBQ.
23. Fischer-Cripps, A.C., *Introduction to contact mechanics*. 2000: Springer.
24. Cappella, B., *Physical Principles of Force–Distance Curves by Atomic Force Microscopy*, in *Mechanical Properties of Polymers Measured through AFM Force-Distance Curves*. 2016, Springer. p. 3-91.
25. Rico, F., et al., *Probing mechanical properties of living cells by atomic force microscopy with blunted pyramidal cantilever tips.* Physical Review E, 2005. **72**(2): p. 021914.
26. Rico, F., et al., *Nanomechanics of lung epithelial cells.* International journal of nanotechnology, 2005. **2**(1-2): p. 180-194.
27. Gavara, N. and R.S. Chadwick, *Determination of the elastic moduli of thin samples and adherent cells using conical atomic force microscope tips.* Nature nanotechnology, 2012. **7**(11): p. 733-736.
28. Rotsch, C. and M. Radmacher, *Drug-induced changes of cytoskeletal structure and mechanics in fibroblasts: an atomic force microscopy study.* Biophysical journal, 2000. **78**(1): p. 520-535.
29. Schäfer, A. and M. Radmacher, *Influence of myosin II activity on stiffness of fibroblast cells.* Acta Biomaterialia, 2005. **1**(3): p. 273-280.
30. Rianna, C., et al. *Cell mechanics as a marker for diseases: Biomedical applications of AFM*. in *AIP Conference Proceedings*. 2016. AIP Publishing.
31. Kumar, S. and V.M. Weaver, *Mechanics, malignancy, and metastasis: the force journey of a tumor cell.* Cancer and Metastasis Reviews, 2009. **28**(1-2): p. 113-127.
32. Prabhune, M., et al., *Comparison of mechanical properties of normal and malignant thyroid cells.* Micron, 2012. **43**(12): p. 1267-1272.
33. Alcaraz, J., et al., *Microrheology of human lung epithelial cells measured by atomic force microscopy.* Biophysical journal, 2003. **84**(3): p. 2071-2079.
34. Andreu, I., et al., *Heterogeneous micromechanical properties of the extracellular matrix in healthy and infarcted hearts.* Acta biomaterialia, 2014. **10**(7): p. 3235-3242.
35. Kaufmann, A., et al., *Amphibian oocyte nuclei expressing lamin A with the progeria mutation E145K exhibit an increased elastic modulus.* Nucleus, 2011. **2**(4): p. 310-319.
36. Oberleithner, H., et al., *Potassium softens vascular endothelium and increases nitric oxide release.* Proceedings of the National Academy of Sciences, 2009. **106**(8): p. 2829-2834.

37. Rianna, C. and M. Radmacher, *Comparison of viscoelastic properties of cancer and normal thyroid cells on different stiffness substrates.* European Biophysics Journal, 2016: p. 1-16.
38. Discher, D.E., P. Janmey, and Y.-l. Wang, *Tissue cells feel and respond to the stiffness of their substrate.* Science, 2005. **310**(5751): p. 1139-1143.
39. Levental, I., P.C. Georges, and P.A. Janmey, *Soft biological materials and their impact on cell function.* Soft Matter, 2007. **3**(3): p. 299-306.
40. Yeung, A. and E. Evans, *Cortical shell-liquid core model for passive flow of liquid-like spherical cells into micropipets*, in *Biophysical journal*. 1989. p. 139-149.
41. Evans, E. and A. Yeung, *Apparent viscosity and cortical tension of blood granulocytes determined by micropipet aspiration.* Biophysical journal, 1989. **56**(1): p. 151.
42. Crick, F. and A. Hughes, *The physical properties of cytoplasm: A study by means of the magnetic particle method Part I. Experimental.* Experimental Cell Research, 1950. **1**(1): p. 37-80.
43. Valberg, P. and H. Feldman, *Magnetic particle motions within living cells. Measurement of cytoplasmic viscosity and motile activity.* Biophysical Journal, 1987. **52**(4): p. 551.
44. Bausch, A.R., W. Möller, and E. Sackmann, *Measurement of local viscoelasticity and forces in living cells by magnetic tweezers.* Biophysical journal, 1999. **76**(1): p. 573-579.
45. Kundu, T., J. Bereiter-Hahn, and K. Hillmann, *Measuring elastic properties of cells by evaluation of scanning acoustic microscopy V (Z) values using simplex algorithm.* Biophysical journal, 1991. **59**(6): p. 1194.
46. Bausch, A.R., et al., *Local measurements of viscoelastic parameters of adherent cell surfaces by magnetic bead microrheometry.* Biophysical journal, 1998. **75**(4): p. 2038-2049.
47. Fabry, B., et al., *Scaling the microrheology of living cells.* Physical review letters, 2001. **87**(14): p. 148102.
48. Kollmannsberger, P. and B. Fabry, *BaHigh-force magnetic tweezers with force feedback for biological applications.* Review of Scientific Instruments, 2007. **78**(11): p. 114301.
49. Radmacher, M., *Studying the mechanics of cellular processes by atomic force microscopy.* Methods in cell biology, 2007. **83**: p. 347-372.
50. Guck, J., et al., *The optical stretcher: a novel laser tool to micromanipulate cells.* Biophysical journal, 2001. **81**(2): p. 767-784.
51. Mietke, A., et al., *Extracting Cell Stiffness from Real-Time Deformability Cytometry: Theory and Experiment.* Biophysical journal, 2015. **109**(10): p. 2023-2036.
52. Kollmannsberger, P. and B. Fabry, *Linear and nonlinear rheology of living cells.* Annual review of materials research, 2011. **41**: p. 75-97.
53. Ahmed, W.W., É. Fodor, and T. Betz, *Active cell mechanics: Measurement and theory.* Biochimica et Biophysica Acta (BBA)-Molecular Cell Research, 2015. **1853**(11): p. 3083-3094.
54. Hecht, F.M., et al., *Imaging viscoelastic properties of live cells by AFM: power-law rheology on the nanoscale.* Soft matter, 2015. **11**(23): p. 4584-4591.
55. Hertz, H., *Über die Berührung fester elastischer Körper.* Journal für die reine und angewandte Mathematik, 1882. **92**: p. 156-171.

56. Sneddon, I.N., *The relation between load and penetration in the axisymmetric Boussinesq problem for a punch of arbitrary profile.* International journal of engineering science, 1965. **3**(1): p. 47-57.
57. Rebelo, L., et al., *Comparison of the viscoelastic properties of cells from different kidney cancer phenotypes measured with atomic force microscopy.* Nanotechnology, 2013. **24**(5): p. 055102.
58. Wu, H., T. Kuhn, and V. Moy, *Mechanical properties of L929 cells measured by atomic force microscopy: effects of anticytoskeletal drugs and membrane crosslinking.* Scanning, 1998. **20**(5): p. 389-397.
59. Moreno-Flores, S., et al., *Stress relaxation and creep on living cells with the atomic force microscope: a means to calculate elastic moduli and viscosities of cell components.* Nanotechnology, 2010. **21**(44): p. 445101.
60. Radmacher, M., R. Tillmann, and H. Gaub, *Imaging viscoelasticity by force modulation with the atomic force microscope.* Biophysical journal, 1993. **64**(3): p. 735.
61. Florin, E.L., et al., *Atomic force microscope with magnetic force modulation.* Review of scientific instruments, 1994. **65**(3): p. 639-643.
62. Puig-De-Morales, M., et al., *Measurement of cell microrheology by magnetic twisting cytometry with frequency domain demodulation.* Journal of Applied Physiology, 2001. **91**(3): p. 1152-1159.
63. Rebêlo, L., et al., *Microrheology of cells with magnetic force modulation atomic force microscopy.* Soft matter, 2014. **10**(13): p. 2141-2149.
64. Kuimova, M.K., *Mapping viscosity in cells using molecular rotors.* Physical Chemistry Chemical Physics, 2012. **14**(37): p. 12671-12686.
65. López-Duarte, I., et al., *A molecular rotor for measuring viscosity in plasma membranes of live cells.* Chemical Communications, 2014. **50**(40): p. 5282-5284.
66. Harris, A.R. and G. Charras, *Experimental validation of atomic force microscopy-based cell elasticity measurements.* Nanotechnology, 2011. **22**(34): p. 345102.
67. Kuznetsova, T.G., et al., *Atomic force microscopy probing of cell elasticity.* Micron, 2007. **38**(8): p. 824-833.
68. Ventre, M., F. Causa, and P.A. Netti, *Determinants of cell–material crosstalk at the interface: towards engineering of cell instructive materials.* Journal of the Royal Society Interface, 2012: p. rsif20120308.
69. Chen, D.T., et al., *Rheology of soft materials.* Condensed Matter Physics, 2010. **1**.
70. Natale, C.F., M. Ventre, and P.A. Netti, *Tuning the material-cytoskeleton crosstalk via nanoconfinement of focal adhesions.* Biomaterials, 2014. **35**(9): p. 2743-2751.
71. Yamaguchi, H. and J. Condeelis, *Regulation of the actin cytoskeleton in cancer cell migration and invasion.* Biochimica et Biophysica Acta (BBA)-Molecular Cell Research, 2007. **1773**(5): p. 642-652.
72. Kumar, S., et al., *Viscoelastic retraction of single living stress fibers and its impact on cell shape, cytoskeletal organization, and extracellular matrix mechanics.* Biophysical journal, 2006. **90**(10): p. 3762-3773.
73. Rianna, C., et al., *Micropatterned azopolymer surfaces modulate cell mechanics and cytoskeleton structure.* ACS applied materials & interfaces, 2015. **7**(38): p. 21503-21510.
74. Wu, G., et al., *Bioassay of prostate-specific antigen (PSA) using microcantilevers.* Nature biotechnology, 2001. **19**(9): p. 856-860.
75. Subramanian, A., et al., *Glucose biosensing using an enzyme-coated microcantilever.* Applied Physics Letters, 2002. **81**(2): p. 385-387.

76. Vashist, S.K., *A review of microcantilevers for sensing applications.* J. of Nanotechnology, 2007. **3**: p. 1-18.
77. Burnham, N., et al., *Comparison of calibration methods for atomic-force microscopy cantilevers.* Nanotechnology, 2003. **14**: p. 1-6.
78. Gates, R.S. and J.R. Pratt, *Accurate and precise calibration of AFM cantilever spring constants using laser Doppler vibrometry.* Nanotechnology, 2012. **23**(37): p. 375702.
79. Grutzik, S.J., et al., *Accurate spring constant calibration for very stiff atomic force microscopy cantilevers.* Review of Scientific Instruments, 2013. **84**(11): p. 113706.
80. Tortonese, M. and M. Kirk. *Characterization of application-specific probes for SPMs*. in *Photonics West'97*. 1997. International Society for Optics and Photonics.
81. Gates, R.S. and M.G. Reitsma, *Precise atomic force microscope cantilever spring constant calibration using a reference cantilever array.* Review of Scientific Instruments, 2007. **78**(8): p. 086101.
82. Gates, R.S., et al., *Atomic force microscope cantilever flexural stiffness calibration: toward a standard traceable method.* Journal of research of the National Institute of Standards and Technology, 2011. **116**(4): p. 703.
83. Sader, J.E., J.W. Chon, and P. Mulvaney, *Calibration of rectangular atomic force microscope cantilevers.* Review of Scientific Instruments, 1999. **70**(10): p. 3967-3969.
84. Song, Y., et al. *Calibration of the lateral spring constant of atomic force microscope cantilevers*. in *Applied Optics and Photonics China (AOPC2015)*. 2015. International Society for Optics and Photonics.
85. Sader, J.E., *Susceptibility of atomic force microscope cantilevers to lateral forces.* Review of Scientific Instruments, 2003. **74**(4): p. 2438-2443.
86. Clifford, C.A. and M.P. Seah, *The determination of atomic force microscope cantilever spring constants via dimensional methods for nanomechanical analysis.* Nanotechnology, 2005. **16**(9): p. 1666.
87. Tasci, T., et al., *Surface-enabled propulsion and control of colloidal microwheels.* Nature communications, 2016. **7**.
88. Sadiku, M.N., *Elements of electromagnetics*. Vol. 428. 2010, New York: Oxford university press New York.
89. Bishop, K.J., et al., *Nanoscale forces and their uses in self‐assembly.* small, 2009. **5**(14): p. 1600-1630.
90. Gupta, A.K. and M. Gupta, *Synthesis and surface engineering of iron oxide nanoparticles for biomedical applications.* Biomaterials, 2005. **26**(18): p. 3995-4021.
91. Kodera, N., et al., *High-resolution imaging of myosin motor in action by a high-speed atomic force microscope*, in *Molecular and Cellular Aspects of Muscle Contraction*. 2003, Springer. p. 119-127.
92. Proksch, R., et al., *Finite optical spot size and position corrections in thermal spring constant calibration.* Nanotechnology, 2004. **15**(9): p. 1344.
93. Tse, J.R. and A.J. Engler, *Preparation of hydrogel substrates with tunable mechanical properties.* Current protocols in cell biology, 2010: p. 10.16. 1-10.16. 16.
94. DREHMEL. *Dremeleurope.com*. 2017 [cited 2017 January 04 2017]; Available from: https://www.dremeleurope.com/nl/nl/imprint/.

95. UHU. *2-Komponenten Klebstoffe*. 2016 [cited 2016 Febraury 02]; Available from: http://www.uhu-profishop.de/klebstoffe/2-komponenten-klebstoffe.html?gclid=CNGU6Zm3qNECFVW4GwodATENuw.
96. AG, C.Z.M. *Germany, Oberkochen - Company Location | Carl Zeiss Meditec AG*. 2017 [cited 2017 January 04]; Available from: https://www.zeiss.com/meditec-ag/about-us/locations/germany-oberkochen-company.html.
97. Yu, Z., et al., *A force calibration standard for magnetic tweezers.* Review of Scientific Instruments, 2014. **85**(12): p. 123114.
98. Rico, F., et al., *Cell dynamic adhesion and elastic properties probed with cylindrical atomic force microscopy cantilever tips.* Journal of Molecular Recognition, 2007. **20**(6): p. 459-466.